

Field Guide to **Infrared Systems**

Arnold Daniels

SPIE Field Guides
Volume FG09

John E. Greivenkamp, Series Editor

SPIE
PRESS

Bellingham, Washington USA

Daniels, Arnold.

Field guide to infrared systems / Arnold Daniels.

p. cm. -- (The Field guide series ; no. 1:9)

Includes bibliographical references and index.

ISBN 0-8194-6361-2 (alk. paper)

1. Infrared technology--Handbooks, manuals, etc. I. Title. II. Series:
Field guide series (Bellingham, Wash.) ; no. 1:9.

TA1570.D36 2006

621.36'2--dc22

2006015467

Published by

SPIE—The International Society for Optical Engineering

P.O. Box 10

Bellingham, Washington 98227-0010 USA

Phone: +1 360 676 3290

Fax: +1 360 647 1445

Email: spe@spie.org

Web: <http://spie.org>

Copyright © 2007 The Society of Photo-Optical Instrumentation Engineers

All rights reserved. No part of this publication may be reproduced or distributed in any form or by any means without written permission of the publisher.

The content of this book reflects the work and thought of the author. Every effort has been made to publish reliable and accurate information herein, but the publisher is not responsible for the validity of the information or for any outcomes resulting from reliance thereon.

Printed in the United States of America.



The International Society
for Optical Engineering

Introduction to the Series

Welcome to the *SPIE Field Guides*—a series of publications written directly for the practicing engineer or scientist. Many textbooks and professional reference books cover optical principles and techniques in depth. The aim of the *SPIE Field Guides* is to distill this information, providing readers with a handy desk or briefcase reference that provides basic, essential information about optical principles, techniques, or phenomena, including definitions and descriptions, key equations, illustrations, application examples, design considerations, and additional resources. A significant effort will be made to provide a consistent notation and style between volumes in the series.

Each *SPIE Field Guide* addresses a major field of optical science and technology. The concept of these *Field Guides* is a format-intensive presentation based on figures and equations supplemented by concise explanations. In most cases, this modular approach places a single topic on a page, and provides full coverage of that topic on that page. Highlights, insights, and rules of thumb are displayed in sidebars to the main text. The appendices at the end of each *Field Guide* provide additional information such as related material outside the main scope of the volume, key mathematical relationships, and alternative methods. While complete in their coverage, the concise presentation may not be appropriate for those new to the field.

The *SPIE Field Guides* are intended to be living documents. The modular page-based presentation format allows them to be easily updated and expanded. We are interested in your suggestions for new *Field Guide* topics as well as what material should be added to an individual volume to make these *Field Guides* more useful to you. Please contact us at fieldguides@SPIE.org.

John E. Greivenkamp, *Series Editor*
Optical Sciences Center
The University of Arizona

The Field Guide Series

Keep information at your fingertips with all of the titles in the Field Guide Series:

Field Guide to Geometrical Optics, John E. Greivenkamp (FG01)

Field Guide to Atmospheric Optics, Larry C. Andrews (FG02)

Field Guide to Adaptive Optics, Robert K. Tyson and Benjamin W. Frazier (FG03)

Field Guide to Visual and Ophthalmic Optics, Jim Schwieglerling (FG04)

Field Guide to Polarization, Edward Collett (FG05)

Field Guide to Optical Lithography, Chris A. Mack (FG06)

Field Guide to Optical Thin Films, Ronald R. Willey (FG07)

Field Guide to Spectroscopy, David W. Ball (FG08)

Field Guide to Infrared Systems, Arnold Daniels (FG09)

Field Guide to Interferometric Optical Testing, Eric P. Goodwin and James C. Wyant (FG10)

Field Guide to Infrared Systems

Field Guide to Infrared Systems is written to clarify and summarize the theoretical principles of infrared technology. It is intended as a reference work for the practicing engineer and/or scientist who requires effective practical information to design, build, and/or test infrared equipment in a wide variety of applications.

This book combines numerous engineering disciplines necessary for the development of an infrared system. It describes the basic elements involving image formation and image quality, radiometry and flux transfer, and explains the figures of merit involving detector performance. It considers the development of search infrared systems, and specifies the main descriptors used to characterize thermal imaging systems. Furthermore, this guide clarifies, identifies, and evaluates the engineering tradeoffs in the design of an infrared system.

I would like to acknowledge and express my gratitude to my professor and mentor Dr. Glenn Boreman for his guidance, experience, and friendship. The knowledge that he passed on to me during my graduate studies at CREOL ultimately contributed to the creation of this book. Thanks are extended to Merry Schnell for her hard work and dedication on this project. I voice a special note of gratitude to my kids Becky and Alex for their forbearance, and to my wife Rosa for her love and support.

Lastly, I would particularly like to thank you, the reader, for selecting this book and taking the time to explore the topics related to this motivating and exciting field. I truly hope that you will find the contents of this book interesting and informative.

This *Field Guide* is dedicated to the memory of my father and brothers.

Arnold Daniels

Table of Contents

Glossary	x
Introduction	1
Electromagnetic Spectrum	1
Infrared Concepts	2
Optics	3
Imaging Concepts	3
Magnification Factors	4
Thick Lenses	5
Stop and Pupils	6
<i>F</i> -number and Numerical Aperture	7
Field-of-View	8
Combination of Lenses	9
Afocal Systems and Refractive Telescopes	10
Cold-Stop Efficiency and Field Stop	11
Image Quality	12
Image Anomalies in Infrared Systems	14
Infrared Materials	15
Material Dispersion	19
Atmospheric Transmittance	21
Radiometry and Sources	22
Solid Angle	22
Radiometry	23
Radiometric Terms	24
Flux Transfer	26
Flux Transfer for Image-Forming Systems	27
Source Configurations	28
Blackbody Radiators	30
Planck's Radiation Law	31
Stefan-Boltzmann and Wien's Displacement Laws	33
Rayleigh-Jeans and Wien's Radiation Laws	34
Exitance Contrast	35
Emissivity	36
Kirchhoff's Law	37
Emissivity of Various Common Materials	38
Radiometric Measure of Temperature	39
Collimators	41

Table of Contents

Performance Parameters for Optical Detectors	42
Infrared Detectors	42
Primary Sources of Detector Noise	43
Noise Power Spectral Density	44
White Noise	45
Noise-Equivalent Bandwidth	46
Shot Noise	48
Signal-to-Noise Ratio: Detector and BLIP Limits	49
Generation-Recombination Noise	50
Johnson Noise	51
$1/f$ Noise and Temperature Noise	52
Detector Responsivity	53
Spectral Responsivity	55
Blackbody Responsivity	56
Noise Equivalent Power	57
Specific or Normalized Detectivity	58
Photovoltaic Detectors or Photodiodes	59
Sources of Noise in PV Detectors	60
Expressions for $D_{PV,BLIP}^*$, $D_{PV,BLIP}^{**}$, and $D_{PV,JOLI}^*$	61
Photoconductive Detectors	62
Sources of Noise in PC Detectors	63
Pyroelectric Detectors	64
Bolometers	66
Bolometers: Immersion Optics	68
Thermoelectric Detectors	69
Infrared Systems	70
Raster Scan Format: Single-Detector	70
Multiple-Detector Scan Formats: Serial Scene	70
Dissection	72
Multiple-Detector Scan Formats: Parallel Scene	73
Dissection	73
Staring Systems	74
Search Systems and Range Equation	75
Noise Equivalent Irradiance	78
Performance Specification: Thermal-Imaging Systems	79
MTF Definitions	80

Table of Contents

Optics MTF: Calculations	83
Electronics MTF: Calculations	85
MTF Measurement Setup and Sampling Effects	86
MTF Measurement Techniques: PSF and LSF	87
MTF Measurement Techniques: ESF and CTF	88
MTF Measurement Techniques: Noiselike Targets	89
MTF Measurement Techniques: Interferometry	92
Noise Equivalent Temperature Difference	93
NETD Measurement Technique	94
Minimum Resolvable Temperature Difference	95
MRTD: Calculation	96
MRTD Measurement Technique	97
MRTD Measurement: Automatic Test	98
Johnson Criteria	99
Infrared Applications	101
Appendix	
Equation Summary	103
Notes	112
Bibliography	113
Index	116

Glossary

A	Area
A_d	Detector area
A_{enp}	Area of an entrance-pupil
A_{exp}	Area of an exit-pupil
$A_{\text{footprint}}$	Footprint area
A_{img}	Area of an image
A_{lens}	Lens area
A_{obj}	Area of an object
A_{opt}	Area of an optical component
A_s	Source area
B	3-db bandwidth
c	Speed of light in vacuum
C_d	Detector capacitance
CTF	Contrast transfer function
d_{diff}	Diameter of a diffraction-limited spot
D^*	Normalized detectivity of a detector
D_{BLIP}^*	D-star under BLIP conditions
D^{**}	Angle-normalized detectivity
D_{enp}	Diameter of an entrance-pupil
D_{exp}	Diameter of an exit-pupil
D_{img}	Image diameter
D_{in}	Input diameter
D_{lens}	Lens diameter
D_{out}	Output diameter
D_{obj}	Object diameter
D_{opt}	Optics diameter
e	Energy-based unit subscript
E_{bkg}	Background irradiance
E_{img}	Image irradiance
E_{source}	Source irradiance
ESF	Edge spread function
\mathcal{E}	Energy of a photon
f_{eff}	Effective focal length
f	Focal length
$b.f.l$	Back focal length
$f.f.l$	Front focal length
$f(x, y)$	Object function
F_B	Back focal point
F_F	Front focal point

Glossary (cont'd)

$F(\xi, \eta)$	Object spectrum
f_0	Center frequency of an electrical filter
FOV	Full-angle field-of-view
$\text{FOV}_{\text{half-angle}}$	Half-angle field-of-view
$F/\#$	F-number
$g(x, y)$	Image function
$G(\xi, \eta)$	Image spectrum
G	Gain of a photoconductive detector
$h(x, y)$	Impulse response
$H(\xi, \eta)$	Transfer function
h	Planck's constant
H	Heat capacity
HIFOV	Horizontal instantaneous field-of-view
HFOV	Horizontal field-of-view
h_{img}	Image height
h_{obj}	Object height
i	Electrical current
\bar{i}	Mean current
i_{avg}	Average electrical current
i_{bkg}	Background rms current
i_{dark}	Dark current
i_j	rms Johnson noise current
$i_{1/f}$	rms $1/f$ -noise current
$i_{G/R}$	Generation-recombination noise rms current
i_{noise}	Noise current
i_{oc}	Open circuit current
i_{pa}	Preamplifier noise rms current
i_{rms}	rms current
i_{sc}	Short circuit current
i_{shot}	Shot noise rms current
i_{sig}	Signal current
J	Current density
k	Boltzmann's constant
$\mathcal{K}(\xi_f)$	Spatial-frequency dependant MRTD proportionality factor
K	Thermal conductance
L	Radiance
LSF	Line spread function

Glossary (cont'd)

L_{bkg}	Background radiance
L_{λ}	Spectral radiance
M	Exitance
M_{meas}	Measured exitance
M_{obj}	Exitance of an object
M_{λ}	Spectral exitance
MRTD	Minimum resolvable temperature difference
MTF	Modulation transfer function
MTF_d	Detector MTF
\mathcal{M}	Magnification
\mathcal{M}_{ang}	Angular magnification
n	Refractive index
n_d	Number of detectors
n_e	Number of photogenerated electrons
n_{lines}	Number of lines
NEI	Noise-equivalent irradiance
NEP	Noise-equivalent power
$\text{NE}\Delta f$	Noise-equivalent bandwidth
OTF	Optical transfer function
P_{avg}	Average power
p	Object distance
PSD	Power spectral density
PSF	Point spread function
q	Image distance
R	Resistance
R_d	Detector resistance
R_{eq}	Equivalent resistance
R_{in}	Input resistance
R_L	Load resistance
R_{out}	Output resistance
SNR	Signal-to-noise ratio
SR	Strehl-intensity ratio
\mathcal{R}	Responsivity
\mathcal{R}_i	Current responsivity
\mathcal{R}_v	Voltage responsivity
$\mathcal{R}(\lambda)$	Spectral responsivity
$\mathcal{R}(T)$	Blackbody responsivity
t	Time

Glossary (cont'd)

T	Temperature
T_B	Brightness temperature
T_{bkg}	Background temperature
T_C	Color temperature
T_d	Detector temperature
T_{load}	Load temperature
T_{rad}	Radiation temperature
T_{source}	Source temperature
T_{target}	Target temperature
VIFOV	Vertical instantaneous field-of-view
VFOV	Vertical field-of-view
\bar{v}	Mean voltage
v_{in}	Input voltage
v_j	Johnson noise rms voltage
v_n	rms noise voltage
v_{oc}	Open-circuit voltage
v_{out}	Output voltage
v_{sc}	Short-circuit voltage
v_s	Shot-noise rms voltage
v_{scan}	Scan velocity
v_{sig}	Signal voltage
V	Abbe number
\mathcal{W}	\mathcal{W} proportionality factor
α	Coefficient of absorption
β	Blur angle caused by diffraction
ε	Emissivity
Δf	Electronic frequency bandwidth
Δt	Time interval
ΔT	Temperature difference
$\Delta \lambda$	Wavelength interval
θ	Angle variable
θ_{max}	Maximum angle subtense
η	Quantum efficiency
η_{scan}	Scan efficiency
λ	Wavelength
λ_{cut}	Cutoff wavelength
λ_{max}	Maximum wavelength
$\lambda_{\text{max-cont}}$	Maximum contrast wavelength
λ_{peak}	Peak wavelength

Glossary (cont'd)

λ_0	Fixed wavelength
ν	Optical frequency
σ^2	Variance
σ	Standard deviation
σ_e	Stefan-Boltzmann constant in energy units
σ_p	Stefan-Boltzmann constant in photon units
ρ	Reflectance
τ	Transmittance
τ_{atm}	Atmospheric transmittance
τ_{dwell}	Dwell time
τ_{ext}	External transmittance
τ_{int}	Internal transmittance
τ_{frame}	Frame time
τ_{line}	Line time
τ_{opt}	Optical transmittance
ϕ	Flux
ϕ_λ	Spectral flux
ϕ_{abs}	Absorbed flux
ϕ_{bkg}	Background flux
ϕ_d	Detector flux
ϕ_{img}	Flux incident on an image
ϕ_{inc}	Incident flux
ϕ_{obj}	Flux radiated by an object
ϕ_{ref}	Reflected flux
ϕ_{sig}	Signal flux
ϕ_{trans}	Transmitted flux
ξ	Spatial frequency in x -direction
ξ_{cutoff}	Spatial cutoff frequency
η	Spatial frequency in y -direction
Ω	Solid angle
Ω_d	Detector solid angle
Ω_s	Source solid angle
Ω_{bkg}	Background solid angle
Ω_{exp}	Exit pupil solid angle
Ω_{enp}	Entrance pupil solid angle
Ω_{img}	Image solid angle
Ω_{lens}	Lens solid angle
Ω_{obj}	Object solid angle

Electromagnetic Spectrum

The **electromagnetic spectrum** is the distribution of **electromagnetic radiation** according to energy, frequency, or wavelength. The electro-magnetic radiation can be described as a stream of **photons**, which are particles traveling in a wavelike pattern, moving at the speed of light.

Type of Radiation	Frequency Range	Wavelength Range
Gamma rays	$<3 \times 10^{20}$	$<1 \text{ fm}$
X rays	3×10^{17} – 3×10^{20}	1 fm – 1 nm
Ultraviolet	7.5×10^{14} – 3×10^{17}	1 nm – 400 nm
Visible	4×10^{14} – 7.5×10^{14}	$0.4 \mu\text{m}$ – $0.75 \mu\text{m}$
Near-infrared	10^{14} – 7.5×10^{14}	$0.75 \mu\text{m}$ – $3.0 \mu\text{m}$
Midwave infrared	5×10^{13} – 10^{14}	$3.0 \mu\text{m}$ – $6 \mu\text{m}$
Long wave infrared	2×10^{13} – 5×10^{13}	$6.0 \mu\text{m}$ – $15 \mu\text{m}$
Extreme infrared	3×10^{11} – 2×10^{13}	$15 \mu\text{m}$ – 1 mm
Micro and radio waves	$<3 \times 10^{11}$	$>1 \text{ mm}$

Frequencies in the visible and infrared spectral bands are measured in the millions of megahertz, commonly referred to as wavelengths rather than frequencies. Wavelength can be measured interferometrically with great accuracy and it is related to the optical frequency by the universal equation

$$c = \lambda\nu,$$

where λ is the wavelength, ν is the optical frequency, and c is the speed of light in free space ($3 \times 10^8 \text{ m/sec}$).

The difference between the categories of electromagnetic radiation is the amount of energy found in their photons. The energy of a photon is inversely proportional to the wavelength, and is given by

$$\mathcal{E} = h\nu = \frac{hc}{\lambda},$$

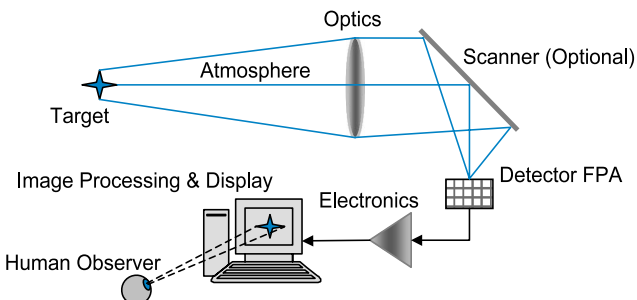
where h is the Planck constant ($6.62 \times 10^{-34} \text{ J}\cdot\text{sec}$).

Radio waves have photons with very low energies while gamma-rays are the most energetic of all. The electromagnetic spectrum is classified based on the source, detector, and materials technologies employed in each of the spectral regions.

Infrared Concepts

Infrared-imaging systems are often used to form images of targets under nighttime conditions. The target is seen because of **self-radiation** rather than the reflected radiation from the sun. Self-radiation is a physical property of all objects that are at temperatures above absolute zero (i.e., 0 K = -273.15°C).

In order to make this radiation visible, the infrared system depends on the interaction of several subsystems.



The self-radiation signature is determined by the **temperature** and the surface characteristics of the target. Gases in the atmosphere limit the frequencies that this radiation is transmitted. The configuration of the optical system defines the **field-of-view (FOV)**, the **flux collection efficiency**, and the **image quality**. These parameters, along with the detector interface, impact the radiometric accuracy and **resolution** of the resulting image. The detector is a transducer that converts the optical energy into an electrical signal, and electronics amplify this signal to useful levels.

For typical terrestrial and airborne targets **Planck's equation** dictates that, within the range of temperatures of 300 K to 1000 K, emission of radiation occurs primarily in the infrared spectrum. However, the background is self-luminous as well, causing terrestrial targets to compete with background clusters of similar temperature. Infrared images have much lower **contrast** than corresponding visual images, which have orders of magnitude higher reflectance and emittance differences.

Imaging Concepts

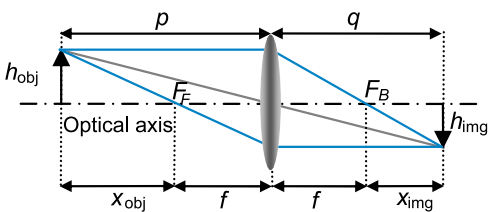
An object is a collection of independent source points, each emitting light rays into all forward directions. Because of **Snell's law**, rays that diverge from each object point intersect at corresponding image-plane points. The image is built up on a point-by-point basis. The power at any image location is proportional to the strength of the corresponding object point, causing a geometrical distribution of power.

The symmetry line that contains the centers of curvature of all optical surfaces is called the **optical axis**. Three ray-trace rules are used to find the image position with respect to the object:

1. rays entering parallel to the optical axis exit through the back focal point F_B ;
2. rays entering the lens through the front focal point F_F exit parallel to the optical axis; and
3. rays entering through the center (chief rays) of the lens do not change direction.

To determine the image-plane location and size, a thin lens and small-angle or **paraxial approximation** is used, which linearizes

the ray trace equations that determine the ray paths through the optical system (i.e., $\sin \theta \approx \tan \theta \approx \theta$).



Gaussian lens equation:
$$\frac{1}{f} = \frac{1}{p} + \frac{1}{q}$$

Newtonian lens equation:
$$x_{\text{obj}}x_{\text{img}} = f^2$$

A **thin lens** has a thickness that is considered negligible in comparison with its focal length.

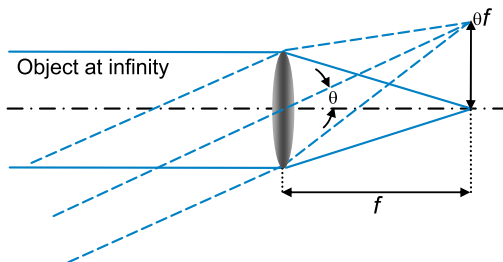
Magnification Factors

As the object gets farther away, the image distance gets closer to f ($f \rightarrow \infty, q \rightarrow f$); and as the object is placed closer to the front focus of the lens, the image gets farther away ($p \rightarrow f, q \rightarrow \infty$).

The **lateral or transverse magnification** of an optical system is given by

$$\mathcal{M} = -\frac{q}{p} = \frac{h_{\text{img}}}{h_{\text{obj}}}.$$

By using the Gaussian lens equation, it can be verified that the minimum distance between a real object and its corresponding image is $4f$ (i.e., $p = q = 2f$, in which case $\mathcal{M} = -1$).

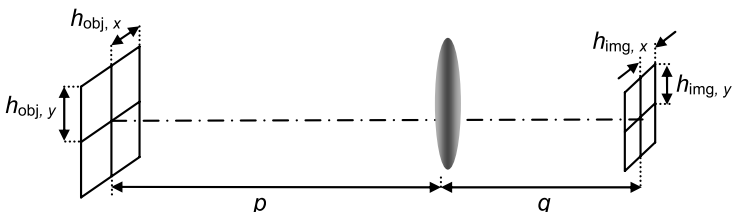


When an off-axis source is located at an infinite distance from the lens; an angle θ [rad] exists between the direction of the collimated rays and the optical axis. The ray focuses at a distance θf away from the optical axis.

Squaring the lateral magnification, the **area or longitudinal magnification** is obtained by

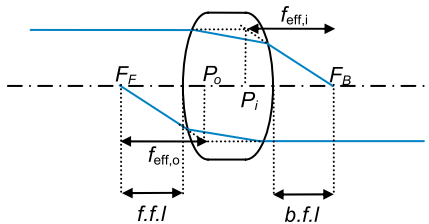
$$\mathcal{M}^2 = \frac{A_{\text{img}}}{A_{\text{obj}}} = \left(-\frac{q}{p} \right)^2,$$

which is used extensively in radiometric calculations.



Thick Lenses

When the thickness of a lens cannot be considered negligible, the lens is treated as a thick lens. F_F and F_B , are the **front** and **back focal points** and when these focal

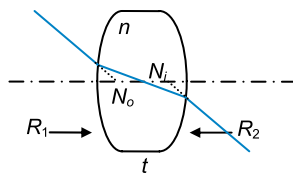


points are measured from the lens vertices they define the **front focal length (f.f.l)** and the **back focal length (b.f.l)** of the optical element.

A diverging ray from F_F emerges parallel to the optical axis, while a parallel incident ray is brought to F_B . In each case, the incident and emerged rays are extended to the point of intersection between the surfaces. Transverse planes through these intersections are termed the **primary and secondary principal planes** and can either lie inside or outside the lens. Points where these planes intersect the optical axis are known as the **first and second principal points P_o and P_i** . Extending incoming and outgoing chief rays until they cross the optical axis locate the **nodal points N_o and N_i** . These six points; two focal, two principal and two nodal, are named the **cardinal points** of the optical system.

The **effective focal lengths** $f_{\text{eff},o}$ and $f_{\text{eff},i}$ are measured from the foci to their respective principal points, and are identical if the medium on each side has the same refractive index:

$$\frac{1}{f_{\text{eff}}} = (n - 1) \left[\frac{1}{R_1} - \frac{1}{R_2} + \frac{(n - 1)t}{n} \frac{1}{R_1 R_2} \right].$$



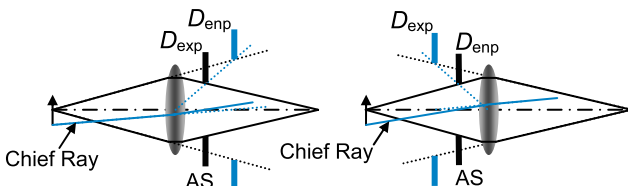
R_1 and R_2 are the lens radii, and n is the index of refraction of the lens material.

A rule of thumb for ordinary glass lenses immersed in air is that the separation between the principal points roughly equal one third of the lens thickness (t).

Stop and Pupils

Aperture stop (AS): the physical opening that limits the angle over which the lens accepts rays from the axial object point.

Entrance pupil (D_{enp}): the image of the AS as seen from the axial point on the object plane through the optical elements preceding the stop. If there are no elements between the object and the AS, the latter operates as the entrance pupil.



Exit pupil (D_{exp}): the image of the AS as seen from the axial point on the image plane through those optical elements that follow the stop. If there are no elements between the AS and the image, the former serves as the exit pupil.

Axial ray: the ray that starts at the axial object point and ends on the axial image point.

Marginal ray: a special axial ray that starts at the axial object point, goes through the edge of the entrance pupil, and ends on the axial image point. Marginal ray is used to define the $F/\#$ and the numerical aperture.

Chief ray: a ray that starts at the edge of the object, passes through the center of the entrance pupil, and defines the height of the image.

Telecentric stop: an aperture stop that is located at a focal point of the optical system. It is used to reduce the magnification error in the size of the projected image for a small departure from best focus.

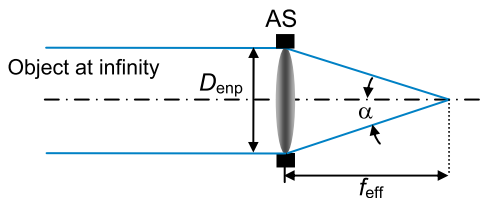
Telecentric system: a system where the entrance or exit pupils located at infinity.

For any point in the object, the amount of radiation accepted by and emitted from the optical system is determined by the sizes and locations of the pupils. The location of the AS is determined by that stop or image of a stop that subtends the smallest angle as seen from the object axial point. An analogous procedure can be carried out from the image plane.

F-number and Numerical Aperture

The **F-number (F/#)** is the parameter used to describe the ratio between the f_{eff} of an optical system and the **diameter** of the entrance pupil. It describes the image-spaced cone for an object at infinity:

$$F/\# \equiv \frac{f_{\text{eff}}}{D_{\text{enp}}}.$$



Although the $F/\#$ also exists in image space as q/D_{enp} for finite conjugate systems, the **numerical aperture (NA)** is usually the parameter used in these cases.

The refractive index n in air is approximately 1 ($n = 1$), the numerical aperture is the axial cone of light in terms of the marginal ray angle α and is defined as $\text{NA} \equiv \sin \alpha$

The NA and the $F/\#$ are related as follows:

$$\text{NA} \equiv \sin\left(\tan^{-1} \frac{1}{2F/\#}\right) \quad \text{or} \quad F/\# = \frac{1}{2\tan(\sin^{-1} \text{NA})}$$

Assuming paraxial approximation, $\sin \alpha \approx \alpha$ yielding

$$F/\# \approx \frac{1}{2\text{NA}}.$$

Example: If an F/3 system has its aperture made larger or smaller by 50% in diameter, what are the new $F/\#$ s?

If $D \uparrow \Rightarrow F/\# \downarrow$; $F/\#_{\text{new}} = f_{\text{eff}}/1.5D = 2/3F/\# = 2$, resulting in faster optics.

If $D \downarrow \Rightarrow F/\# \uparrow$; $F/\#_{\text{new}} = f_{\text{eff}}/0.5D = 2F/\# = 6$, resulting in slower optics.

Field-of-View

The **field-of-view (FOV)** is the angular coverage of an optical system. It can be defined either in full or half angles. Using the half-angle principle

$$\text{FOV}_{\text{half-angle}} = \theta_{1/2} = \left| \tan^{-1} \frac{h_{\text{obj}}}{p} \right| = \left| \tan^{-1} \frac{h_{\text{img}}}{q} \right|.$$

The element that limits the size of the object to be imaged is called the **field stop**, which determines the system's FOV. In an infrared camera, it is the edge of the detector array itself that bounds the image plane and serves as the field stop.

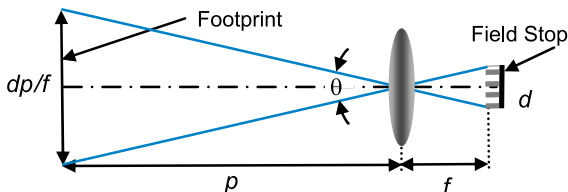
For an object at infinity, the full-angle FOV is determined by the ratio between the detector size and the system's focal length:

$$\text{FOV} = \theta = \frac{d}{f}.$$

The detector has a **footprint**; the image of the detector projected onto the object plane. It defines the area of the object that contributes flux onto the detector. Given the focal length and the size of the detector, the resolution element at the object plane can be determined.

A smaller FOV is attained by increasing the focal length, causing an increment in the **magnification**; a shorter focal length widens the FOV but decreases the magnification.

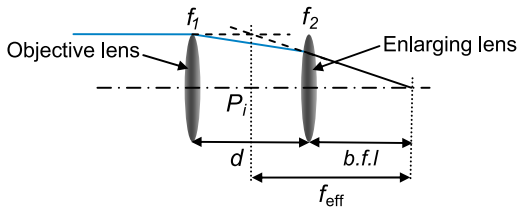
The **$F/\#$** and **FOV** are inversely proportional, and are affected by both



flux transfer and **optical aberrations**. There is a trade-off between the amount of light that reaches the detector, and the **image quality**. A system with a small $F/\#$ and large FOV has high flux-transfer efficiency, but the image quality worsens. A large $F/\#$ and small FOV restricts the system's flux, but the quality of the image is improved.

Combination of Lenses

Consider two lenses separated by a distance d .



The f_{eff} of this optical system is given by the expression

$$\frac{1}{f_{\text{eff}}} = \frac{1}{f_1} + \frac{1}{f_2} - \frac{d}{f_1 f_2},$$

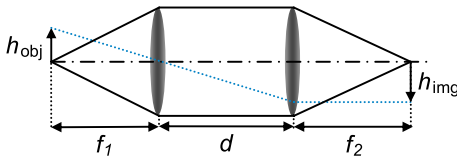
where f_1 and f_2 are the focal lengths of the **objective** and **enlarging lenses**, respectively. The back focal length is the distance from the last surface of the enlarging lens to the focal plane of the system, and is given by

$$b.f.l = \frac{f_2(d - f_1)}{d - (f_1 + f_2)}.$$

When the two lenses are placed in contact (i.e., $d \rightarrow 0$), the combination acts as a single lens yielding

$$\frac{1}{f_{\text{eff}}} = \frac{1}{f_1} + \frac{1}{f_2}.$$

A special configuration of the two-lens combination system is the so called “relay lens pair.” In this case, a source is placed at the front focal point of the optical system; the objective lens projects this source to infinity which is then imaged by the enlarging lens.



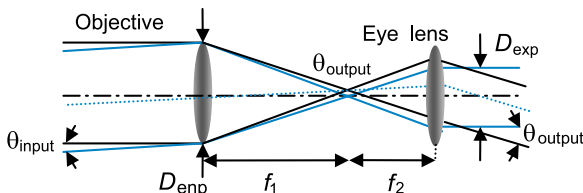
$$\mathcal{M} = \frac{h_{\text{img}}}{h_{\text{obj}}} = -\frac{f_2}{f_1}$$

The separation of the lenses affect the location of the principal planes and thereby the effective focal length of the system. Furthermore, as the lenses move apart, the size the detector lens must be increased in size to avoid vignetting.

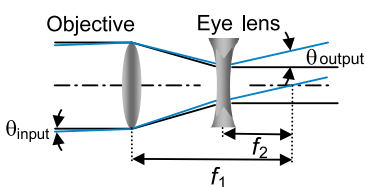
Afocal Systems and Refractive Telescopes

Afocal systems do not have focal lengths. Telescopes are afocal systems with their object and image located at infinity. Their primary function is to enlarge the apparent size of a distant object. There are three main types of refractive telescopes as defined below.

Astronomical (or Keplerian) telescope: comprised of two convergent lenses spaced by the sum of their focal lengths. The objective is usually an achromatic doublet forming a real inverted and reverted image at its focal point; the eye lens then reimages the object at infinity, where it may be erected by the use of an auxiliary lens. The aperture stop and the entrance pupil are located at the objective to minimize its size and cost.



Galilean telescope: comprised of a positive objective and a negative eye lens, where spacing is the difference between the absolute values of the focal lengths since f_2 is negative. There is no real internal image, and a reticle or



crosshair cannot be introduced into the optical system. The final image is erect. The aperture stop is usually the pupil of the viewer's eye, which is also the exit pupil.

Terrestrial (or erecting) telescope: an astronomical telescope with an erecting system inserted between the eye lens and objective so that the final image is erected.

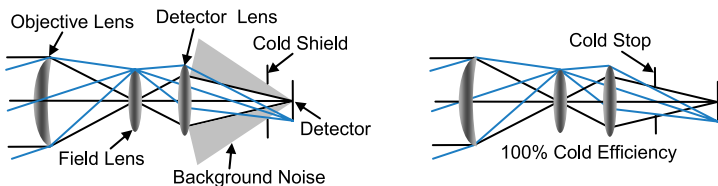
The **angular magnification** of these afocal systems is given by the ratio between the angle subtended by the image and then angle subtended by the object:

$$\mathcal{M}_{\text{angular}} = \frac{\theta_{\text{output}}}{\theta_{\text{input}}} = \left| \frac{f_2}{f_1} \right|.$$

Cold-Stop Efficiency and Field Stop

To reduce **thermal noise**, infrared photon detectors are cooled to **cryogenic temperatures**. The detector is housed in a vacuum bottle called a **Dewar**. An aperture stop is adjacent to the detector plane, which prevents **stray radiation** from reaching the detector. This **cold shield** is located inside the evacuated Dewar, and limits the angle over which the detector receives radiation.

The **cold-stop efficiency** is the percentage of the total scene source power reaching the detector. The perfect **cold stop** is defined as one that limits the reception of background radiation to the cone established by the $F/\#$ (i.e., 100% cold-stop efficiency). This is achieved when the cold shield is located at the exit pupil of the infrared optical system.



The FOV of an optical system may be increased without increasing the diameter of the detector lens by placing a **field lens** at the internal image of the system. This lens redirects the ray bundles back toward the optical axis, which would otherwise miss the detector. The insertion of this lens has no effect on the system's magnification. This arrangement is good for flux-collection systems (i.e., search systems), but not for imaging systems since the object is not imaged onto the detector, but rather into the field lens.

If the field lens is moved to the detector plane, it becomes an **immersion lens**, which increases the numerical aperture by a factor of the **index of refraction** of the lens material, without modifying the characteristics of the system. This configuration allows the object to be imaged onto the detector array.

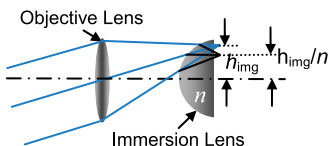
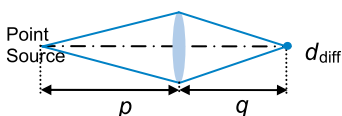


Image Quality

The assumption thus far has been that all points in object space are mapped to points in image space. However, more detailed information such as the size of the image and its energy distribution is required to properly design an optical system. Due to effects of **diffraction** and **optical aberrations**, point sources in the object are seen in the image as **blur spots**, producing a blurred image.

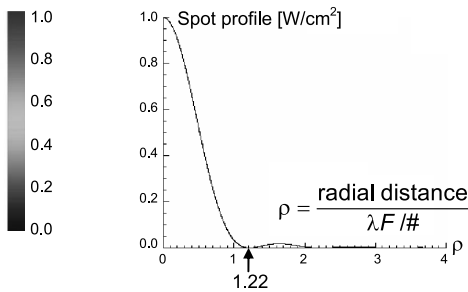
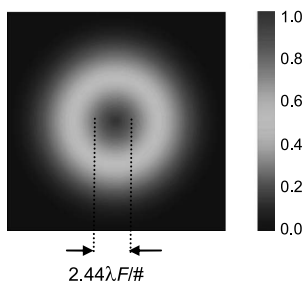


Better quality is achieved for smaller blur spots.

Diffraction is a consequence of the wave nature of radiant energy. It is a physical limitation of the optical system over which there is no control. On the other hand, optical aberrations are image defects that arise from the deviation of the paraxial approximation; and therefore, they can be controlled through proper design.

Even in the absence of optical aberrations, diffraction phenomena still cause a point to be imaged as a blur circle. Such an optical system is said to be **diffraction limited**, and it represents the best in optical performance.

The diffraction pattern of a point source appears as a bright central disk surrounded by several alternative bright and dark rings. The central disk is called the Airy disk and contains 84% of the total flux.



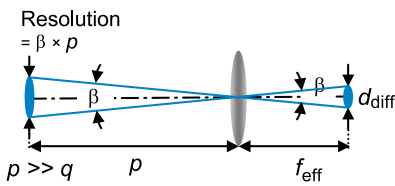
The linear diameter of the diffraction-limited blur spot is given by

$$d_{\text{diff}} = 2.44\lambda F/\#.$$

Image Quality (cont'd)

The effects of diffraction may also be expressed in angular terms. The full-angular blur is the diameter of the diffraction spot divided by f_{eff} , yielding

$$\beta = 2.44 \frac{\lambda}{D}$$



It can also be defined as the angular subtense of the minimum resolution feature in object space viewed from the entrance pupil.

The size of the blur spot depends on the $F/\#$ and the spectral band in which the imaging system operates.

Low $F/\#$ systems have the smallest diffraction-limited spot sizes, thus the best potential performance. However, the aberration effects generally become worse as the $F/\#$ decreases. Therefore, low $F/\#$ systems are harder to correct to diffraction-limited performance. Alternatively, longer wavelength systems have larger diffraction spots, and are easier to correct to a diffraction-limited level of performance.

For example, an $F/1$ diffraction-limited system operating at 10 μm forms a spot diameter of 24.4 μm . The same system operating at $F/7$ would form a spot diameter of 170.8 μm . The same $F/1$ system operating in the visible spectrum at 0.5 μm , forms a spot diameter of 1.22 μm , while the $F/7$ system produces a diffraction spot of 8.5 μm in diameter.

Optical aberrations depend on the refractive and dispersive effects of the optical materials and on the geometrical arrangement of the optical surfaces. Inherent aberrations in the performance of the system with spherical surfaces include

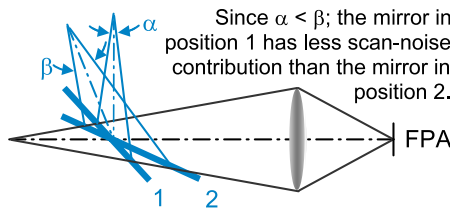
- spherical
- astigmatism
- field curvature
- distortion
- coma
- axial and lateral chromatic aberration

Image Anomalies in Infrared Systems

There are three common image anomalies associated with IR systems.

Shading: the gradual fall off in the scene radiance toward the edges of the detector, caused by fall of ($\cos^4 \theta$) dependence of the effective exitance of a uniform source. It is controlled by optical design techniques that keep the angle of the chief ray small in image space.

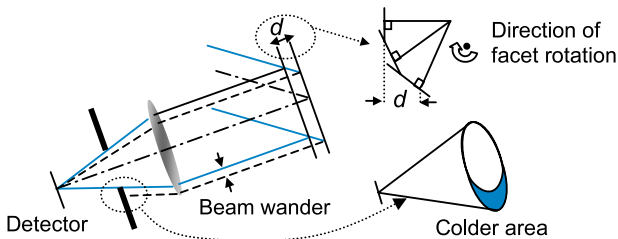
Scan noise: the amount of self-radiation reaching the detector due to room-temperature internal housing, and



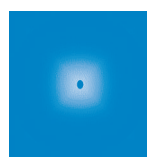
Since $\alpha < \beta$, the mirror in position 1 has less scan-noise contribution than the mirror in position 2.

optical elements as a function of scan position. Scan noise can also be caused by vignetting in an image-side scanner (e.g., rotating polygon). There is a final displacement d from the center of the facet in the direction normal to the initial position. Then the interactive scanning moves in and out, and the exit beam wanders left and right, causing vignetting.

Then the interactive scanning moves in and out, and the exit beam wanders left and right, causing vignetting.



The narcissus effect: the result of a cold reflection of the detector array into itself; it appears as a dark spot at the center of the scan. It is controlled by using the appropriate antireflective coatings on the optical elements, and by optical design techniques that ensure the cold-reflected image is out of focus at the detector plane. Its magnitude is often expressed as a multiple of the system's noise level.



Infrared Materials

The choice of infrared materials is dictated by the application. The most important material parameters to consider are its **transmission range**, and its **material dispersion**. Other properties to be considered are the **absorption coefficient**, **reflection loss**, **rupture modulus**, **thermal expansion**, **thermal conductivity**, and **water-erosion resistance**.

The **refractive index n** is defined as

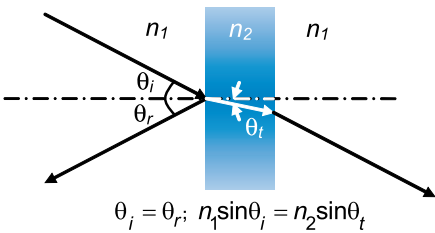
$$n = \frac{c}{v},$$

where c is the speed of light (3×10^{10} cm/sec) in free space and v is the speed of light in the medium.

Whenever a ray crosses a boundary between two materials of different refractive indexes, there is some power transmitted, reflected, and absorbed (i.e., conservation of energy):

$$\phi_{\text{inc}} = \phi_{\text{trans}} + \phi_{\text{ref}} + \phi_{\text{abs}}; \quad \phi \equiv \text{power [Watts].}$$

The direction of the transmitted light is given by **Snell's law**; and the direction of the reflected beam is determined by the **law of reflection**.



The distribution of power from a plane-parallel plate at normal incidence is determined by the **Fresnel equations**:

$$\rho = \left(\frac{n_2 - n_1}{n_1 + n_2} \right)^2 \text{ and } \tau = \frac{4n_1 n_2}{(n_1 + n_2)^2}, \text{ where}$$

$$\rho = \frac{\phi_{\text{ref}}}{\phi_{\text{inc}}} \text{ and } \tau = \frac{\phi_{\text{trans}}}{\phi_{\text{inc}}}.$$

The **absorption** is described as the attenuation coefficient α [1/cm], and it takes power out of the beam radiation, raising the temperature of the material:

$$\phi(z) = \phi_{\text{inc}} e^{-\alpha z},$$

where z is the propagation distance within the material.

Infrared Materials (cont'd)

The **internal transmittance** is defined as the transmittance through a distance in the medium, excluding the Fresnel reflection loss at the boundaries:

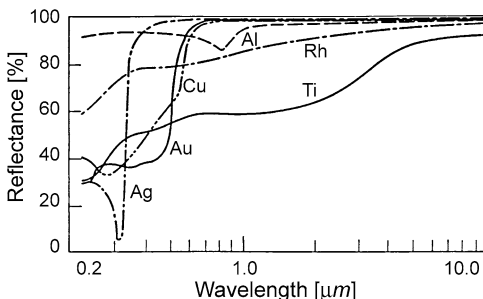
$$\tau_{\text{internal}} = \frac{\phi(z)}{\phi_{\text{incident}}} = e^{-\alpha z}.$$

Conversely, the **external transmittance** is the transmittance through a distance in the medium that includes the Fresnel loss at the boundaries:

$$\tau_{\text{external}} = \tau^2 e^{-\alpha z} = \tau^2 \tau_{\text{internal}}.$$

When examining material specifications from a vendor, it is necessary to take into account the distinction between internal and external transmittances.

Mirrors are characterized by their surface reflectivity and polish, as well as by the properties of the blanks on which these polishes are established. Plots of reflectance versus wavelength for commonly used metallic coating materials are shown below. Aluminum is widely used because it offers an average reflectance of 96% throughout the visible, near-infrared, and near-ultraviolet regions of the spectrum. Alternatively, silver exhibits higher reflectance (98%) through most of the visible and IR spectrum, but it oxidizes faster reducing its reflectance and causing light to scatter. Bare gold, on the other hand, combines good tarnish resistance with consistently high reflectance (99%) through the near, middle, and far infrared regions. All of the metals exhibit higher reflectance at long wavelengths.

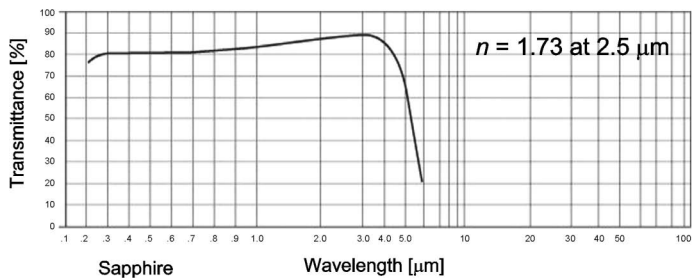


Data from Wolfe & Zissis, *The Infrared Handbook* (1990).

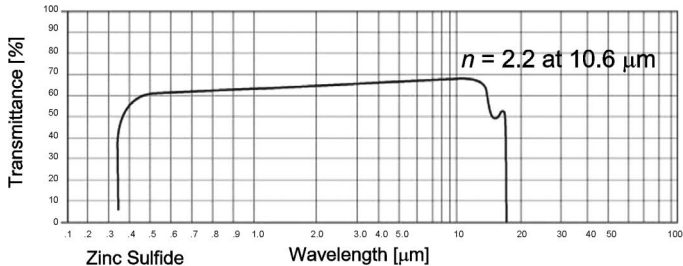
Infrared Materials (cont'd)

Metallic reflective coatings are delicate and require care during cleaning. Therefore, metallic coatings that are over-coated with a single, hard dielectric layer of half-wave optical thickness improve abrasion and tarnish resistance. Depending on the dielectric used, such coatings are referred to as **durable**, **protected**, or **hard coated**. The reflectance of metallic coatings can also be increased over the desired spectral range or for different angles of incidence by over-coating it with a quarter-wave stack of multilayer dielectric film, said to be **enhanced**.

The most versatile materials commonly used for systems operating in the MWIR and LWIR spectral regions are sapphire (Al_2O_3), zinc sulfide (ZnS), zinc selenide (ZnSe), silicon (Si), and germanium (Ge).



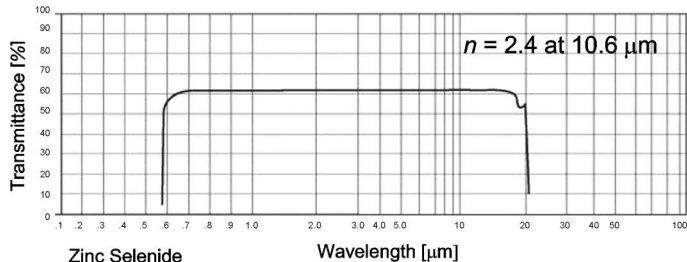
Sapphire is an extremely hard material, which is useful for visible, NIR, and IR applications through $5 \mu\text{m}$. It is practical for high-temperature and pressure applications.



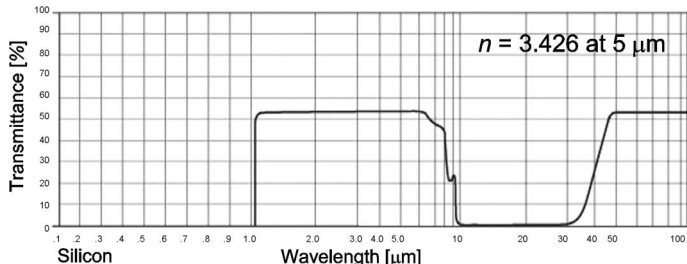
ZnS comes in two grades. The regular grade transmits in the $1\text{--}12 \mu\text{m}$ with reasonable hardness and good strength. The other grade is water-clear called CLEARTRAN and transmits in the $0.4\text{--}12 \mu\text{m}$ spectral band.

Infrared Materials (cont'd)

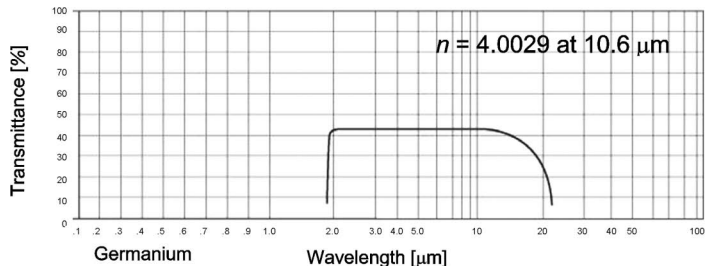
ZnSe has low absorbance and is an excellent material used in many laser and imaging systems. It transmits well from 0.6–18 μm .



Si is a good substrate for high-power lasers due to its high thermal conductivity. It is useful in the 3–5 μm , and 48–100 μm (astronomical applications).



Ge has good thermal conductivity, excellent surface hardness and good strength. It is used for IR instruments operating in the 2–14 μm spectral band.



Other popular infrared materials are calcium fluoride (CaF_2), magnesium fluoride (MgF_2), barium fluoride (BAF_2), gallium arsenide (GaAs), thallium bromoiodide (KRS-5), and cesium iodide (CsI).

Material Dispersion

Dispersion is the variation in the index of refraction with wavelength [$dn/d\lambda$] and it is an important material property when considering large-spectral-bandwidth optical systems. The dispersion is greater at short wavelengths and decreases at longer wavelengths; however, for most of the materials, it increases again when approaching the long infrared wavelength absorption band.

For historical reasons, the dispersion is often quoted as a unitless ratio called the **reciprocal relative dispersion** or **Abbe number** defined by:

$$V = \frac{n_{\text{mean}} - 1}{\Delta n} = \frac{n_{\text{mean}} - 1}{n_{\text{final}} - n_{\text{initial}}},$$

where n_{initial} and n_{final} are the initial and final index of refraction values of the spectral band of interest, and n_{mean} is the mean center value. Δn is basically the measured value of the dispersion and $n_{\text{mean}} - 1$ specifies the refractive power of the material. The smaller the Abbe number the larger the dispersion. For example, the V number for a germanium lens in the 8- to 12- μm spectral band is

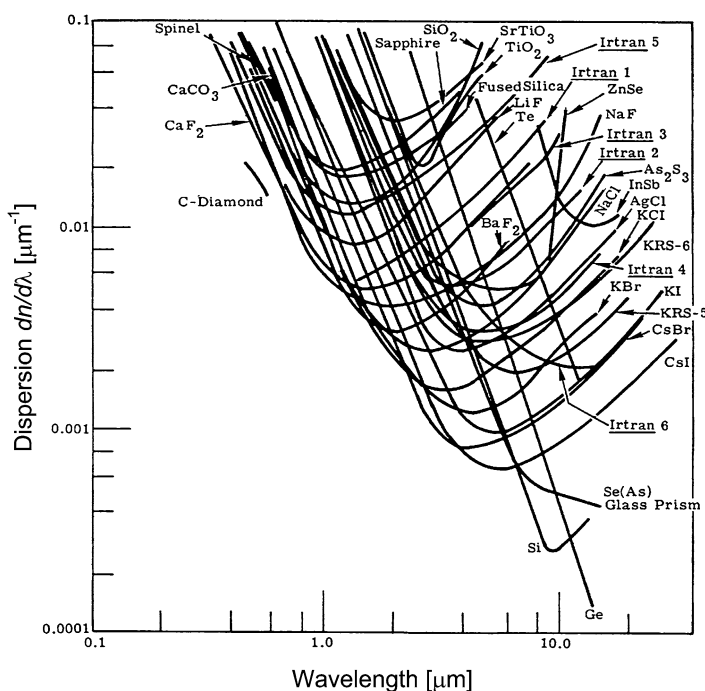
$$V = \frac{n(10 \mu\text{m}) - 1}{n(12 \mu\text{m}) - n(8 \mu\text{m})} = \frac{4.0038 - 1}{4.0053 - 4.0023} = 1001.27.$$

Another useful definition is the **relative partial dispersion** given by

$$P = \frac{n_{\text{mean}} - n_{\text{initial}}}{n_{\text{final}} - n_{\text{initial}}},$$

which is a measure of the rate of change of the slope of the index as a function of wavelength (i.e., $d^2n/d\lambda^2$).

Material Dispersion (cont'd)



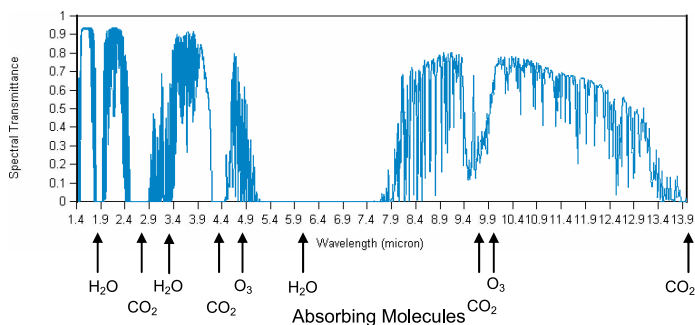
¹Figure adapted from Wolfe & Zissis, *The Infrared Handbook*.

Atmospheric Transmittance

The **absorption** and **emission** of radiation in the atmosphere are critical parameters that must be considered when developing infrared systems. Because of the sun's radiation, aerosols and molecular scattering are particularly important background sources in the visible spectrum. However, in the IR this effect is minimal since the wavelengths are much longer. According to the Rayleigh principle, the **scattered flux density** is inversely proportional to the fourth power of the driving wavelength.

The atmosphere is comprised primarily of CO₂, H₂O, and O₃. High absorption occurs in different parts of the infrared spectrum due to molecular vibrations of these elements. For example, the NIR is greatly affected by water vapor as well as the short and long wave sides of the LWIR large window. The MWIR has two dips due to carbon dioxide and ozone.

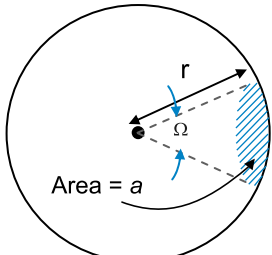
There are three main atmospheric windows in the infrared: NIR, 3 to 5 μm , and 8 to 14 μm . System technologies have evolved independently, optimizing the operation in each of these spectral bands.



The atmosphere is problematic for high-energy laser systems. Small temperature variations cause random changes in wind velocity, or turbulence motion. These changes in temperature give rise to small changes in the index of refraction of air, acting like little lenses that cause intensity variations. These fluctuations distort the laser beam wavefront, producing unwanted effects such as beam wander, beam spreading, and scintillation.

Solid Angle

The **solid angle “ Ω ”** in 3D space measures a range of pointing directions from a point to a surface. It is defined, assuming paraxial approximation, as the element of the



$$\Omega = \frac{a}{r^2} \quad a \ll r^2$$

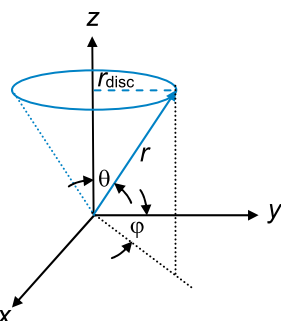
area of a sphere divided by the square of the radius of the sphere. It is dimensionless and measured in square radians or **steradians [ster]**.

For example, the area of a full sphere is given by $4\pi r^2$; therefore, its solid angle is 4π . A hemisphere contains half as many radians as a sphere (i.e., $\Omega = 2\pi$).

When large angles are involved, a more exact definition is required. Using spherical coordinates the solid-angular subtense can be expressed as a function of a flat disc or planar angle θ as

$$d\Omega = \frac{da}{r^2} \sin \theta d\theta d\varphi.$$

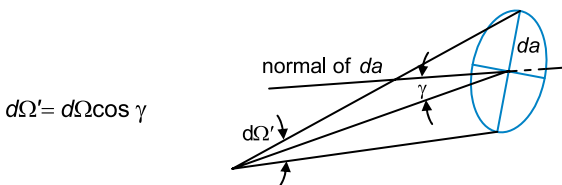
Integrating over the acceptance cone



$$\Omega = \int_0^{2\pi} d\varphi \int_0^{\theta_{\max}} \sin \theta d\theta = 2\pi(1 - \cos \theta_{\max}) = 4\pi \sin^2 \frac{\theta_{\max}}{2}$$

is obtained.

If the disc is tilted at a selected angle γ , its differential solid angular subtense is decreased by a factor of $\cos \gamma$.



$$d\Omega' = d\Omega \cos \gamma$$

Radiometry

Radiometry is a quantitative understanding of flux transfer through an optical system. Given the radiation from a thermal source transmitted through the optics of an infrared system, the fundamental question is how much of the source power is collected by the infrared sensor. Radiometric calculations predict the system's **signal-to-noise ratio (SNR)**.

Understanding the radiometric terms and their units are the key to performing radiometric calculations.

Symbol	Radiometric Term	Units
Q_e	Radiant energy	Joule
ϕ_e	Radiant power or flux	Watt
I_e	Radiant intensity	Watt/ster
M_e	Radiant exitance	Watt/cm ²
E_e	Irradiance	Watt/cm ²
L_e	Radiance	Watt/cm ² ·ster
Q_p	Photon energy	Photon or quantum
ϕ_p	Photon flux	Photon/sec
I_p	Photon intensity	Photon/sec·ster
M_p	Photon exitance	Photon/cm ² ·sec
E_p	Photon irradiance	Photon/cm ² ·sec
L_p	Photon radiance	Photon/sec·cm ² ·ster

Subscript e = energy derived units; subscript p = photon rate quantities.

Conversion between the two sets of units is done with the formula that determines the amount of energy carried per photon:

$$\mathcal{E} = \frac{hc}{\lambda}; \quad \Rightarrow \quad \phi_e[\text{Watt}] = \phi_p[\text{Photon/sec}] \cdot \mathcal{E},$$

where h is Planck's constant, c is the speed of light, and λ is the wavelength. Photon derived units are useful when considering an infrared sensor that responds directly to photon (e.g., photovoltaic) events, rather to thermal energy (e.g., microbolometer).

The energy carried per photon is inversely proportional to the wavelength; therefore, a short-wavelength photon carries more energy than a long-wavelength photon. It can also be interpreted as how many photons per second it takes to produce 1 W.

Radiometric Terms

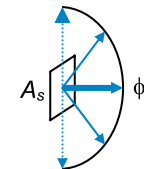
Flux: a quantity propagated or spatially distributed according to the laws of geometrical optics.

Both **irradiance** and **exitance** have units of spatial power density; however, the terms have different interpretations. The exitance is the power per unit area leaving a surface, thus describing a self-luminous source. It is defined as the ratio of the differential flux to the source area from which it is radiating as the area is reduced to a point:

$$M = \frac{\partial \phi}{\partial A_s},$$

where the total flux radiated into a hemisphere is given by:

$$\phi = \int M \cdot \partial A_s.$$

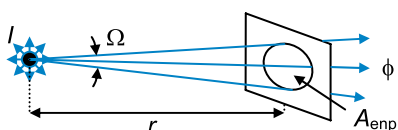


$$\phi = M A_s \text{ for small but final quantities.}$$

Equivalently, irradiance is a measure of the total incident flux per unit area on a passive receiver surface (e.g., sensor). It is defined as the ratio of power to the area upon which it is incident as the area is reduced to a specific position.

$$E = \frac{\partial \phi}{\partial A_d} \Rightarrow \phi = \int E \cdot \partial A_d.$$

The **intensity** is the radiant power per unit solid angle as the solid angle is reduced in value to a specific direction,



$$I = \frac{\partial \phi}{\partial \Omega} \Rightarrow \phi = \int I \cdot \partial \Omega$$

and is used to characterize the amount of flux radiated from a **point source** that is collected by the entrance pupil.

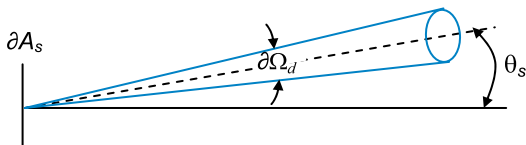
The intensity varies as a function of the view angle, and can be written as $I = I_0 \cos \theta$, where I_0 is the intensity in direction normal to the surface.

Both the flux and the irradiance decrease as “one-over-r-square falloff”:

$$\phi = I \cdot \Omega = I \frac{A_{\text{entr}}}{r^2}; \quad E = \frac{\phi}{A_{\text{entr}}} = \frac{I}{r^2}.$$

Radiometric terms (cont'd)

Radiance is the most general term to describe source flux, because it includes both positional and directional characterization. It is used to characterize extended sources; that is, one that has appreciable area compared to the square of the viewing distance. The visual equivalent of the radiance is the term “brightness.”



The radiance is defined for a particular ray direction, as the radiant power per unit projected source area (perpendicular to the ray) per unit solid angle:

$$L \equiv \frac{\partial^2 \phi}{\partial A_s \cos \theta_s \partial \Omega_d}; \Rightarrow \quad \partial^2 \phi = L \partial A_s \cos \theta_s \partial \Omega_d,$$

which is the fundamental equation of **radiation transfer**. The term $\partial^2 \phi$ is the power radiated into the cone, and it is incremental with respect to both the area of the source and the solid angle of the receiver.

For small but final source area and detector solid angle quantities

$$\phi \cong L A_s \cos \theta_s \Omega_d.$$

A **Lambertian radiator** emits radiance that is independent of angle (i.e., the radiance is isotropic and is equally uniform in each direction within the hemisphere). The transfer equation can be applied to a Lambertian emitter to obtain the relationship between radiance and exitance:

$$M = \frac{\partial \phi}{\partial A_s} = \int_{\Omega_d} L \cos \theta_s \partial \Omega_d = \int_0^{2\pi} d\varphi \int_0^{\pi/2} L \cos \theta_s \sin \theta_s d\theta_s = \pi L.$$

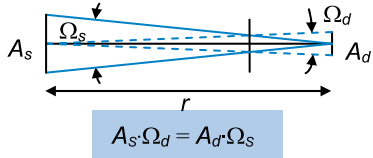
Similarly, the intensity can be obtained by integrating the fundamental equation with respect to the source area:

$$I = \frac{\partial \phi}{\partial \Omega_d} = \int L \cos \theta_s dA_s = L A_s \cos \theta_s.$$

Flux Transfer

The fundamental equation of radiation transfer states that an element of power is given by the radiance times the product of two projected areas, divided by the square of the distance between them.

Assuming normal angles of incidence (i.e., $\theta_s = \theta_d = 0$),



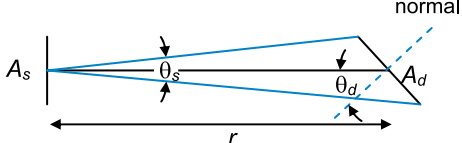
$$\phi = L A_s \Omega_d = L \frac{A_s A_d}{r^2} = L \Omega_s A_d.$$

Two equivalent expressions in terms of area solid angle product are obtained by grouping either the source or the detector area with r^2 .

This relationship, defined as the so called **AΩ product**, is completely symmetrical, and can be used to calculate the power in either direction of the net power flow. It is also known as the **optical invariant** or **throughput**.

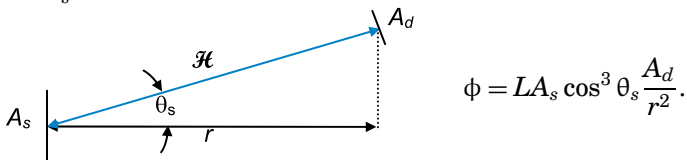
In the case where the detector is tilted ($\theta_d \neq 0$), the flux decreases by the cosine of the angle:

$$\phi = L A_s \frac{A_d \cos \theta_d}{r^2}.$$



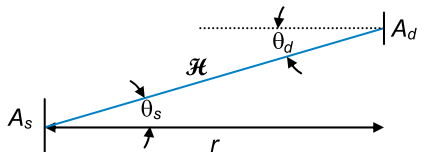
Consider the case

for $\theta_s \neq 0$ but $\theta_d = 0$, the flux decreases proportional to $\cos^3 \theta_s$:



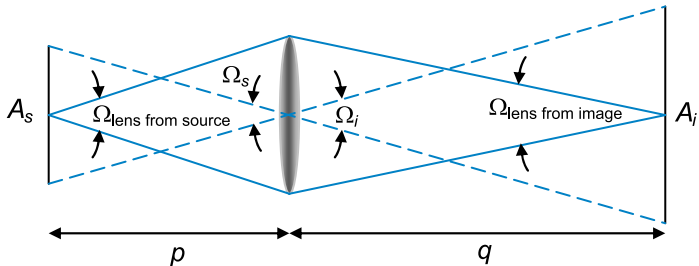
The last case is when both $\theta_d = \theta_s \equiv \theta \neq 0$, which leads to the most realistic situation; the so-called “cosine to the fourth law.”

$$\phi = L A_s \cos^4 \theta \frac{A_d}{r^2}$$



Flux Transfer for Image-Forming Systems

For purposes of simplification, the cosine projections are dropped (i.e., paraxial approximation), in which case the flux transfer is simply described in terms of the $A\Omega$ product.



Recalling the area or longitudinal magnification equation, the total flux collected by the optical system may be calculated by either one of the following flux-transfer equations:

$$\phi = L_s A_s \Omega_{\text{lens from source}} = L_s A_s \frac{A_{\text{lens}}}{p^2},$$

$$\phi = L_s A_i \Omega_{\text{lens from image}} = L_s A_i \frac{A_{\text{lens}}}{q^2},$$

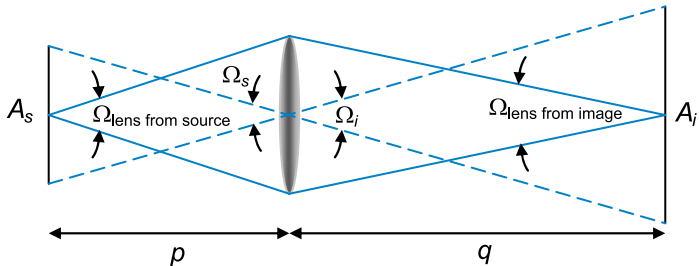
$$\phi = L_s A_{\text{lens}} \Omega_s = L_s A_{\text{lens}} \frac{A_s}{p^2},$$

$$\phi = L_s A_{\text{lens}} \Omega_i = L_s A_{\text{lens}} \frac{A_i}{q^2}.$$

In this case, the lens aperture acts as the intermediate receiver. In more complex optical systems, the entrance pupil is the intermediate receiver.

Flux Transfer for Image-Forming Systems

For purposes of simplification, the cosine projections are dropped (i.e., paraxial approximation), in which case the flux transfer is simply described in terms of the $A\Omega$ product.



Recalling the area or longitudinal magnification equation, the total flux collected by the optical system may be calculated by either one of the following flux-transfer equations:

$$\phi = L_s A_s \Omega_{lens \text{ from source}} = L_s A_s \frac{A_{lens}}{p^2},$$

$$\phi = L_s A_i \Omega_{lens \text{ from image}} = L_s A_i \frac{A_{lens}}{q^2},$$

$$\phi = L_s A_{lens} \Omega_s = L_s A_{lens} \frac{A_s}{p^2},$$

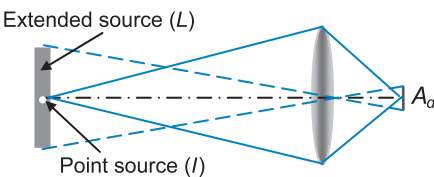
$$\phi = L_s A_{lens} \Omega_i = L_s A_{lens} \frac{A_i}{q^2}.$$

In this case, the lens aperture acts as the intermediate receiver. In more complex optical systems, the entrance pupil is the intermediate receiver.

Source Configurations

The source may be idealized as either a **point source** or a uniform **extended-area source**. The point source is a source that cannot be resolved by the optical system. It is smaller than the projection of the resolution spot at the object plane. An extended source, on the other hand,

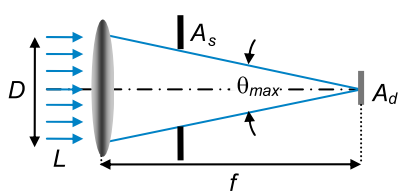
is the one that has an appreciable area compared to the detector's footprint.



The entity of **radiance** is the most appropriate for the de-

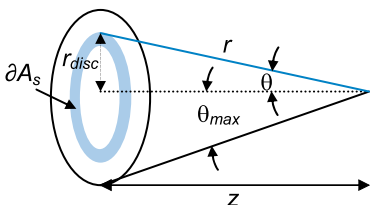
scription of radiant flux from an extended-area source; while **intensity** is the quantity that must be used in order to characterize the radiation originated from a point source.

The power collected by the lens is reformatted to form an image of the source. The **image irradiance** for a distant extended-area source can be calculated directly using a large **Lambertian disc**, which can be the actual extended source or an intermediate source such as a lens.



The extended source is filling the FOV; and the solid angle is bounded by the marginal rays and limited by the aperture stop.

From the Lambertian disc, the following relationships are derived:



$$r_{disc} = z \tan \theta \Rightarrow dr_{disc} = d(z \tan \theta) = z \sec^2 \theta d\theta = \frac{z}{\cos^2 \theta} d\theta,$$

$$A_s = \pi r_{disc}^2 \Rightarrow dA_s = 2\pi r_{disc} dr_{disc} = 2\pi z^2 \tan \theta \frac{d\theta}{\cos^2 \theta}.$$

Source Configurations (cont'd)

The transfer flux is obtained by integrating the fundamental equation of radiation transfer over the source and detector areas:

$$\phi_d = L \iint_{A_s A_d} \partial A_s \cos \theta_s \partial \Omega_d = L \iint_{A_s A_d} \partial A_s \cos \theta_s \frac{\partial A_d \cos \theta_d}{r^2},$$

$$\phi_d = L \iint_{\theta A_d} 2\pi z^2 \tan \theta \frac{d\theta}{\cos^2 \theta} \cos^2 \theta \left(\frac{\cos^2 \theta}{z^2} \right) \partial A_d,$$

$$\phi_d = 2\pi L A_d \int_0^{\theta_{\max}} \sin \theta \cos \theta d\theta = \pi L A_d \sin^2 \theta_{\max}.$$

The irradiance on a detector from an extended-area source is then obtained by dividing the flux transferred by the area of the detector:

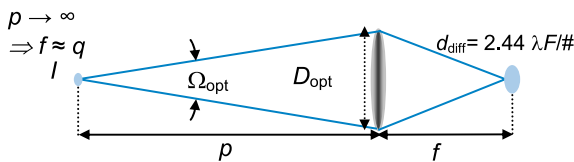
$$E_{\text{extended source}} = \frac{\phi}{A_d} = \pi L \sin^2 \theta = \frac{\pi L}{4F_{/\#}^2 + 1}.$$

For an extended-area source the image irradiance depends only on the source radiance and the $F/\#$ of the optical system.

In the case of a point source, the collected power is defined by the intensity times the solid angle of the optics:

$$\phi = I \cdot \Omega_{\text{opt}} = I \cdot \frac{A_{\text{opt}}}{p^2}.$$

and it is defined as:



If the optics is diffraction-limited, 84% of the flux transfer is concentrated into the image spot; therefore, the average irradiance of a point source at the detector plane is given by

$$E_{\text{point source}} = \frac{\phi}{A_d} \times 0.84 = \frac{0.84 I \Omega_{\text{opt}}}{\frac{\pi}{4} d_{\text{diff}}^2} = \frac{0.84 I \Omega_{\text{opt}}}{\frac{\pi}{4} [2.44 \lambda (F/\#)]^2}.$$

Blackbody Radiators

Empirically, it is found that solid bodies heated to incandescent temperatures emit radiation primarily in the infrared portion of the spectrum, and these incandescent sources emit their radiation in a continuous wavelength rather than at discrete spectral lines.

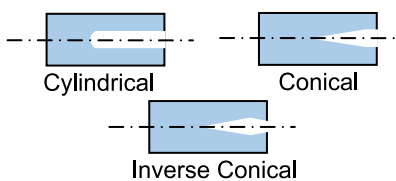
To describe a radiation that emits a finite total power distributed continuously over wavelength, **spectral radiometric quantities** with units per micron of wavelength interval are used. The weighted spectral quantities are denoted with a subscript λ (e.g., $M_{e,\lambda}$ is the spectral exitance in $\text{W/cm}^2 \mu\text{m}$). In-band nonspectral quantities are obtained by integrating the spectral terms over any spectral interval, for example,

$$L = \int_{\lambda_1}^{\lambda_2} L_\lambda d\lambda, \quad M = \int_{\lambda_1}^{\lambda_2} M_\lambda d\lambda, \quad \phi = \int_{\lambda_1}^{\lambda_2} \Phi_\lambda d\lambda.$$

The term **blackbody (BB)** is used to describe a perfect radiator (i.e., an idealized thermal source). It absorbs all the radiant energy; and as a consequence, it is the perfect emitter. BBs have maximum spectral exitance possible for a body at a specified temperature, either over a particular spectral region, or integrated over all wavelengths. They are a convenient baseline for radiometric calculations, since any thermal source at a specified temperature is constrained to emit less radiation than a blackbody source at the same temperature.

BB radiation is also called **cavity radiation**. Virtually any heated cavity with a small aperture produces high-quality radiation. These blackbody simulators are used primarily as laboratory calibration standards. The most popular

blackbody cavities are cylinders and cones, the latter being the most common. The aperture of the cavity defines the area of the source.



Some commercial blackbodies have an aperture wheel that allows the choice of this area.

Planck's Radiation Law

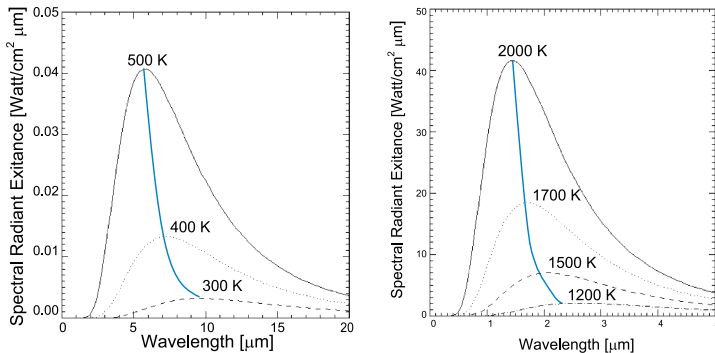
The radiation characteristics of ideal blackbody surfaces are completely specified if the temperature is known. Blackbody radiation is specified by Planck's equation, and it defines the spectral exitance as a function of absolute temperature and wavelength:

$$M_{e,\lambda} = \frac{2\pi hc^2}{\lambda^5} \frac{1}{\exp(hc/\lambda kT) - 1}$$

$$= \frac{c_1}{\lambda^5} \frac{1}{\exp(c_2/\lambda T) - 1} \text{ [W/cm}^2 \cdot \mu\text{m}],$$

where h is Planck's constant; 6.62×10^{-34} Joule·sec; k is Boltzmann's constant; 1.3806×10^{-23} Joule/K; T is the absolute temperature in degrees Kelvin [K]; λ is the wavelength in centimeters [cm]; c is the speed of light in vacuum; 2.998×10^{10} cm/sec; c_1 is the first radiation constant; $2\pi hc^2 = 3.7415 \times 10^4$ W/cm $^2 \cdot \mu$ 4 ; c_2 is the second radiation constant; $hc/k = 1.4382$ cm · K.

Planck's equation generates spectral exitance curves that are quite useful for engineering calculations.



Planck's curves illustrating the following characteristics:

- The shape of the blackbody curves does not change for any given temperature.
- The temperature is inversely proportional to wavelength; the peak exitance shifts toward shorter wavelengths as the temperature increases.

Planck's Radiation Law (cont'd)

- The individual curves never cross one another; the exittance increases rapidly for increased temperatures at all wavelengths.

The Planck radiation formula models system design and analysis problems. For example, the radiant emittance of a blackbody at temperatures from 400 to 900 K includes the temperature of the hot metal tailpipes of jet aircrafts.

Stefan-Boltzmann and Wien's Displacement Laws

Stefan-Boltzmann law relates the total blackbody exitance at all wavelengths to source temperature, and it is obtained by integrating out the wavelength dependence of the Planck's radiation law:

$$M_e(T) = \int_0^{\infty} M_{e,\lambda}(\lambda, T) d\lambda = \int_0^{\infty} \frac{2\pi hc^2}{\lambda^5} \frac{d\lambda}{\exp(hc/\lambda kT) - 1} = \frac{2\pi^5 k^4 T^4}{15 c^2 h^3}$$

$$M_e(T) = \sigma_e T^4,$$

where σ_e is the **Stefan-Boltzmann constant** and has a value of $5.7 \times 10^{-12} \text{ W/cm}^2 \text{ K}^4$. Stefan-Boltzmann law only holds for exitance integrated from zero to infinity at the interval of wavelength.

The total exitance at all wavelengths multiplied by the source area results in the total power radiated, which increases as the fourth power of the absolute source temperature in Kelvin. For example, at room temperature (300 K), a perfect blackbody of an area equal to 1 cm^2 emits a total power of $4.6 \times 10^{-2} \text{ W}$. Doubling the temperature to 600 K, the total power increases 16 fold to 0.74 W.

The derivative of Planck's equation with respect to wavelength yields the **Wien's displacement law**, which gives the wavelength for which the peak of the spectral-exitance function occurs as a function of temperature:

$$\frac{\partial M_{e,\lambda}(\lambda, T)}{\partial \lambda} = 0 \Rightarrow \lambda_{\max} T = 2898 \text{ [\mu m}\cdot\text{K].}$$

Thus the wavelength at which the maximum spectral radiant exitance varies is inversely proportional to the absolute temperature. The plot of λ_{\max} as a function of temperature is a hyperbola (see plots on page 31).

For example, a blackbody source at 300 K has its maximum exitance at $9.7 \text{ }\mu\text{m}$; however, if the temperature of this source is changed to 1000 K, the maximum value at which the peak exitance occurs is at $2.9 \text{ }\mu\text{m}$. The sun is a blackbody source at approximately 6000 K. Applying Wien's law it is found that its maximum wavelength occurs at $0.5 \text{ }\mu\text{m}$, which corresponds to the peak response of the human eye.

Rayleigh-Jeans and Wien's Radiation Laws

Two well-known approximations to Planck's radiation law are the Rayleigh-Jeans and Wien's radiation laws. The former occurs at long wavelengths:

$$hc/\lambda kT \ll 1 \Rightarrow M_{e,\lambda} \cong \frac{2\pi ckT}{\lambda^4},$$

while the latter is valid only at short wavelengths:

$$hc/\lambda kT \gg 1 \Rightarrow M_{e,\lambda} \cong \frac{2\pi hc^2}{\lambda^5} \exp\left(-\frac{hc}{\lambda kT}\right).$$

As the temperature increases, the peak wavelength decreases (Wien's law), and the area under the Planck curve increases much faster (Stefan-Boltzmann law).

Thermal Equations in Photon-Derived Units

In photon derived units Planck's radiation, Boltzmann and Wien's displacement, Wien's radiation, and Rayleigh-Jeans formulae are given by:

Planck's radiation equation:

$$M_{p,\lambda} = \frac{2\pi c}{\lambda^4} \frac{1}{\exp(hc/\lambda kT) - 1} \quad [\text{Photon/sec} \cdot \text{cm}^2 \cdot \mu\text{m}]$$

Stefan-Boltzmann law:

$$M_p(T) = \sigma_p T^3$$

where σ_p has a value of 1.52×10^{-11} photons/sec·cm²·K³.

Wien's displacement law:

$$\lambda_{\max} T = 3662 \quad [\mu\text{m} \cdot \text{K}]$$

Rayleigh-Jeans radiation law:

$$hc/\lambda kT \ll 1 \Rightarrow M_{p,\lambda} \cong \frac{2\pi kT}{\lambda^3 h}$$

Wien's radiation laws:

$$hc/\lambda kT \gg 1 \Rightarrow M_{p,\lambda} \cong \frac{2\pi c}{\lambda^4} \exp\left(-\frac{hc}{\lambda kT}\right)$$

Exitance Contrast

In terrestrial infrared systems, the target and background are often of similar temperatures, in which case the target has very low contrast. The proper choice of spectral passband wavelength $\Delta\lambda$ becomes essential to maximize the visibility of the target. This pass band should straddle the wavelength for which the exitance changes the most as a function of temperature.

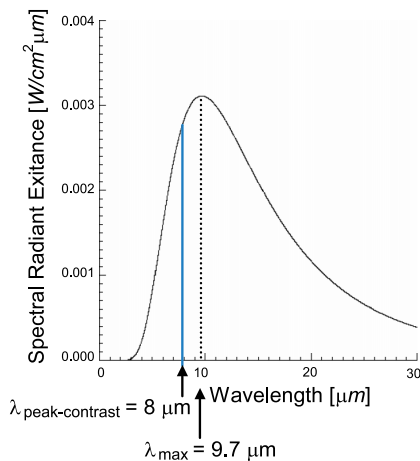
This consideration of exitance contrast involves the following second order partial derivative, where the system operating within a finite passband is most sensitive to small changes in temperature:

$$\text{Finds } \lambda_{\text{peak contrast}} \frac{\partial}{\partial \lambda} \left[\frac{\partial M_\lambda(\lambda, T)}{\partial T} \right] = 0 \quad \begin{array}{l} \text{Finds best sensitivity} \\ (\text{steepest slope}) \end{array}$$

Carrying out these derivatives yields a constraint on wavelength and temperature in a similar fashion to the Wien's displacement law, yielding:

$$\lambda_{\text{peak-contrast}} T = 2410 \text{ [μm·K].}$$

For a given blackbody temperature, the maximum exitance contrast occurs at shorter wavelengths than the wavelength of the peak exitance. For example, at 300 K the peak exitance occurs at 9.7 μm while the peak exitance contrast occurs at 8 μm.



Emissivity

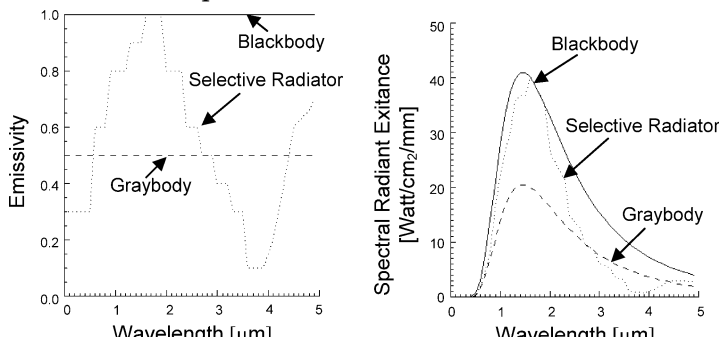
Emissivity is the ratio of the spectral exitance of a real source at a given temperature, to that of a blackbody at the same temperature:

$$\varepsilon(\lambda, T) = \frac{M_{\lambda, \text{source}}(\lambda, T)}{M_{\lambda, \text{BB}}(\lambda, T)}.$$

The spectral exitance of any real source at a given temperature is bounded by the spectral exitance of a perfect radiator at the same kinetic temperature; hence ε is constrained between zero and unity.

The emissivity characterizes how closely the radiation spectrum of a real heated body corresponds to that of a blackbody. It is a spectrally varying quantity, and can be either referred to as spectral (measured over a finite passband) or total (measured over all wavelengths) quantity. This emission efficiency parameter depends also on the surface temperature. However, emissivity data for most materials are typically a constant and are seldom given as a function of λ and T unless it is an especially well characterized material.

There are three types of sources that can be differentiated depending on how their spectral emissivity varies: (1) a blackbody or perfect radiator, for which its emissivity is equal to unity for all wavelengths; (2) a graybody when its emissivity is a constant fraction of what the corresponding blackbody would radiate at the same temperature ($\varepsilon < 1$). It is independent of wavelength and it has the same spectral shape as a blackbody; (3) a selective radiator where ε is an explicit function of λ .



Kirchhoff's Law

If a solid body of a certain mass is located within a colder isothermal cavity, according to the second law of thermodynamics, there will be a net flow of heat from the object to the walls of the hollow space. Once the body reaches thermal equilibrium with its surroundings, the first law of thermodynamics or conservation of energy requires that:

$$\phi_{\text{incident}} = \phi_{\text{absorbed}} + \phi_{\text{transmitted}} + \phi_{\text{reflected}},$$

where ϕ_{incident} is the incident flux on the solid body. Dividing both sides of the equation by ϕ_{incident} yields

$$1 = \alpha + \tau + \rho,$$

where α is the absorbance, τ the transmittance, and ρ is the reflectance. For an opaque body (i.e., $\tau = 0$) either the incident radiation is absorbed or reflected, yielding

$$\alpha = 1 - \rho,$$

which indicates that surfaces with low reflectance are high emitters.

If the body absorbs only a portion of the radiation that is incident on it, then it emits less radiation in order to remain in thermal equilibrium; that is

$$E = \varepsilon M,$$

which leads to **Kirchhoff's law**, which states that the absorbance of a surface is identical to the emissivity of that surface. Kirchhoff's law also holds for spectral quantities; it is a function of temperature and can vary with the direction of measurement. This law is sometimes verbalized as “**good absorbers are good emitters.**”

Integrated absorbance = $\alpha(\lambda, T) \equiv \varepsilon(\lambda, T)$ = Integrated emittance

For polished metals, the emissivity is low; however, it increases with temperature, and may increase substantially with the formation of an oxide layer on the object surface. A thin-film of oil and surface roughness can increase the emissivity by an order of magnitude, compared to a polished metal surface. The emissivity of nonmetallic surfaces is typically greater than 0.8 at room temperature, and it decreases as the temperature increases.

Emissivity of Various Common Materials

Metals and Other Oxides	Emissivity
Aluminum: Polished sheet Sheet as received Anodized sheet, chromatic-acid process Vacuum deposited	0.05
	0.09
	0.55
	0.04
Brass: highly polished Rubbed with 80-grit emery Oxidized	0.03
	0.20
	0.61
Copper: Highly polished Heavily oxidized	0.02
	0.78
Gold: Highly polished	0.21
Iron: Cast polished Cast, oxidized Sheet, heavily rusted	0.21
	0.64
	0.69
Nickel: Electroplated, polished Electroplated, not polished Oxidized	0.05
	0.11
	0.37
Silver: polished	0.03
Stainless Steel: type 18-8 buffed Type 18-8, oxidized	0.16
	0.85
Steel: Polished Oxidized	0.07
	0.79
Tin: Commercial tin-plated sheet iron	0.07

Nonmetallic Materials	Emissivity
Brick: Red common	0.93
Carbon: Candle soot Graphite, filed surface	0.95
	0.98
Concrete	0.92
Glass: Polished plate	0.94
Lacquer: White Matte black	0.92
	0.97
Oil, lubricant (Thin film of Nickel base): Nickel base alone Oil film: 1, 2, 5 × 10-3 in Thick coating	0.05
	0.27, 0.46, 0.72
	0.82
Paint, oil: Average of 16 colors	0.94
Paper: White bond	0.93
Plaster: Rough coat	0.91
Sand	0.90
Human skin	0.98
Soil: Dry Saturated with water	0.92
	0.95
Water: Distilled Ice, smooth Frost crystals Snow	0.96
	0.96
	0.98
	0.90
Wood: Planed oak	0.9

Data from Wolfe & Zissis, *The Infrared Handbook* (1990).

Radiometric Measure of Temperature

There are many applications in the infrared where the actual kinetic temperature of a distant object must be known. However, infrared systems can only measure the apparent spectral exitance emitted by targets and/or backgrounds, which are a function of both temperature and emissivity. The temperature of the infrared source can be measured if emissivity of the viewing source within the appropriate spectral region is known. Discrepancies in emissivity values produce built-in errors in the calculation of this kinetic temperature.

There are three main types of temperature measurements as discussed below.

Radiation temperature (T_{rad}): a calculation based on Stefan-Boltzmann law because it is estimated over the whole spectrum:

$$M_{\text{meas}} = \sigma T_{\text{rad}}^4,$$

where M_{meas} is the measured exitance. If the source is a graybody with a known emissivity, then T_{true} can be calculated from T_{rad} :

$$M_{\text{meas}} = \sigma T_{\text{rad}}^4 = \varepsilon \sigma T_{\text{true}}^4 \Rightarrow T_{\text{true}} = \frac{T_{\text{rad}}}{\sqrt[4]{\varepsilon}}.$$

Due to its strong dependence on emissivity, T_{rad} cannot be corrected to find T_{true} if ε is an unknown. Similarly, T_{rad} is affected by the attenuation in the optical system, especially in harsh environments where the optical elements might be dirty.

Brightness temperature (T_b): a measurement performed using Planck's radiation law because it is estimated over a single wavelength λ_0 , or in a narrow spectral region ($\Delta\lambda$) around a fix wavelength λ_0 . For a blackbody source $T_b = T_{\text{true}}$; therefore, the Planck equation can be solved for T_b :

$$T_b = \frac{c_2}{\lambda_0 \ln \left\{ 1 + \frac{c_1}{\lambda_0^5 M_\lambda(\lambda_0, T_b)} \right\}},$$

where $c_1 = 3.7415 \times 10^4 \text{ W/cm}^2 \mu\text{m}^4$ and c_2 is $= 1.4382 \mu\text{m}\cdot\text{K}$.

Radiometric Measure of Temperature (cont'd)

If the source is a graybody with a known emissivity, then T_{true} can be calculated from T_b as follows:

$$\frac{c_1}{\lambda_0^5} \frac{1}{\exp(c_2/\lambda_0 T_b) - 1} = \frac{c_1}{\lambda_0^5} \frac{\varepsilon}{\exp(c_2/\lambda_0 T_{\text{true}}) - 1},$$

yielding

$$T_{\text{true}} = \frac{c_2}{\lambda_0 \ln\{1 + \varepsilon[\exp(c_2/\lambda_0 T_b) - 1]\}}.$$

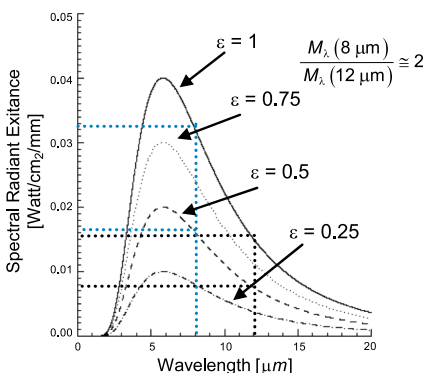
The exitance levels measured for T_b are lower than the levels for T_{rad} because of the narrowband filtering involved. The best sensitivity for this measurement is obtained by choosing λ_0 near the wavelength of the peak exitance contrast, where M_λ changes most with temperature.

The brightness temperature is a convenient measurement, but is not robust to incomplete knowledge of the emissivity or to the attenuation in the optical system.

Color temperature (T_c): is the temperature of a blackbody that best matches the spectral composition of the target source. This spectral composition is defined as the ratio of the measured spectral exitance at two different wavelengths given by

$$\frac{M_\lambda(\lambda_1)}{M_\lambda(\lambda_2)} = \frac{\lambda_2^5 \exp(c_2/\lambda_2 T_c) - 1}{\lambda_1^5 \exp(c_2/\lambda_1 T_c) - 1}.$$

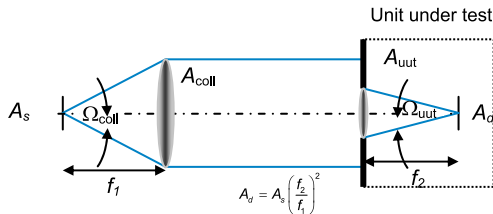
Under these circumstances, the emissivity cancels out because of the ratio, and $T_c = T_{\text{true}}$ for both black and gray bodies.



This method is strongly affected when the target source is a selective radiator. In this case, the measurement of the spectral exitance must be performed at many wavelengths.

Collimators

A collimator is an optical assembly that places a target at infinity, and produces a controllable irradiance that is independent of distance. It is widely used for testing the sensitivity and the resolution of infrared systems.



Assume a Lambertian source that is radiating at all wavelengths, the total flux emitted can be written using Stefan-Boltzmann's law:

$$\phi = L_s A_s \Omega_{\text{coll}} = \frac{\sigma T^4}{\pi} \frac{A_s A_{\text{coll}}}{f_1^2}.$$

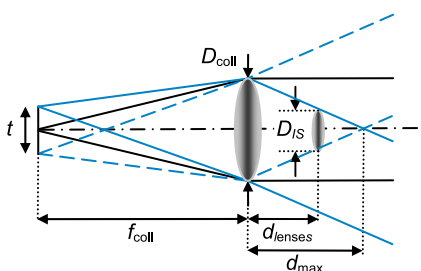
The source exitance and/or the irradiance falling on the detector surface can be obtained by dividing the radiant flux over the area of the collimator, yielding

$$M = \frac{\sigma T^4}{\pi} \frac{A_s}{f_1^2} = \frac{\sigma T^4}{\pi} \frac{A_d}{f_2^2} = E.$$

An extended source placed at the focal plane of a collimator, can only be seen in a well-defined region. The maximum distance at which the infrared imaging system can be placed from the collimator is

$$d_{\max} = \frac{f_{\text{coll}}}{t} D_{\text{coll}}.$$

If the imaging system is placed at a distance greater than d_{\max} , the target's outer edges are clipped and only the central portion of the target is seen.



The distance between the collimating and imaging system optical components is

$$d_{\text{lenses}} = \frac{f_{\text{coll}}}{t} (D_{\text{coll}} - D_{\text{IS}}).$$

Infrared Detectors

Infrared detectors are transducers that sample the incident radiation and produce an electrical signal proportional to the total flux incident on the detector surface. There are two main classes of infrared detectors: **thermal** and **photon detectors**. Both types respond to absorbed photons, but use different response mechanisms, which lead to variations in speed, spectral responsivity, and sensitivity. Thermal detectors depend on the changes in the electrical or mechanical properties of the sensing materials (e.g., resistance, capacitance, voltage, mechanical displacement) that result from temperature changes caused by the heating effect of the incident radiation. The change in these electrical properties with input flux level is measured by an external electrical circuit. The thermal effects do not depend on the photonic nature of the incident infrared radiation; they have no inherent long-wavelength cutoff. Their sensitivity limitation is due to thermal flux and/or the spectral properties of the protective window in front of them. The response rate of a thermal detector is slow because of the time required for the device to heat up after the energy has been absorbed. Examples of different classes of thermal detectors are **bolometer**, **pyroelectric**, **thermopile**, **Golay cells**, and **superconductors**.

The two basic types of semiconductor-photon detectors are photoconductors and photovoltaics, or photodiodes. The photonic effects in these devices result from direct conversion of incident photons into conducting electrons within the material. An absorbed photon excites an electron from the nonconducting state into a conducting state instantaneously, causing a change in the electrical properties of the semiconductor material that can be measured by an external circuit. Photon detectors are very fast; however, their response speed is generally limited by the RC product of the readout circuit.

Detector performance is described in terms of **responsivity**, **noise-equivalent power**, or **detectivity**. These figures of merit enable a quantitative prediction and evaluation of the system as well as to compare relative performance between different detector types.

Primary Sources of Detector Noise

Noise is a random fluctuation in electrical output from a detector, and must be minimized to increase the performance sensitivity of an infrared system. Sources of optical-detector noise can be classified as either external or internal. However, the focus here is on the internal generated detector noises that include shot, generation-recombination, one over frequency ($1/f$), and temperature fluctuation, which are a function of the detector area, bandwidth, and temperature.

It is possible to determine the limits of detector performance set by the statistical nature of the radiation to which it responds. Such limits set the lower level of sensitivity, and can be ascertained by the fluctuations in the signal or background radiation falling on the detector.

Random noise is expressed in terms of an electrical variable such as a voltage, current, or power. If the voltage is designated as a random-noise waveform $v_n(t)$ and a certain probability-density function is assigned to it, its statistics are found as a function of the following statistical descriptors:

Mean: $\bar{v}_n = \frac{1}{T} \int_0^T v_n(t) dt$ [volts],

Variance or mean-square:

$$\overline{v_n^2} = \overline{(v_n(t) - \bar{v}_n)^2} = \frac{1}{T} \int_0^T [v_n(t) - \bar{v}_n]^2 dt \quad [\text{volts}^2],$$

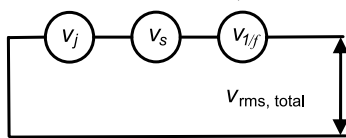
Standard deviation:

$$v_{\text{rms}} = \overline{\Delta v_n} = \sqrt{\frac{1}{T} \int_0^T [v_n(t) - \bar{v}_n]^2 dt} \quad [\text{volts}],$$

where T is the time interval. The standard deviation represents the rms noise of the random variable.

Linear addition of independent intrinsic noise sources is carried out in power (variance) not in voltage noise (standard deviation); the total rms noise of random quantities are added in quadrature:

$$\Delta v_{\text{rms},\text{total}} = \sqrt{\Delta v_{\text{rms},1} + \Delta v_{\text{rms},2} + \dots + \Delta v_{\text{rms},n}}.$$



Assuming three sources of noise are present; Johnson, shot, and $1/f$ noise:

$$v_{\text{rms},\text{total}}^2 = v_j^2 + v_s^2 + v_{1/f}^2$$

Noise Power Spectral Density

Noise can also be described in the frequency domain. The **power spectral density (PSD)**, or the mean-square fluctuation per unity frequency range, provides a measurement of frequency distribution of the mean-square value of the data (i.e., distribution of power).

For random processes, frequency can be introduced through the autocorrelation function. The time average **autocorrelation** function of a voltage waveform may be defined as

$$c_n(\tau) = \lim_{T \rightarrow \infty} \frac{1}{T} \int_{-T/2}^{T/2} v_n(t)v_n(t + \tau) dt,$$

where the autocorrelation is the measure of how fast the waveform changes in time. The PSD of a wide-sense stationary random process is defined as the Fourier transform of the autocorrelation function (Wiener-Kinchine theorem)

$$\text{PSD} = N(f) = \mathcal{F}\{c_n(\tau)\} = \int_{-\infty}^{\infty} c_n(\tau) e^{-j2\pi f \tau} d\tau.$$

The inverse relation is

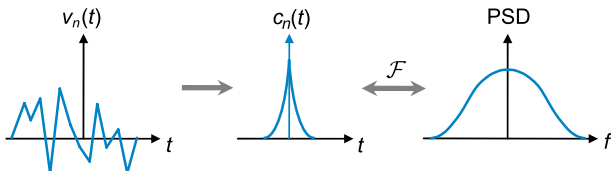
$$c_n(\tau) = \mathcal{F}^{-1}\{N(f)\} = \int_{-\infty}^{\infty} N(f) e^{j2\pi f \tau} df.$$

Using the central ordinate theorem yields

$$c_n(0) = \int_{-\infty}^{\infty} N(f) df = \int_{-\infty}^{\infty} v_n^2(t) dt = \overline{v_n^2(t)}.$$

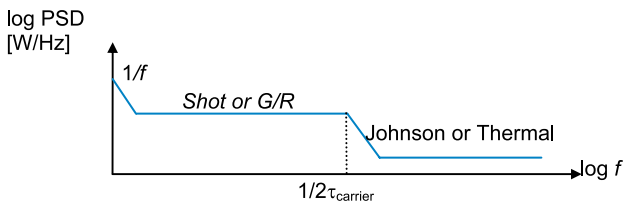
The average power of the random voltage waveform is obtained by integrating the PSD over its entire range of definition.

Uncorrelated noise such as white noise implies that its autocorrelation function is a delta function. The PSD of such random processes is a constant over the entire frequency range, but in practice, the PSD is constant over a wide but final range (i.e., band-pass limited).



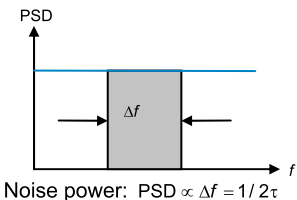
White Noise

Detector noise curves have different frequency contents. A typical PSD plot for a sensor system is shown.



- $1/f$ noise can be partly excluded by ac coupling (i.e., cutoff the system dc response by using a high pass filter with a cutoff between 1 Hz to 1 KHz).
- Shot noise and generation-recombination (G/R) noise have a roll-off frequency in the midband range (≈ 20 KHz–1 MHz), proportional to the inverse of carrier-lifetime.
- Johnson noise and amplifier noise are usually flat to high frequencies past $1/2\tau_{\text{carrier}}$.
- In a photon sensor, the charge carriers transmit both signal and noise, therefore, the upper cut-off frequency of the electronics bandwidth should not be higher than $1/2\tau_{\text{carrier}}$; wider bandwidth includes more noise, but not more signal.

Most system-noise calculations are done in the **white noise** region, where the PSD is flat over sufficient broadband relative to the signal band of interest. Shot and G/R noises are white up to $f \approx 1/2\tau_{\text{carrier}}$; beyond that, they roll-off. For white noise, the noise power is directly proportional to the detector bandwidth; consequently, the rms noise voltage is directly proportional to the square root of the detector bandwidth.



$$\text{Noise power: } \text{PSD} \propto \Delta f = 1/2\tau$$

$$\text{rms noise voltage: } V_{\text{rms}} \propto \sqrt{\Delta f} = \sqrt{1/2\tau}$$

Detectors have temporal impulse response with a width of τ . This response time or integration time is related to its frequency bandwidth as $\Delta f = 1/2\tau$.

If the input noise is white, then the noise-equivalent bandwidth of the filter determines how much noise power is passed through the system. As the integration time shortens, the noise-equivalent bandwidth widens and the system becomes noisier; while using a measurement circuit with longer response time yields a system with less noise.

Noise-Equivalent Bandwidth

The **noise-equivalent bandwidth** ($\text{NE}\Delta f$ or simply Δf) of an ideal electronic amplifier has a constant power-gain distribution between its lower and upper frequencies, and zero elsewhere. It can be represented as a rectangular function in the frequency domain. However, real electronic frequency responses do not have such ideal rectangular characteristics; so it is necessary to find an equivalent bandwidth that would provide the same amount of noise power.

The noise-equivalent bandwidth is defined as:

$$\text{NE}\Delta f \equiv \frac{1}{G^2(f_0)} \int_{-\infty}^{\infty} |G(f)|^2 df,$$

where $G(f)$ is the power gain as a function of frequency, and $G(f_0)$ is the maximum value of the power gain. The most

common definition of bandwidth is the frequency interval within which the power gain exceeds one-half of its maximum value (i.e., 3-dB bandwidth),

width, which it is usually denoted by the symbol B .

The above definition of noise-equivalent bandwidth assumes white noise; that is, the power spectrum of noise is flat. However, if the noise power spectrum exhibits strong frequency dependence, the noise-equivalent bandwidth should be calculated from

$$\text{NE}\Delta f = \frac{1}{G^2(f_0)\overline{v_n^2}} \int_{-\infty}^{\infty} \overline{v_n^2(f)} G^2(f) df,$$

where $\overline{v_n^2(f)}$ is the mean-square noise voltage per unit bandwidth, and $\overline{v_0^2}$ is the mean-square noise voltage per unit bandwidth measured at a frequency high enough that the PSD of the noise is flat.

NE Δf (cont'd)

For noise-equivalent bandwidth calculations, two impulse response forms are commonly considered: square and exponential. The square impulse response is most commonly used to relate response time and noise-equivalent bandwidth. The exponential impulse response arises from charge-carrier lifetime, or measuring the RC time constants in electrical circuits.

A square impulse response with a pulse width τ can be expressed as a rectangular function as

$$v(t) = v_0 \operatorname{rect}[(t - t_0)/\tau].$$

Applying the Fourier transform, the normalized voltage transfer function is obtained:

$$\frac{V(f)}{V_0} = e^{-j2\pi ft_0/\tau} \operatorname{sinc}(\pi f \tau).$$

Substituting into the NE Δf equation and solving the integral:

$$\text{NE}\Delta f = \int_{-\infty}^{\infty} |e^{-j2\pi ft_0/\tau} \operatorname{sinc}(\pi f \tau)|^2 df = \frac{1}{2\tau}.$$

The calculation of the noise-equivalent bandwidth from an exponential impulse response is obtained as follows.

The exponential impulse response can be specified as:

$$v(t) = v_0 \exp(t/\tau) \operatorname{step}(t),$$

Fourier transforming:

$$\frac{V(f)}{V_0} = \frac{1}{1 + j2\pi f \tau},$$

taking the absolute value squared:

$$\left| \frac{V(f)}{V_0} \right|^2 = \frac{1}{1 + (2\pi f \tau)^2}.$$

Integrating, it yields the following noise-equivalent bandwidth:

$$\text{NE}\Delta f = \int_{-\infty}^{\infty} \frac{df}{1 + (2\pi f \tau)^2} = \frac{1}{4\tau}.$$

Shot Noise

The **shot noise** mechanism is associated with the nonequilibrium conditions in a potential energy barrier of a photovoltaic detector through which a dc current flows. It is a result of the discrete nature of the current carriers and therefore of the current-carrying process. The dc current is viewed as the sum total of very many short and small current pulses, each contributed by the passage of a single electron or hole through the junction depletion layer. This type of noise is practically white, considering the spectral density of a single narrow pulse.

The generation of the carriers is random according to photon arrival times. However, once a carrier is generated, its recombination is no longer random; it is actually determined by transit-time considerations that obey Poisson statistics, which state that the variance equals the mean.

To determine the expression for the mean-square current fluctuation at the output of the measuring circuit, the current is measured during a time interval τ :

$$\bar{i} = \frac{n_e q}{\tau},$$

where n_e is the number of photo-generated electrons within τ . The average current can be related to the average number of electrons created by

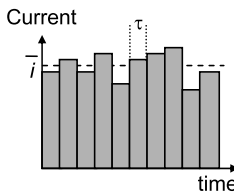
$$\bar{i} = \frac{\bar{n}_e q}{\tau} \Rightarrow \bar{n}_e = \frac{\bar{i}\tau}{q}.$$

The mean-square fluctuation averaged over many independent measuring times τ is

$$\overline{i_{n,\text{shot}}^2} = \overline{(i - \bar{i})^2} = \frac{q^2}{\tau^2} \overline{(n_e - \bar{n}_e)^2} = \frac{q^2}{\tau^2} \bar{n}_e,$$

which yields the expression of the shot noise:

$$\overline{i_{n,\text{shot}}^2} = \frac{\bar{i}q}{\tau} = 2q\bar{i}\Delta f \Rightarrow i_{n,\text{shot}} = \sqrt{2q\bar{i}\Delta f}.$$



τ = interval of integration.

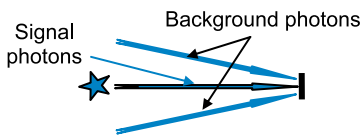
Faster circuit \rightarrow bigger Δf \rightarrow more noise

Signal-to-Noise Ratio: Detector and BLIP Limits

Is **signal-to-noise ratio (SNR)** predominantly generated by the signal or the background?

Considering the current generated primarily by signal photons, without any extraneous radiation present, the signal current from the detector is

$$i_{\text{sig}} = \phi_{p,\text{sig}} \eta q,$$



where η is the quantum efficiency [electrons per photon]. Similarly, the current generated by the background flux is

$$\text{Detector current: } i_{\text{total}} = i_{\text{sig}} + i_{\text{bkg}}$$

$$i_{\text{bkg}} = \phi_{p,\text{bkg}} \eta q.$$

The SNR is that of the signal current to the shot noise, namely

$$\text{SNR} = \frac{i_{\text{sig}}}{i_{n,\text{shot}}} = \frac{\phi_{p,\text{sig}} \eta q}{\sqrt{2q\bar{i}\Delta f}} = \frac{\phi_{p,\text{sig}} \eta q}{\sqrt{2q(\phi_{p,\text{sig}} \eta q + \phi_{p,\text{bkg}} \eta q)\Delta f}}.$$

Assuming that the dominant noise contribution is the shot noise generated by the signal-power envelope (i.e., $\phi_{\text{sig}} \gg \phi_{\text{bkg}}$)

$$\text{SNR} \cong \frac{\phi_{p,\text{sig}} \eta}{\sqrt{2\phi_{p,\text{sig}} \eta \Delta f}} = \sqrt{\phi_{p,\text{sig}} \eta \tau},$$

which states that the SNR increases as the square root of the signal-flux, thus improving the sensitivity of the system.

With a weak signal source detected against a large background, the most common situation in infrared applications, the dominant noise contribution is associated with the shot noise of the background (i.e., $\phi_{\text{bkg}} \gg \phi_{\text{sig}}$). The photodetector is said to be background limited, yielding

$$\text{SNR}_{\text{BLIP}} \cong \frac{\phi_{p,\text{sig}} \eta}{\sqrt{2\phi_{p,\text{bkg}} \eta \Delta f}} = \phi_{p,\text{sig}} \sqrt{\frac{\eta \tau}{\phi_{p,\text{bkg}}}}.$$

SNR_{BLIP} is inversely proportional to the square root of the background flux; so reducing the background photon flux increases the SNR **background-limited infrared photodetector (BLIP)**.

Generation-Recombination Noise

Generation-recombination (G/R) noise is caused by fluctuations in the rates of thermal generation and recombination of free carriers in semiconductor devices without potential barriers (e.g., photoconductors), thereby giving rise to a fluctuation in the average carrier concentration. Thus, the electrical resistance of the semiconductor material changes, which can be observed as fluctuating voltage across the sample when the bias current flows through it.

The transverse photoconductivity geometry and circuit are shown.

Once a carrier is generated, it travels under the influence of an applied electric field. The carrier lasts until recombination occurs at a random time consistent with the mean carrier lifetime τ_{carrier} . The statistical fluctuation in the concentration of carriers produces white noise.

The current noise expression for generation-recombination noise is given by

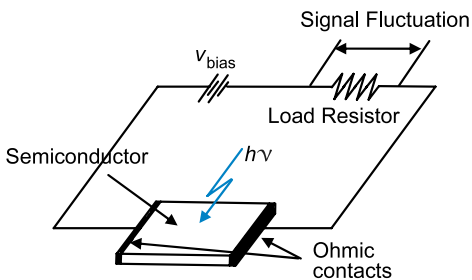
$$i_{n,G/R} = 2qG\sqrt{\eta E_p A_d \Delta f + g_{th} \Delta f},$$

where G is the photoconductive gain and g_{th} is the thermal generation of carriers. Since photoconductors are cooled cryogenically, the second term in the above equation can be neglected. Assuming G equals unity,

$$i_{n,G/R} = \sqrt{2q\eta E_p A_d \Delta f + 2q\eta E_p A_d \Delta f} = 2\sqrt{q\eta E_p A_d \Delta f},$$

$$i_{n,G/R} = \sqrt{2}i_{n,\text{shot}}.$$

Note that the rms G/R noise is $\sqrt{2}$ larger than for shot noise, since both generation and recombination mechanisms are random processes.

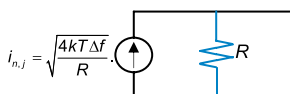


Johnson Noise

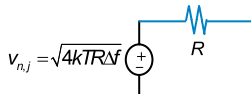
If the background flux is reduced enough, the noise floor is determined by the **Johnson noise**, also known as Nyquist or thermal noise. The fluctuation is caused by the thermal motion of charge carriers in resistive materials, including semiconductors, and occurs in the absence of electrical bias as a fluctuating rms voltage or current.

Johnson noise is an ideal noise-free resistor of the same resistance value, combined either in series with an rms noise voltage or in parallel with an rms noise current.

Norton model: R in parallel with rms noise current



Thevenin model: R in series with rms noise voltage



When multiplying the Johnson noise in terms of noise-voltage and current spectra:

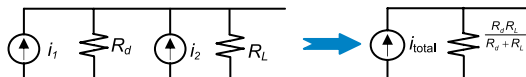
$$\sqrt{4kT R} \text{ [volt}/\sqrt{\text{Hz}}\text{]} \text{ and } \sqrt{\frac{4kT}{R}} \text{ [amp}/\sqrt{\text{Hz}}\text{]},$$

the power spectral density of the Johnson noise depends only on temperature, and not on resistance:

$$\text{PSD} = 4kT \text{ [watt}/\text{Hz}\text{]}.$$

Often the detector is cooled to cryogenic temperatures, while the load resistance is at room temperature. In combination, both parallel resistors are added as usual, but the rms noises are added in quadrature, yielding

$$i_{\text{Johnson}} = \sqrt{i_d^2 + i_L^2} = \sqrt{4k\Delta f \left[\frac{T_d}{R_d} + \frac{T_L}{R_L} \right]}.$$



The SNR in the Johnson noise limit is given by

$$\text{SNR}_{\text{Johnson}} \cong \frac{\Phi_{p,\text{sig}} \eta q}{\sqrt{\frac{4kT}{R} \Delta f}}.$$

Johnson noise is independent of the photogeneration process, and thus the SNR is directly proportional to the quantum efficiency.

1/f Noise and Temperature Noise

1/f noise is found in semiconductors, and becomes worse at low frequencies. It is characterized by a spectrum in which the noise power depends approximately inversely on the frequency. The general expression for 1/f noise current is given by

$$i_{n,f} = \sqrt{\mathcal{K} \frac{\bar{i}^\alpha \Delta f}{f^\beta}},$$

where \mathcal{K} is a proportionality factor, \bar{i} is the average dc current, f is the frequency, Δf is the measuring bandwidth, and α is a constant of ~ 2 , and β ranges from ~ 0.5 to 1.5 .

Although the cause of 1/f noise is not fully understood, it appears to be associated with the presence of potential barriers at the nonohmic contacts and the surface of the semiconductor.

1/f noise is typically the dominant noise to a few hundred hertz, and is often significant to several kilohertz. It is always present in microbolometers and photoconductors, because there is always a dc-bias current flowing within the detector material. However, 1/f noise can be eliminated in photovoltaic detectors operating in open-circuit voltage mode, when no dc-bias current is allowed to flow through the diode.

Temperature noise is caused by fluctuations in the temperature of the detector due to fluctuations in the rate at which heat is transferred from the sensitive element to its surroundings (i.e., radiative exchange and/or conductance with heat sink). The spectrum of the mean-square fluctuation in temperature is given by

$$\overline{\Delta T^2} = \frac{4kKT^2}{K^2 + (2\pi f)^2 C^2},$$

where k is Boltzmann's constant, K is the thermal conductance, C is the heat capacity, and T is the temperature.

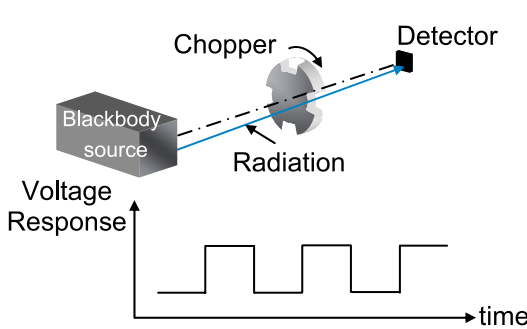
Temperature noise is mostly observed in thermal detectors, and being temperature-noise limited is the utmost performance level. The power spectrum of the temperature noise is flat.

Detector Responsivity

Responsivity gives the response magnitude of the detector. It provides information on gain, linearity, dynamic range, and saturation level. Responsivity is a measure of the transfer function between the input signal photon power or flux and the detector electrical signal output:

$$\mathcal{R} = \frac{\text{output signal}}{\text{input flux}},$$

where the output can be in volts or amperes, and the input in watts or photons/sec. \mathcal{R}_i is **current responsivity** and \mathcal{R}_v is **voltage responsivity**. A common technique in detection is to modulate the radiation to be detected and to measure the modulated component of the electrical output of the detector. This technique provides some discrimination against electrical noise since the signal is contained only within the Fourier component of the electrical signal at the modulation frequency, whereas electrical noise is often broadband. Furthermore, it avoids baseline drifts that affect electronic amplifiers due to ac coupling. The output voltage would vary from peak-to-valley.



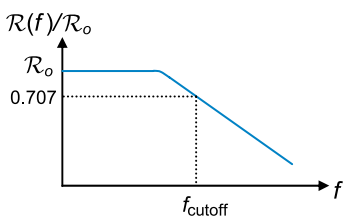
An important characteristic of a detector is how fast it responds to a pulse of optical radiation. The voltage response to radiation modulated at frequency f is defined as:

$$\mathcal{R}_v(f) = \frac{v_{\text{sig}}(f)}{\phi_{\text{sig}}(f)},$$

where $\phi_{\text{sig}}(f)$ is the rms value of the signal flux contained within the harmonic component at frequency f , and $v_{\text{sig}}(f)$ is the rms output voltage within this same harmonic component.

Detector Responsivity (cont'd)

In general, the responsivity $\mathcal{R}(f)$ of a detector decreases as the modulation frequency f increases. Changing the angular speed of the chopper, the responsivity can be obtained as a function of frequency. A typical responsivity-versus-frequency curve is plotted.



The cutoff frequency f_{cutoff} is defined as the modulation frequency at which $|\mathcal{R}_v(f_{\text{cutoff}})|^2$ falls to one-half its maximum value, and is related to response time as

$$f_{\text{cutoff}} = \frac{1}{2\pi\tau}.$$

The response time of a detector is characterized by its **responsive time constant**, the time that takes for the detector output to reach 63% ($1 - 1/e$) of its final value after a sudden change in the irradiance. For most sensitive devices, the response to a change in irradiance follows a simple exponential law. As an example, if a delta-function pulse of radiation $\delta(t)$ is incident on the detector, an output voltage signal (i.e., the impulse response) of the form

$$v(t) = v_0 e^{-t/\tau} \quad t \geq 0$$

is produced, where τ is the time constant of the detector. Transforming this time-dependent equation into the frequency domain by using the corresponding Fourier transform yields

$$V(f) = \frac{v_0\tau}{1 + j2\pi f\tau},$$

which can be extended to responsivity as

$$\mathcal{R}_v(f) = \frac{\mathcal{R}_0}{1 + j2\pi f\tau},$$

where $\mathcal{R}_0 = v_0\tau$ is the dc value of the responsivity. The modulus is written as

$$|\mathcal{R}_v(f)| = \frac{\mathcal{R}_0}{\sqrt{1 + (2\pi f\tau)^2}}.$$

Spectral Responsivity

Responsivity depends on the wavelength of the incident radiation beam, thus the spectral response of a detector can be specified in terms of its responsivity as a function of wavelength. **Spectral responsivity $\mathcal{R}(\lambda, f)$** is the output signal response to monochromatic radiation incident on the detector, modulated at frequency f . It determines the amplifier gain required to bring the detector output up to acceptable levels. To measure the spectral responsivity of a detector, a tunable narrowband source is required.

In energy-derived units, the spectral responsivity for a thermal detector is independent of wavelength (i.e., 1 W of radiation produces the same temperature rise at any spectral line). Therefore, its spectral response is limited by the spectral properties of the material of the window placed in front of the detector.

In a photon detector, the ideal spectral responsivity is linearly proportionate to the wavelength:

$$\mathcal{R}_{v,e}(\lambda) = \mathcal{R}_{v,e}(\lambda_{\text{cutoff}}) \frac{\lambda}{\lambda_{\text{cutoff}}}.$$

Photons with $\lambda > \lambda_{\text{cutoff}}$, are not absorbed by the material of the detector; and therefore not detected.

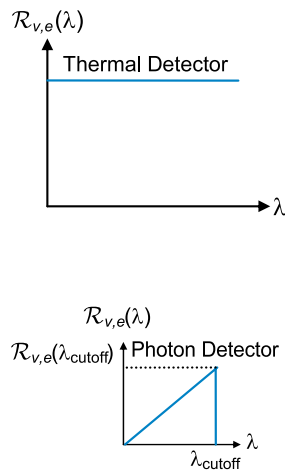
Long-wavelength cutoff is the longest wavelength detected by a sensor made of a material with a certain energy gap, and it is given by

$$\lambda_{\text{cutoff}} = hc / \mathcal{E}_{\text{gap}}.$$

A expression to determine the energy gap in electron-volt units is

$$\mathcal{E}_{\text{gap}}[\text{eV}] = \frac{hc}{\lambda_{\text{cutoff}}} \cdot \frac{1 \text{ eV}}{1.6 \times 10^{-19} \text{ J}} = \frac{1.24}{\lambda_{\text{cutoff}}}.$$

The energy gap of silicon is 1.12 eV; therefore, photons with $\lambda > 1.1 \mu\text{m}$ are not detected.



Blackbody Responsivity

Blackbody responsivity $\mathcal{R}(T, f)$ is interpreted as the output produced in response to a watt of input optical radiation from a blackbody at temperature T modulated at electrical frequency f . Since a BB source is widely available and rather inexpensive compared to a tunable narrowband source, it is more convenient to measure $\mathcal{R}(T)$ and calculate its corresponding $\mathcal{R}(\lambda)$.

For a blackbody that produces a spectral flux $\phi_\lambda(\lambda)$ the **detector output voltage** is calculated from the following integral:

$$v_{\text{out,det}} = \int_0^{\lambda_{\text{cutoff}}} \phi_\lambda(\lambda) \mathcal{R}_v(\lambda) d\lambda \text{ [volt]},$$

which determines the contribution to the detector output in those regions where the spectral flux and the voltage spectral responsivity overlap.

When measuring blackbody responsivity, the radiant power on the detector contains all wavelengths of radiation, independent of the spectral response curve of the detector. Using Stefan-Boltzmann's law and some of the basic radiometric principles studied previously, the blackbody responsivity is

$$\mathcal{R}(T) = \frac{v_{\text{out,det}}}{\phi_e} = \frac{\int_0^{\lambda_{\text{cutoff}}} \phi_\lambda(\lambda) \mathcal{R}_v(\lambda) d\lambda}{\frac{\sigma T^4}{\pi} A_{\text{source}} \Omega_{\text{det}}} = \frac{\int_0^{\lambda_{\text{cutoff}}} M_{e,\lambda}(\lambda) \mathcal{R}_v(\lambda) d\lambda}{\sigma T^4}.$$

Substituting the ideal response of a photon detector:

$$\mathcal{R}(T) = \frac{\frac{\mathcal{R}_v(\lambda_{\text{cutoff}})}{\lambda_{\text{cutoff}}} \int_0^{\lambda_{\text{cutoff}}} M_{e,\lambda}(\lambda) \lambda d\lambda}{\sigma T^4}.$$

The ratio of $R(T)$ and $R(\lambda_{\text{cutoff}})$ is defined by the \mathcal{W} -factor:

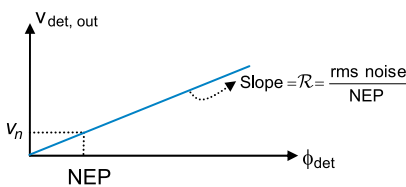
$$\mathcal{W}(\lambda_{\text{cutoff}}, T) = \frac{\mathcal{R}_v(\lambda_{\text{cutoff}})}{\mathcal{R}(T)} = \frac{\sigma T^4}{\frac{1}{\lambda_{\text{cutoff}}} \int_0^{\lambda_{\text{cutoff}}} M_{e,\lambda}(\lambda) \lambda d\lambda} = \frac{\sigma T^4}{\frac{hc}{\lambda_{\text{cutoff}}} \int_0^{\lambda_{\text{cutoff}}} M_{p,\lambda}(\lambda) d\lambda}.$$

Two standard blackbody temperatures are used to evaluate detectors: (1) 500 K for mid-wave and long-wave infrared measurements; and (2) 2850 K for visible and NIR measurements.

Noise Equivalent Power

Although the responsivity is a useful measurement to predict a signal level for a given irradiance, it gives no indication of the minimum radiant flux that can be detected. In other words, it does not consider the amount of noise at the output of the detector that ultimately determines the SNR.

The ability to detect small amounts of radiant energy is inhibited by the presence of noise in the detection process. Since noise produces a random fluctuation in the output of a radiation detector, it can mask the output that is



produced by a weak optical signal. Noise thus sets limits on the minimum input spectral flux that can be detected under given conditions.

One convenient description of this minimum detectable signal is the **noise equivalent power (NEP)**, which is defined as the radiant flux necessary to give an output signal equal to the detector noise. In other words, is the radiant power, ϕ_e , incident on the detector that yields an $\text{SNR} = 1$, and is expressed as the rms noise level divided by the responsivity of the detector:

$$\text{NEP} = \frac{v_n}{\mathcal{R}_v} = \frac{v_n}{v_{\text{sig}}/\phi_{\text{sig}}} = \frac{\phi_{\text{sig}}}{\text{SNR}} \quad [\text{watt}],$$

where v_n denote the rms voltage produced by a radiation detection system. A smaller NEP implies better sensitivity.

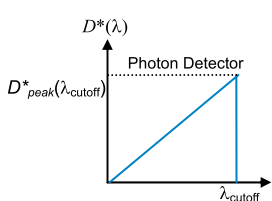
The disadvantage of using the NEP to describe detector performance is that the NEP does not allow a direct comparison of the sensitivity of different detector mechanisms or materials. This is because of its dependence on both the square root of the detector area, and the square root of the electronic bandwidth. A descriptor that circumvents this problem is called D^* (pronounced “dee star”) which normalized the inverse of the NEP to a 1-cm² detector area and 1 Hz of noise bandwidth.

Specific or Normalized Detectivity

The use of NEP is a situation-specific descriptor useful for design purposes but does not allow direct comparison of the sensitivity of different detector mechanisms of materials. The **specific or normalized detectivity (D^*)** is often used to specify detector performance. It normalizes the noise-equivalent bandwidth and the area of the detector; however, in order to predict the SNR, the sensor area and bandwidth must be chosen for a particular application.

D^* is independent of detector area and the electronic bandwidth, because the NEP is also directly proportional to the square root of these parameters as well. D^* is directly proportional to the SNR as well as to the responsivity:

$$D^* = \frac{\sqrt{A_d \Delta f}}{\text{NEP}} = \frac{\sqrt{A_d \Delta f}}{\phi_d} \text{SNR} = \frac{\sqrt{A_d \Delta f}}{v_n} R_v \quad [\text{cm}\sqrt{\text{Hz}}/\text{watt}].$$



Plots of spectral D^* for photon detectors have the same linear dependency with λ :

$$D^*(\lambda) = D^*_{\text{peak}}(\lambda_{\text{cutoff}}) \frac{\lambda}{\lambda_{\text{cutoff}}}.$$

The same \mathcal{W} -factor applies between $D^*(\lambda)$ peak and $D^*(T)$.

The cutoff value of $D^*(\lambda)$ is defined as the peak spectral $D^*_{\text{peak}}(\lambda_{\text{cutoff}})$, and corresponds to the largest potential SNR. In addition, any optical radiation incident on the detector at a wavelength shorter than the cutoff wavelength, λ_{cutoff} , has $D^*(\lambda)$ reduced from the peak $D^*_{\text{peak}}(\lambda_{\text{cutoff}})$ in proportion to the ratio $\lambda/\lambda_{\text{cutoff}}$.

Unlike the NEP, this descriptor increases with the sensitivity of the detector. Depending on whether the NEP is spectral or blackbody, D^* can also be either spectral or blackbody. $D^*(\lambda, f)$ is the detector's SNR when 1 W of monochromatic radiant flux (modulated at f) is incident on a 1-cm² detector area, within a noise equivalent bandwidth of 1 Hz. The blackbody $D^*(T, f)$ is the signal-to-noise output when 1 W of blackbody radiant power (modulated at f) is incident on a 1-cm² detector, within a noise equivalent bandwidth of 1 Hz.

Photovoltaic Detectors or Photodiodes

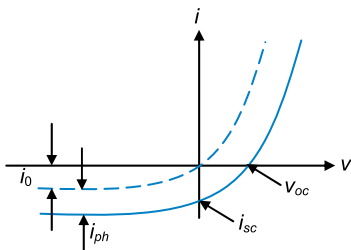
In **photovoltaic (PV) detectors**, more commonly called **photodiodes**, the optical radiation is absorbed at the PN junction, which produces an output current or voltage.

The photodiode equation is given by:

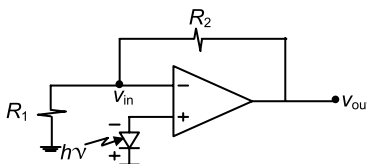
$$i = i_{\text{diode}} - i_{\text{ph}} = i_0 \left[\exp\left(\frac{qv}{kT}\right) - 1 \right] - \eta q \phi_p,$$

where i_{ph} is the photo-generated current, i_0 is the dark current, q is the charge of an electron, v is the voltage, k is the Boltzmann's constant, and T is the temperature.

The photodiode operating in each quadrant has different electro-optical characteristics. The most common operating points are open circuit, reverse bias, and short circuit.



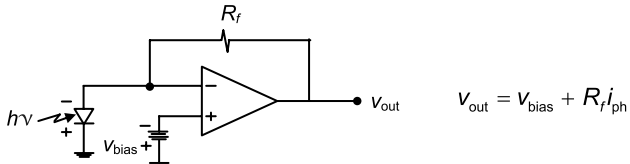
Open circuit:



$$V_{\text{oc}} = \frac{kT}{q} \ln \left(\frac{i_{\text{ph}}}{i_0} + 1 \right)$$

$$\frac{V_{\text{out}}}{V_{\text{in}}} = 1 + \frac{R_2}{R_1}$$

Reverse bias:



$$V_{\text{out}} = V_{\text{bias}} + R_f i_{\text{ph}}$$

If C decreases then RC decreases, the junction widens and the detector response increases.

Short circuit: the voltage is zero across the photodiode and i_{ph} is forced to flow into an electrical short circuit:

$$i = i_{\text{ph}} = \eta q \phi_p = \eta q E_p A_d.$$

Sources of Noise in PV Detectors

The sources of noise in a PV detector are

1. shot noise due to the dark current;
2. shot noise due to the feedback noise of the signal and background;
3. Johnson noise due to detector resistance;
4. Johnson noise due to the load resistors;
5. $1/f$ noise associated with the current flow;
6. preamplifier circuit noise; and
7. preamplifier voltage noise.

The noise expression for the photodiode is then

$$i_n^2 = 4q^2 i_0^2 \Delta f + 2q^2 \eta \phi_{p,\text{sig}} \Delta f + 2q^2 \eta \phi_{p,\text{bkg}} \Delta f + \\ 4k \Delta f \left(\frac{T_d}{R_d} + \frac{T_f}{R_f} \right) + \frac{\beta_0 \bar{i} \Delta f}{f} + i_{pa}^2 + v_{pa}^2 (R_f \parallel R_d).$$

The preamplifier noise can be made negligible by using low-noise transistors or by cooling the preamplifier to cryogenic temperatures. $1/f$ noise is almost zero if the device is operating in either open or reverse circuit modes. It is assumed that the dark current is also negligible compared to both the background and signal currents (i.e., $i_0 \ll i_{\text{sig}} + i_{\text{bkg}}$), and that BLIP conditions are in effect. Under these conditions, the rms shot noise current is approximately

$$i_n \cong \sqrt{2q^2 \eta \phi_{p,\text{bkg}} \Delta f} = \sqrt{2q^2 \eta \phi_{e,\text{bkg}} \frac{\lambda}{hc} \Delta f}.$$

Recalling that the peak signal current generated by a photovoltaic detector is

$$i_{\text{signal}} = \phi_{p,\text{sig}} \eta q = \phi_{e,\text{sig}} \eta q \frac{\lambda}{hc},$$

the SNR for a photovoltaic detector is then

$$\text{SNR}_{\text{PV}} = \frac{\phi_{e,\text{sig}} \eta q \frac{\lambda}{hc}}{\sqrt{2q^2 \phi_{e,\text{bkg}} \eta \frac{\lambda}{hc} \Delta f}}.$$

Setting the $\text{SNR}_{\text{PV}} = 1$, the spectral NEP_{PV,BLIP} is obtained:

$$\text{NEP}_{\text{PV,BLIP}}(\lambda) = \sqrt{\frac{hc}{\lambda} \frac{2\phi_{e,\text{bkg}} \Delta f}{\eta}}.$$

Expressions for $D_{\text{PV,BLIP}}^*$, $D_{\text{PV,BLIP}}^{**}$, and $D_{\text{PV,JOLI}}^*$

Spectral $D_{\text{PV,BLIP}}^*$ for a PV detector is obtained from the definition of D^* in terms of NEP:

$$D_{\text{PV,BLIP}}^*(\lambda) = \sqrt{\frac{A_d \Delta f}{\text{NEP}_{\text{BLIP}}}} = \sqrt{\frac{\lambda}{hc} \frac{\eta}{2E_{\text{bkg}}}} = \frac{\lambda}{hc} \sqrt{\frac{\eta}{2E_{\text{bkg}}}}.$$

If the background is not monochromatic, E_{bkg} needs to be integrated over the sensor response from 0 to λ_{cutoff} :

$$\begin{aligned} D_{\text{PV,BLIP}}^*(\lambda) &= \frac{\lambda_{\text{cutoff}}}{hc} \sqrt{\frac{\eta}{2 \int_0^{\lambda_{\text{cutoff}}} E_{\text{bkg}}(\lambda) d\lambda}} \\ &= F/\# \frac{\lambda_{\text{cutoff}}}{hc} \sqrt{\frac{2\eta}{\pi \int_0^{\lambda_{\text{cutoff}}} L_{\text{bkg}}(\lambda) d\lambda}}, \end{aligned}$$

where $E_{\text{bkg}} = \pi L_{\text{bkg}} \sin^2 \theta \cong \pi L_{\text{bkg}} (1/2F/\#)^2$.

D_{BLIP}^* increases when increasing the $F/\#$, which illuminates the detector with a smaller cone of background radiation.

D^{**} normalizes the dependence on $\sin \theta$, allowing a comparison of detectors normalized to hemispherical background:

$$D_{\text{PV,BLIP}}^{**}(\lambda) = \sin \theta D_{\text{PV,BLIP}}^*(\lambda).$$

Johnson-limited noise performance (JOLI) occurs in deep space applications when the shot noise has been decreased. It becomes negligible compared to the Johnson noise:

$$2q^2\eta(\phi_{p,\text{sig}} + \phi_{p,\text{sig}})\Delta f \ll 4k\Delta f \left(\frac{T_d}{R_d} + \frac{T_f}{R_f} \right),$$

where T_d and R_d are the temperature and resistance of the detector, respectively. The SNR of the PV detector under this condition becomes:

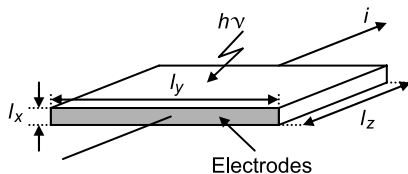
$$\text{SNR}_{\text{PV,JOLI}} = \frac{q\eta\phi_{e,\text{sig}} \frac{\lambda}{hc}}{4k\Delta f \left(\frac{T_d}{R_d} + \frac{T_f}{R_f} \right)} \cong \frac{q\eta\phi_{e,\text{sig}} \frac{\lambda}{hc}}{4k\Delta f \frac{T_d}{R_d}} \quad R_f \gg R_d.$$

Setting $\text{SNR}_{\text{PV,JOLI}} = 1$, converting the noise-equivalent photon flux to $\text{NEP}_{\text{PV,JOLI}}$, and substituting the NEP expression in terms of D^*

$$D_{\text{PV,JOLI}}^* = \frac{\lambda q \eta}{2hc} \sqrt{\frac{R_d A_d}{k T_d}}.$$

Photoconductive Detectors

Shot noise occurs in diodes and other devices with a potential-energy barrier for which the generation is a random process, while recombination is a deterministic process.



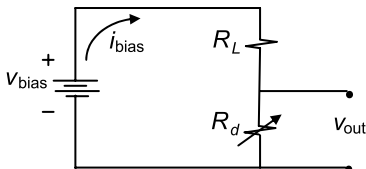
In devices such as **photoconductive (PC) detectors** without junctions or other potential barriers, both generation and recombination are random processes.

Photoconductors respond to light by changing the resistance or conductance of the detector's material:

$$R_d \propto \frac{1}{\phi_p} \Rightarrow dR_d \propto \frac{d\phi_p}{\phi_p^2},$$

where ϕ_p is the photon flux.

Photoconductive detectors have no junction; therefore, there is no intrinsic field. They cannot operate under open circuit conditions, and do not generate voltage independently (i.e., a must use bias current). In order to detect the change in resistance, a biasing circuit with an applied field must be utilized.



The output voltage is given by

$$V_{out} = \frac{R_d}{R_d + R_L} V_{bias},$$

where a small change in the detector resistance produces a change in signal voltage, which is directly proportional to the change in the photon flux incident on the photoconductive detector:

$$dv_{out} = \frac{dR_d}{(R_d + R_L)^2} V_{bias} \propto \frac{d\phi_p}{(R_d + R_L)^2 \phi_p^2} V_{bias}.$$

Sources of Noise in PC Detectors

The sources of noise in **photoconductors** are listed as

1. $1/f$ noise associated with the current flow;
2. generation-recombination (R/G) noise;
3. Johnson noise due to detector resistance;
4. Johnson noise due to the load resistors;
5. preamplifier circuit noise; and
6. preamplifier voltage noise.

The noise expression for the photoconductive detector is then

$$i_n^2 = 4q^2\eta E_p A_d G^2 \Delta f + 4q^2 g_{th} G^2 \Delta f + 4k \Delta f \left(\frac{T_d}{R_d} + \frac{T_f}{R_f} \right) + \frac{\beta_0 \bar{i} \Delta f}{f} + i_{pa}^2 + v_{pa}^2 (R_f \parallel R_d),$$

where g_{th} is the thermal generation rate of carriers and G is the photoconductive gain. G is proportional to the number of times an electron can transit the detector electrodes in its lifetime (i.e., excess signal electrons through the PC). It depends on the detector size, material, and doping, and can vary between $1 < G < 10^5$. If $G < 1$, the electron does not reach the electrode before recombining. Usually PC detectors are cooled cryogenically; in which case, the thermal term in the generation recombination noise is negligible. A photoconductor for BLIP- and Johnson-limited conditions are defined in the table.

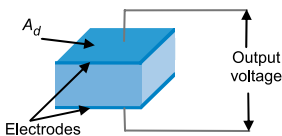
BLIP	JOLI
$\text{NEP}_{\text{PC,BLIP}} = \frac{2hc}{\lambda G} \sqrt{\frac{E_{\text{bkg}} A_d \Delta f}{\eta}}$	$\text{NEP}_{\text{PC,JOLI}} \equiv \frac{i_j}{R_{i,\text{PC}}} = \frac{\sqrt{4k \Delta f T / R_{\text{eq}}}}{\frac{\lambda q \eta}{hc} G}$
$D_{\text{PC,BLIP}}^* = \frac{\lambda}{2hc} G \sqrt{\frac{\eta}{E_{\text{bkg}}}}$	$D_{\text{PC,JOLI}}^* = \frac{\lambda q \eta}{2hc} G \sqrt{\frac{R_{\text{eq}} A_d}{kT}}$

where:
 $T \equiv T_d \approx T_L \& R_{\text{eq}} = R_d \parallel R_L$

For a given photon flux and a photoconductive gain of unity, the generation-recombination noise is larger than the shot noise by a factor of $\sqrt{2}$.

Pyroelectric Detectors

A **pyroelectric detector** is comprised of a slice of ferroelectric material with metal electrodes in opposite faces,



perpendicular to the polar axis. This material possesses an inherent electrical polarization, the magnitude of which is a strong function of temperature. The rate of change of electric polarization with respect to temperature, dP/dT , is defined as the pyroelectric coefficient at the operating temperature, \mathbf{p} .

A change in irradiance causes a temperature variation, which expands or contracts the crystal lattice, changing the polarization of the material. This change in polarization (i.e., realignment of the electric dipole concentration) appears as a charge on the capacitor formed by the pyroelectric with its two electrodes. A voltage is then produced by the charge on the capacitor. Thus, there is an observable voltage in the external circuit as long as the detector experiences a change in irradiance (i.e., it can only be used in an ac mode). In order to detect these small charges, low-noise high-impedance amplifiers are necessary.

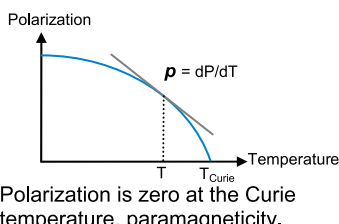
The temperature difference ΔT between the pyroelectric and the heat sink is related to the incident radiation by the heat balance differential equation:

$$H \frac{d\Delta T}{dt} + K\Delta T = \varepsilon\phi_e,$$

where H is the heat capacity, K is the thermal conductance, ε is the emissivity of the surface, and ϕ_e is the flux in energy derived units.

Since the radiation is modulated at an angular frequency ω , it can be expressed as an exponential function $\phi_e = \phi_{e,o}e^{j\omega t}$, in which case the heat balance equation provides the following solution:

$$|\Delta T| = \frac{\varepsilon\phi_{e,o}}{K\sqrt{1 + \omega^2\tau_{th}^2}} \Rightarrow \tau_{th} \equiv \frac{H}{K} = R_{th}C_{th},$$



Polarization is zero at the Curie temperature, paramagnetism.

Pyroelectric Detectors (cont'd)

where τ_{th} is the thermal time constant, R_{th} is the thermal resistance, and C_{th} is the thermal capacitance.

The current flowing through the pyroelectric detector is given by:

$$i = A_d p \frac{d\Delta T}{dt},$$

Thus the current responsivity is defined as:

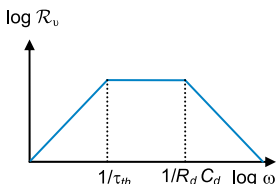
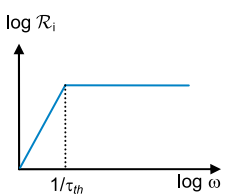
$$\mathcal{R}_i = \left| \frac{i}{\Phi_{e,o}} \right| = \frac{A_d p \varepsilon \omega}{K \sqrt{1 + \omega^2 \tau_{th}^2}} = \frac{A_d R_{th} p \varepsilon \omega}{\sqrt{1 + \omega^2 \tau_{th}^2}}$$

The current times the parallel electrical impedance yields the detector voltage:

$$v = \frac{i R_d}{1 + j \omega R_d C_d},$$

and the voltage responsivity is simply:

$$\mathcal{R}_v = \left| \frac{v}{\Phi_e} \right| = \frac{A_d R_d R_{th} p \varepsilon \omega}{\sqrt{1 + \omega^2 \tau_{th}^2} \sqrt{1 + \omega^2 (R_d C_d)^2}}$$



At high frequencies, the voltage responsivity is inversely proportional to frequency; while at low frequencies this is modified by the electric and thermal constants. The dominant noise in pyroelectric detectors is most commonly Johnson noise, in which:

$$v_{\text{Johnson}} = \sqrt{4kT R_d \Delta f}$$

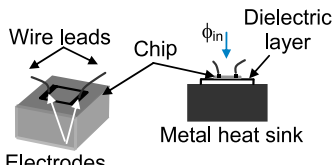
Then both NEP and D^* may be calculated by:

$$\text{NEP} = \frac{v_{\text{Johnson}}}{\mathcal{R}_v} = \frac{\sqrt{4kT \Delta f} \sqrt{1 + \omega^2 \tau_{th}^2} \sqrt{1 + \omega^2 (R_d C_d)^2}}{A_d \sqrt{R_d} R_{th} p \varepsilon \omega}$$

$$D^* = \frac{\sqrt{A_d^3 R_d} R_{th} p \varepsilon \omega}{\sqrt{4kT} \sqrt{1 + \omega^2 \tau_{th}^2} \sqrt{1 + \omega^2 (R_d C_d)^2}}.$$

Bolometers

Thermal detectors that change their electrical resistance as a function of temperature are called **bolometers** or **thermistors**. Bolometer-semiconductor elements are thin chips made by sintering a powdered mixture of ferrous oxides such as manganese, nickel and/or cobalt, which have temperature coefficients of resistance of the order of 4.2% per degree Celsius. These chips are mounted on a dielectric substrate that is, in turn, mounted on a metallic heat sink to provide high speed of response and dissipate bias current power. After assembly, the sensitive area is blackened to improve the emissivity to IR radiation.



The resistance of a semiconductor varies exponentially with temperature:

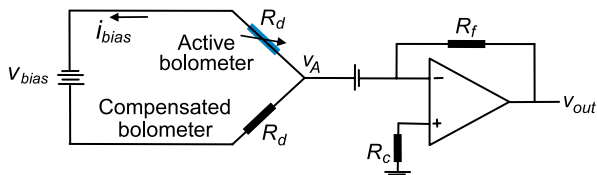
$$R_d = R_o e^{\mathcal{C}(1/T - 1/T_o)},$$

where R_o is the ambient resistance at a nominal temperature T_o , and \mathcal{C} is a material characteristic ($\mathcal{C} = 3400$ K for a mixture of manganese, nickel, and cobalt).

The resistance change that results from the optically induced temperature change is obtained by differentiation, yielding a temperature coefficient of:

$$\alpha = \frac{1}{R_d} \frac{dR_d}{dT} = -\frac{\mathcal{C}}{T^2}.$$

When infrared radiation is absorbed into the bolometer, its temperature rises slightly causing a small decrease in resistance. In order to produce an electrical current from this change in resistance, a bias voltage must be applied across the bolometer. This is accomplished by interfacing two identical bolometer chips into a bridge circuit.



Bolometers (cont'd)

The chip exposed to radiation is called the active chip, while the other is shielded from input radiation and is called the compensation chip.

Setting up the expression that equates the heat inflow and heat outflow:

$$H \frac{d\Delta T}{dt} + K \Delta T = \varepsilon \phi_e.$$

Assuming that the radiant power incident on the active device is periodic $\phi_e = \phi_{e,o} e^{j\omega t}$; the heat-balance differential equation provides the following solution:

$$|\Delta T| = \frac{\varepsilon \phi_{e,o}}{K \sqrt{1 + \omega^2 \tau_{th}^2}} \Rightarrow \tau_{th} \equiv \frac{H}{K}.$$

The radiation-induced change in resistance is then

$$\frac{dR_d}{R_d} = \alpha \Delta T = \frac{\alpha \varepsilon \phi_{e,o}}{K \sqrt{1 + \omega^2 \tau_{th}^2}}.$$

The bias current flowing through the active bolometer produces a change in the output voltage v_A given by

$$dv_A = i_{bias} dR_d = \frac{v_{bias}}{2} \frac{dR_d}{R_d}.$$

Therefore, the voltage responsivity becomes

$$\mathcal{R}_v = \frac{\alpha \varepsilon v_{bias}}{2K \sqrt{1 + \omega^2 \tau_{th}^2}}.$$

Note that if K decreases, \mathcal{R}_v increases; however, τ_{th} also increases yielding a lower cutoff frequency.

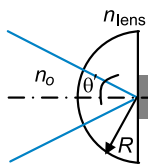
At small bias voltages, the bolometer obeys Ohm's law; however, as the bias voltage is increased, the self-heating of the chip due to the bias current causes a decrease in resistance and further increases the bias current. Eventually, there is a point where the detector burns out unless the current is limited in some manner.

Since the primary noise in a bolometer is Johnson noise, the NEP and D^* are stated as

$$\text{NEP} = \frac{4K \sqrt{1 + \omega^2 \tau_{th}^2} \sqrt{kTR_d \Delta f}}{\alpha \varepsilon v_{bias}}, \quad D^* = \frac{\alpha \varepsilon v_{bias} \sqrt{A_d}}{4K \sqrt{1 + \omega^2 \tau_{th}^2} \sqrt{kTR_d}}.$$

Bolometers: Immersion Optics

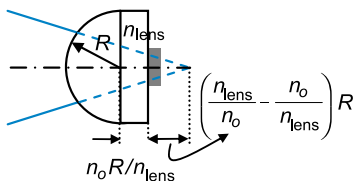
The detectivity of a bolometer is inversely proportional to the square root of its area; therefore it is desirable to make use of an immersion lens with high refractive index n_{lens} to minimize the radiation on the sensing area. By increasing n_{lens} , the detector area is decreased; the size of the entrance pupil and the ray angle in object space remain constant. However, the limit to such compression is regulated by the optical invariant and Abbe's sine condition given by



pupil and the ray angle in object space remain constant. However, the limit to such compression is regulated by the optical invariant and Abbe's sine condition given by

$$n_{\text{lens}}^2 A_{\text{det}} \sin \theta' = n_o^2 A_{\text{enp}} \sin \theta.$$

This hemispherical immersion lens is used with the bolometer located at the center of curvature. This is an aplanatic condition, thus no spherical aberration or coma is produced by the lens. A hyperhemispheric lens can also be used alternatively, and becomes aplanatic when the distance between the detector and center of curvature is $n_o R / n_{\text{lens}}$.

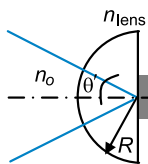


In a germanium hemispherical immersion lens, where $n_{\text{lens}} = 4$, the detector area is reduced by a factor of 16, which theoretically increases its detectivity by a factor of 4. This full gain is limited and cannot be practically achieved; however, if the immersion lens is antireflection coated, D^* improves to ~ 3.5 .

An adhesive layer glues the chip and the immersion lens together. The material for this layer must have good infrared transmission, high-quality electrical and thermal insulation properties, a high dielectric strength to prevent breakdown under the bias voltage, and a high refractive index to optically match the immersion lens to the bolometer. Arsenic-doped amorphous selenium or Mylar may be used. The index of refraction of selenium is 2.5, while that of the bolometer materials is ~ 2.9 . When a germanium immersion lens is used, total internal reflection (TIR) occurs at the selenium when the angle of incidence exceeds 38 deg. Suitable optical design techniques must be used to avoid this situation.

Bolometers: Immersion Optics

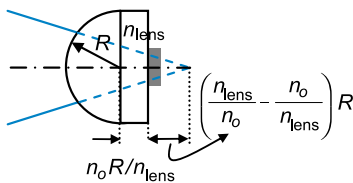
The detectivity of a bolometer is inversely proportional to the square root of its area; therefore it is desirable to make use of an immersion lens with high refractive index n_{lens} to minimize the radiation on the sensing area. By increasing n_{lens} , the detector area is decreased; the size of the entrance pupil and the ray angle in object space remain constant. However, the limit to such compression is regulated by the optical invariant and Abbe's sine condition given by



pupil and the ray angle in object space remain constant. However, the limit to such compression is regulated by the optical invariant and Abbe's sine condition given by

$$n_{\text{lens}}^2 A_{\text{det}} \sin \theta' = n_o^2 A_{\text{enp}} \sin \theta.$$

This hemispherical immersion lens is used with the bolometer located at the center of curvature. This is an aplanatic condition, thus no spherical aberration or coma is produced by the lens. A hyperhemispheric lens can also be used alternatively, and becomes aplanatic when the distance between the detector and center of curvature is $n_o R / n_{\text{lens}}$.

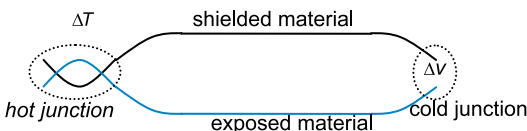


In a germanium hemispherical immersion lens, where $n_{\text{lens}} = 4$, the detector area is reduced by a factor of 16, which theoretically increases its detectivity by a factor of 4. This full gain is limited and cannot be practically achieved; however, if the immersion lens is antireflection coated, D^* improves to ~ 3.5 .

An adhesive layer glues the chip and the immersion lens together. The material for this layer must have good infrared transmission, high-quality electrical and thermal insulation properties, a high dielectric strength to prevent breakdown under the bias voltage, and a high refractive index to optically match the immersion lens to the bolometer. Arsenic-doped amorphous selenium or Mylar may be used. The index of refraction of selenium is 2.5, while that of the bolometer materials is ~ 2.9 . When a germanium immersion lens is used, total internal reflection (TIR) occurs at the selenium when the angle of incidence exceeds 38 deg. Suitable optical design techniques must be used to avoid this situation.

Thermoelectric Detectors

A **thermoelectric detector** or **thermocouple** is comprised of two junctions between two dissimilar conductors having a large difference in their thermoelectric power (i.e., a large **Seebeck coefficient Θ**). The hot junction is an efficient absorber exposed to incident radiation, while the cold junction is purposely shielded.



Seebeck effect where two semiconductor materials are joined together at a hot point and a cold point; ΔT is maintained between the hot and cold junctions; an open-circuit voltage Δv is developed between these materials at the cold point:

$$\Delta v = \Theta \Delta T \rightarrow \Theta [\mu\text{V/K}]$$

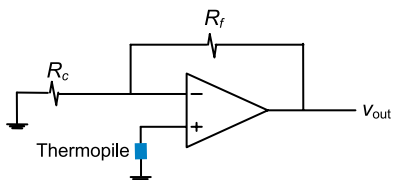
To obtain efficient and large electrical conductivity σ , both the thermal conductivity K and the Joulean heat loss must be minimized. This is achieved by maximizing the coefficient $\sigma\Theta^2/K$ found in some heavily doped semiconductors.

The voltage output between the two dissimilar materials is increased by connecting numerous thermocouples in series; a device called radiation **thermopile**. The responsivity of a thermopile is given by

$$\mathcal{R}_v = \frac{\varepsilon \Theta N}{K \sqrt{1 + \omega^2 \tau_{th}^2}},$$

where N is the number of thermocouples in electrical series.

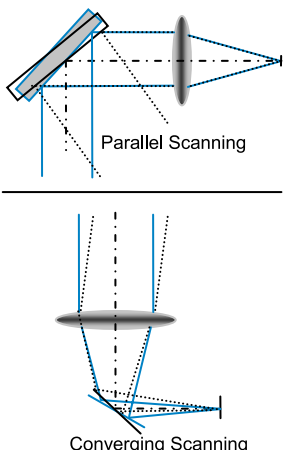
The thermopile device may then be interfaced to an operational amplifier circuit to increase the voltage to usable levels.



Thin-film techniques enable chip thermopiles to be fabricated as complex arrays with good reliability.

Raster Scan Format: Single-Detector

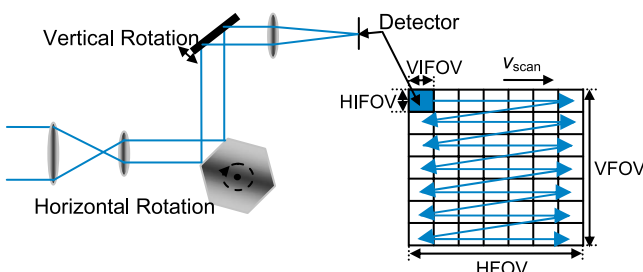
Scanning mechanisms are often necessary in infrared systems to cover a 2D FOV with a reasonable number of detector elements, or when a substantial FOV is required. The many applications that need scanning usually depend on opto-mechanical elements to direct and focus the infrared radiation. There are two basic types of scanners: pre-objective or **parallel beam scanner**, and post-objective or **converging beam scanner**.



In parallel scanning, the scanning element is out in front of the final image-forming element, and must be the entrance pupil of the optical system. The converging scanner has the moving element between the final optical element and the image, and works on axis.

There are three basic scan formats: raster, parallel, and the staring focal plane array.

In the raster scan mechanisms, a single detector is scanned in two orthogonal directions in a 2D raster across the FOV. The moving footprint sensed by the detector is called the **instantaneous field-of-view (IFOV)**, and the specific time required for the footprint to pass across the detector is called the **dwell time (τ_{dwell})**.



One-hundred percent scan efficiency (η_{scan}) is assumed. Scan inefficiencies include overlap between scan lines, over scanning of the IFOV beyond the region sensed, and finite retrace time to move the detector to the next line.

Raster Scan Format: Single-Detector (cont'd)

The number of horizontal lines to make up a 2D scene is given by

$$n_{\text{lines}} = \frac{\text{VFOV}}{\text{VIFOV}}.$$

The time taken to scan one particular line is

$$\tau_{\text{line}} = \frac{\tau_{\text{frame}}}{n_{\text{lines}}} = \tau_{\text{frame}} \frac{\text{VFOV}}{\text{VIFOV}}.$$

The dwell time is the line time divided by the number of horizontal pixels contained in that line:

$$\tau_{\text{dwell}} = \frac{\tau_{\text{line}}}{\text{HFOV}/\text{HIFOV}}.$$

The scan velocity and the dwell time can be written as

$$v_{\text{scan}} = \frac{\text{HFOV}}{\tau_{\text{line}}} \Rightarrow \tau_{\text{dwell}} = \frac{\text{HIFOV}}{v_{\text{scan}}}.$$

The dwell time can be also interpreted as the frame time divided by the total number of pixels within the 2D FOV:

$$\tau_{\text{dwell}} = \frac{\tau_{\text{frame}}}{(\text{VFOV}/\text{VIFOV}) \cdot (\text{HFOV}/\text{HIFOV})} = \frac{\tau_{\text{frame}}}{n_{\text{pixels}}},$$

where the frame time can be found by

$$\tau_{\text{frame}} = n_{\text{lines}} \cdot \tau_{\text{line}} = \frac{\text{VFOV}}{\text{VIFOV}} \cdot \frac{\text{HFOV}}{v_{\text{scan}}}.$$

The electronic bandwidth can be written in terms of the dwell time as

$$\Delta f = \frac{1}{2\tau_{\text{dwell}}}.$$

A scanning system that covers the entire FOV with a single-detector considerably lowers the duration that the sensing element remains on a particular IFOV; hence resulting in a higher noise-equivalent bandwidth.

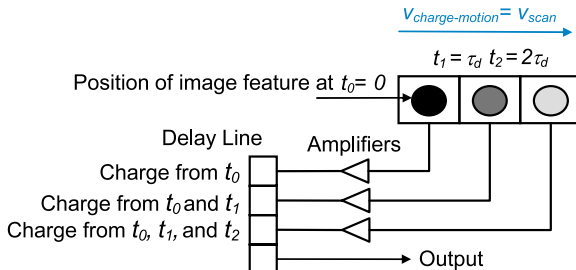
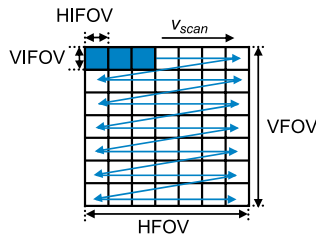
A longer dwell time is obtained using a multiple-detector system. In this case, the noise is reduced by the square root of the number of sensing elements, thus improving the SNR of the infrared system.

Multiple-Detector Scan Formats: Serial Scene Dissection

Serial scan uses multiple sensors along the scan direction, in such a way that each point in the image is scanned by all detectors.

The number of detectors used in a practical system varies between two and ten.

The main mechanism used to implement a serial scan is called **time delay and integration (TDI)**. TDI requires a synchronized delay line (typically a charge-coupled device), to move the signal charge along with the optical-scan motion. A particular IFOV is looked n_d times; being n_d the number of detectors in series dissecting the overall system's FOV of the scanned system. The output charge from each detector is added together as the serial scan moves on. As a result, the amplitude of the added charge signal is incremented n_d times, and the uncorrelated noise, since it is added in quadrature, is intensified by a factor of $\sqrt{n_d}$. Thereby, the overall SNR of the system is improved by the square root of the number of sensor elements.



Advantage: The nonuniformity of the detectors is improved.

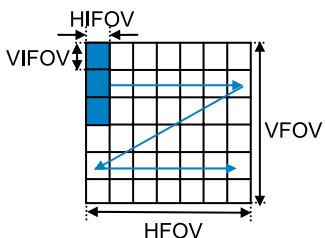
Disadvantages: High-mirror speeds are necessary to cover the 2D FOV. TDI circuit increases the weight and power of the electronics subsystem.

Assumption: The $\sqrt{n_d}$ increment in the SNR assumes that all the detectors are identical in noise and level responsivity. The practical result is around 10% short of the ideal.

Parallel Scene Dissection

Parallel scanning uses multiple sensors in cross-scan directions. For a given fixed frame time, a slower scan is used since multiple vertical lines are covered at once.

If $n_d < \text{VFOV}/\text{VIFOV}$, a 2D raster is required, with the scan format such that any given detector will drop $n_d \times \text{VIFOV}$.

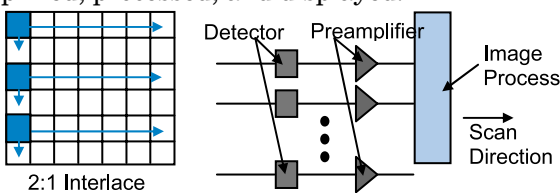


If there are sufficient detectors to cover a full line only horizontal scan motion is required.

Advantage: Lower mirror speeds are required.

Disadvantage: D^* variations produce image nonuniformities.

In second generation forward-looking infrared (FLIR) imagers, TDI/parallel scan is used to perform 2:1 interlacing. A full line is stored and summed to the next line. Here, TDI is applied along the scan direction, and all the detectors are preamplified, processed, and displayed.



For a system with a fixed frame time, an n_d sensor has a time line of

$$\tau_{\text{line}} = \frac{\tau_{\text{frame}}}{n_{\text{lines}}/n_d} = \tau_{\text{frame}} n_d \frac{\text{VFOV}}{\text{VIFOV}},$$

where, longer dwell time is achieved by a factor of n_d yielding

$$\tau_{\text{dwell}} = \frac{\tau_{\text{line}}}{\text{HFOV}/\text{HIFOV}} = \frac{\tau_{\text{frame}} n_d}{(\text{VFOV}/\text{VIFOV}) \cdot (\text{HFOV}/\text{HIFOV})} = \frac{\tau_{\text{frame}} n_d}{n_{\text{pixels}}}.$$

Bandwidth decreases inversely proportional to n_d , and the noise is proportional to the square root of the bandwidth, yielding

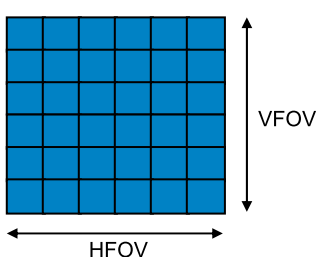
$$\Delta f = \frac{1}{2\tau_{\text{dwell}}} = \frac{n_{\text{pixels}}}{2\tau_{\text{frame}} n_d} \Rightarrow v_n \propto \sqrt{\Delta f} = \sqrt{\frac{n_{\text{pixels}}}{2\tau_{\text{frame}} n_d}}.$$

Therefore, the overall SNR increases by $\text{SNR} \propto \sqrt{n_d}$.

Staring Systems

Staring systems cover the 2D FOV in its entirety, so the number of detector elements is equal to resolution elements in the image. As a result, the dwell time is equal to the frame time of the system increasing the SNR significantly:

$$\tau_{\text{dwell}} = \tau_{\text{frame}}.$$



Each detector reduces the bandwidth because of the increment in the dwell time, so the SNR increases by a factor of $\sqrt{n_d}$.

Nonuniformities and dead pixels are implicit in a staring array.

The SNR square root dependence can be used to compare the potential performance of the various system configurations. For example, a 320×256 staring array produces a SNR that is higher by a factor of 25.3 in comparison to a parallel scanned system with a linear array of 128 detectors.

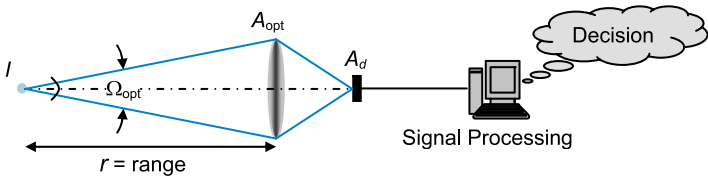
Staring Systems	Scanning Systems
Good SNR	Low SNR
No moving parts	Moving parts
Uniformity problems	Good uniformity
More complex electronically	More complex mechanically
Under-sampling problems	Prone to line-of-sight jitter
More prone to aliasing	Need more flux for a given SNR
Lower bandwidth for a given τ_{frame}	Higher bandwidth for a given τ_{frame}
D^* for the array is lower	Good D^* for individual detectors
Expensive	Cheaper

Search Systems and Range Equation

Search systems are also called **detection, warning, or go-no-go systems**. Their intent is to detect and locate a target that has a prescribed minimum intensity within a prescribed search volume. They operate on an unresolved point-source basis (that does not fill the IFOV of the system); therefore, the spectral radiant intensity [W/ster·μm] is the variable of interest.

The principal concern is to assess the maximum SNR required for specified values of the probability of correct detection, and minimizing false-alarm rate. The result is a statistical decision about the existence or state of a target phenomenon within a search volume. Linear fidelity is unimportant for these systems because they do not produce an image.

The objective is to establish the maximum range at which an infrared search system can detect or track a point source target. The **range equation** states the distance at which a given point source can be detected and establishes the design tradeoffs available.



The amount of flux reaching the detector as a function of the radiant intensity is

$$\phi_d = I \cdot \Omega_{\text{opt}} \tau_{\text{opt}} \tau_{\text{atm}} = \frac{I \cdot A_{\text{opt}}}{r^2} \tau_{\text{opt}} \tau_{\text{atm}},$$

where τ_{opt} is the optical transmittance and τ_{atm} is the atmospheric transmittance between the point source and the search system. The signal voltage from the detector is given by

$$v_s = \mathcal{R}_v \cdot \phi_d = \mathcal{R}_v \frac{I \cdot A_{\text{opt}}}{r^2} \tau_{\text{opt}} \tau_{\text{atm}}.$$

The SNR is found by dividing each side of the equation by the rms value of the noise from the detector, yielding

$$\text{SNR} = \frac{v_s}{v_n} = \frac{\mathcal{R}_v}{v_n} \frac{I \cdot A_{\text{opt}}}{r^2} \tau_{\text{opt}} \tau_{\text{atm}}.$$

Search Systems and Range Equation (cont'd)

Using the definition of NEP, and recasting in terms of D^* :

$$\text{SNR} = \frac{1}{\text{NEP}} \frac{I \cdot A_{\text{opt}}}{r^2} \tau_{\text{opt}} \tau_{\text{atm}} = \frac{D^*}{\sqrt{A_d \Delta f}} \frac{I \cdot A_{\text{opt}}}{r^2} \tau_{\text{opt}} \tau_{\text{atm}},$$

where Δf is the noise equivalent bandwidth. Recasting in terms of $F/\#$ and the IFOV, and solving for the range

$$r = \sqrt{\frac{ID^*}{\text{SNR} \sqrt{\Delta f}} \frac{\pi D_{\text{opt}}^2}{4f \sqrt{\Omega_d}}} \tau_{\text{opt}} \tau_{\text{atm}} = \sqrt{\frac{ID^*}{\text{SNR} \sqrt{\Delta f}} \frac{\pi D_{\text{opt}}}{4F/\# \sqrt{\Omega_d}}} \tau_{\text{opt}} \tau_{\text{atm}},$$

where D_{opt} is the diameter of the entrance pupil and f is the effective focal length of the optics. When the range equation is used to find the maximum detection or tracking range, the SNR is the minimum required for the system to work appropriately.

To analyze how the various factors affect the detection range, the range equation is regrouped in terms of optics, target and atmospheric transmittance, detector, and signal processing, respectively, yielding

$$r = \sqrt{\frac{\pi D_{\text{opt}} \tau_{\text{opt}}}{4F/\#}} \sqrt{I \tau_{\text{atm}}} \sqrt{D^*} \sqrt{\frac{1}{\text{SNR} \sqrt{\Omega_d \Delta f}}}.$$

In the first term, the diameter, the speed of the optics, and the transmittance characterize the optics. The first two terms are written separately to facilitate their independent solutions in the tradeoff process. The range is directly proportional to the square root of D_{opt} , where the bigger the optics, the more flux is collected. However, scaling up the entrance pupil changes the $F/\#$ of the system, and requires a corresponding increase in both the focal length and the linear size of the detector to maintain the original FOV.

The second term contains the radiant intensity of the target and the transmittance along the line of sight. The amount of attenuation caused by the atmosphere, and the shot-noise contribution from the background can be optimized by choosing the best spectral band for the specific optical system. For example, if the emitting flux from the target is high, the spectral band that yields the best contrast is selected; however, if the flux is low, the spectral band that produces the optimum SNR is selected.

Search Systems and Range Equation (cont'd)

The third factor pertains to the characteristics of the detector. The range is proportional to the square root of the normalized detectivity of the detector. Therefore, an increment in the detection range can be achieved by enhancing the sensitivity of the system using serial TDI approaches, or by effectively shielding the detector from background radiation. Also notice that since the radiation is collected from a point source, increasing the area of the detector reduces the SNR of the system.

The final factor describes the range in terms of the signal processing parameters. It shows that decreasing either the FOV or the noise equivalent bandwidth slowly increases the range because of the inverse fourth root dependence. The product $\Delta f \Omega_d$ represents the angular scan rate in steradian per second, increasing the integration time of the system averages away random noises resulting in longer detection ranges. The SNR in this type of system is interpreted as the minimum SNR required to reach a detection decision with an acceptable degree of certainty. For example, if the search system requires a higher SNR to improve the probability of correct detection, the system will have a shorter range.

The range equation for BLIP search systems is obtained by substituting D_{BLIP}^* for D^* , which in photon-derived units translates to

$$r_{\text{BLIP}} = \sqrt{\frac{\pi D_{\text{opt}} \tau_{\text{opt}}}{4}} \sqrt{I \tau_{\text{atm}}} \frac{\lambda}{hc} \sqrt{\frac{2\eta}{\pi L_{\text{bkg}}}} \sqrt{\frac{1}{\text{SNR} \sqrt{\Omega_d \Delta f}}}.$$

Note that the $F/\#$ term has dropped out of the equation. So a BLIP search system is influenced by the diameter of its optics but not by its speed.

There are several design concepts that can be used to decrease the background noise: the detector cold stop is designed so that it produces a 100% cold efficiency; a spectral filter is used to limit the spectral pass band to the most favorable region to the corresponding target flux; avoid the wavelengths at which the atmosphere absorbs strongly; minimize the emissivity of all the optical and opto-mechanical components, and, if necessary, cool the elements by the detector's angular subtense.

Noise Equivalent Irradiance

The **noise equivalent irradiance** or better known as **NEI** is one of the main descriptors of infrared warning devices. It is the flux density at the entrance pupil of the optical system that produces an output signal equal to the system's noise (i.e., $\text{SNR} = 1$). It is used to characterize the response of an infrared system to a point source target.

The irradiance from a point source target is given by

$$E = \frac{\phi}{A_{\text{opt}}} = \frac{I \cdot \Omega_{\text{opt}}}{A_{\text{opt}}} = \frac{I}{r^2},$$

substituting the range expression and setting the SNR equal to 1

$$\text{NEI} = E|_{\text{SNR}=1} = \frac{\sqrt{A_d \Delta f}}{A_{\text{opt}} D^* \tau_{\text{opt}} \tau_{\text{atm}}} = \frac{\text{NEP}}{A_{\text{opt}}} \frac{1}{\tau_{\text{opt}} \tau_{\text{atm}}}.$$

Recasting in terms of $F/\#$ and the IFOV

$$\text{NEI} = \frac{4F/\# \sqrt{\Omega_d \Delta f}}{\pi D_{\text{opt}} D^* \tau_{\text{opt}} \tau_{\text{atm}}}.$$

In BLIP conditions the NEI is independent of the $F/\#$, yielding:

$$\text{NEI}_{\text{BLIP}} = \frac{4hc}{\lambda A_{\text{opt}} \tau_{\text{opt}} \tau_{\text{atm}}} \sqrt{\frac{L_{p,bkg} \Omega_d \Delta f}{2\pi\eta}}.$$

NEI is especially useful when it is plotted as a function of wavelength. Such plot defines the irradiance at each wavelength necessary to give a signal output equal to the system's rms noise. It can be interpreted either as an average value over the spectral measuring interval, or as the peak value.

Although NEI has a broader usage in characterizing the performance of an entire system, it also may be used to evaluate the performance of a detector alone. In this case, it is defined as the radiant flux density necessary to produce an output signal equal to the detector noise, and compares the ability of different sized devices to detect a given irradiance.

$$\text{NEI} = \frac{E}{\text{SNR}} = \frac{\text{NEP}}{A_d}.$$

Performance Specification: Thermal-Imaging Systems

A **thermal imaging system (TIS)** collects, spectrally filters, and focuses the infrared radiation onto a multielement detector array. The detectors convert the optical signals into analog signals, which are then amplified, digitized, and processed for display on a monitor. Its main function is to produce a picture that maps temperature differences across an extended-source target; therefore, radiance is the variable of interest.

Two parameters are measured to completely specify TIS and produce good thermal imagery: **thermal sensitivity** and **spatial resolution**. Spatial resolution is related to how small an object can be resolved by the thermal system, and thermal sensitivity concerns the minimum temperature difference discerned above noise level.

Modulation transfer function (MTF): characterizes both the spatial resolution and image quality of an imaging system in terms of spatial frequency response. The MTF is a major parameter used for system specifications and design analysis.

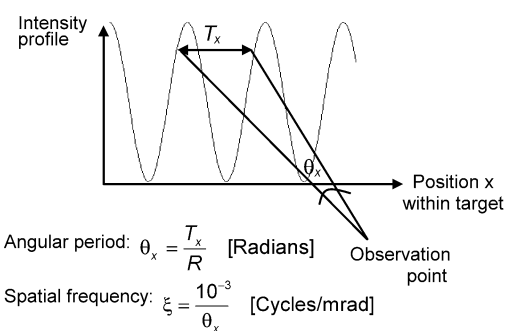
Noise-equivalent temperature difference (NETD): measures the thermal sensitivity of TIS. While the NETD is a useful descriptor that characterizes the target-to-background temperature difference, it ignores the spatial resolution and image quality of the system.

Minimum resolvable temperature difference (MRTD): a subjective measurement that depends on the infrared imaging system's spatial resolution and thermal sensitivity. At low spatial frequencies, the thermal sensitivity is more important; while at high spatial frequencies, the spatial resolution is the dominant factor. The MRTD combines both the thermal sensitivity and the spatial resolution into a single measurement. The MRTD is not an absolute value but is a perceivable temperature differential relative to a given background.

Johnson criteria: another descriptor that accounts for both the thermal sensitivity and spatial resolution. This technique provides a real way of describing real targets in terms of simpler square-wave patterns.

MTF Definitions

Spatial frequency is defined as the reciprocal crest-to-crest distance (i.e., the spatial period) of a sinusoidal wave-front used as a basic function in the Fourier analysis of an object or image. Typically it is specified in [cycles/mm] in the image plane, and in angular spatial frequency [cycles/milliradian] in object space. For an object located at infinity, these two representations are related through the focal length (f) of the image-forming optical system.



$$\xi_{\text{ang,obj}}[\text{cycles/mmrad}] = \xi_{\text{img}}[\text{cycles/mm}] \times \frac{f[\text{mm}]}{10^3}$$

The **image quality** of an optical or electro-optical system is characterized either by the system's **impulse response** or its Fourier transform, the **transfer function**.

function. The impulse response $h(x, y)$ is the 2D image form in response to an impulse or delta-function object. Because of the limitations imposed by diffraction and aberrations, the image quality produced depends on the wavelength distribution of the source, the $F/\#$ at which the system operates, the field angle at which the point is located, and the choice of focus position.

A continuous object $f(x, y)$ is decomposed using the shifting property of delta functions, into a set of point sources, each with a strength proportional to the brightness of their original object at that location. The final image $g(x, y)$ obtained is the superposition of the individual weighted impulse responses. This is equivalent to the convolution of the object with the impulse response:

$$g(x, y) = f(x, y) * * h(x, y),$$

where the double asterisk denotes a 2D convolution.

MTF Definitions (cont'd)

The validity of this requires **shift invariance** and **linearity**; a condition called **isoplanatism**. These assumptions are often violated in practice; however, to preserve the convenience of a transfer function analysis, the variable that causes nonisoplanatism is allowed to assume a set of discrete values. Each set has separate impulse responses and transfer functions. Although $h(x, y)$ is a complete specification of image quality, additional insight is gained by use of the transfer function. A transfer-function analysis considers the imaging of sinusoidal objects, rather than point objects. It is more convenient than the impulse-response analysis because the combined effect of two or more subsystems can be calculated by a point-by-point multiplication of the transfer functions, rather than convolving the individual impulse responses.

Using the convolution theorem of Fourier transforms, the product of the corresponding spectra is given by

$$G(\xi, \eta) = F(\xi, \eta) \times H(\xi, \eta),$$

where $F(\xi, \eta)$ is the object spectrum, $G(\xi, \eta)$ is the image spectrum, and $H(\xi, \eta)$ is the transfer function, which is the Fourier transform of the impulse response. ξ and η are spatial frequencies in the x and y directions, respectively.

The transfer function $H(\xi, \eta)$ is normalized to have a unit value at zero spatial frequency. This normalization is appropriate for optical systems because the transfer function of an incoherent optical system is proportional to the 2D autocorrelation of the exit pupil, and the autocorrelation is the necessary maximum at the origin. In its normalized form, the transfer function $H(\xi, \eta)$ is referred to as the **optical transfer function (OTF)**, which plays a key role in the theoretical evaluation and optimization of an optical system as a complex function that has both a magnitude and a phase portion:

$$\text{OTF}(\xi, \eta) = H(\xi, \eta) = |H(\xi, \eta)| \cdot e^{j\theta(\xi, \eta)}.$$

The absolute value or magnitude of the OTF is the MTF, while the phase portion of the OTF is referred to as the **phase transfer function (PTF)**. The system's MTF and PTF alter the image as it passes through the system.

MTF Definitions (cont'd)

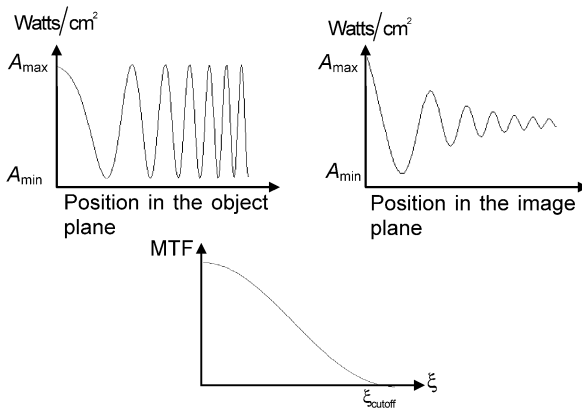
For linear-phase-shift invariant systems, the PTF is of no special interest since it indicates only a spatial shift with respect to an arbitrary selected origin. An image in which the MTF is drastically altered is still recognizable, where large nonlinearities in the PTF can destroy recognizability. PTF nonlinearity increases at high spatial frequencies. Since the MTF is small at high spatial frequencies, the linear phase shift effect is diminished.

The MTF is then the magnitude response of the imaging system to sinusoids of different spatial frequencies. This response can also be defined as the attenuation factor in modulation depth:

$$M = \frac{A_{\max} - A_{\min}}{A_{\max} + A_{\min}},$$

where A_{\max} and A_{\min} refer to the maximum and minimum values of the waveform that describe the object or image in W/cm^2 versus position. The modulation depth is actually a measure of visibility or contrast. The effect of the finite-size impulse response (i.e., not a delta function) of the optical system is to decrease the modulation depth of the image relative to that in the object distribution. This attenuation in modulation depth is a function of position in the image plane. The MTF is the ratio of image-to-object modulation depth as a function of spatial frequency:

$$\text{MTF}(\xi, \eta) = \frac{M_{\text{img}}(\xi, \eta)}{M_{\text{obj}}(\xi, \eta)}.$$



Optics MTF: Calculations

The overall transfer function of an electro-optical system is calculated by multiplying individual transfer functions of its subsystems. The majority of thermal imaging systems operate with broad spectral band-passes and detect noncoherent radiation. Therefore, classical diffraction theory is adequate for analyzing the optics of incoherent electro-optical systems. The OTF of diffraction-limited optics depends on the radiation wavelength and the shape of the entrance pupil. Specifically, the OTF is the autocorrelation of the entrance pupil function with entrance pupil coordinates x and y replaced by spatial frequency coordinates ξ and η , respectively. The change of variable for the coordinate x is

$$\xi = \frac{x}{\lambda d_i},$$

where x is the autocorrelation shift in the pupil, λ is the working wavelength, and d_i is the distance from the exit pupil to the image plane. The image-spaced cutoff frequency with a full width D is

$$\xi_{\text{cutoff}} = \frac{1}{\lambda F/\#},$$

which is when the autocorrelation reaches zero. The same analytical procedure is performed for the y coordinate.

A system without wave-distortion aberrations but accepts the image faults due to diffraction is called **diffraction-limited**. The OTF for such a near perfect system is purely real and nonnegative (i.e., MTF), and represents the best performance that the system can achieve, for a given $F/\#$ and λ .

Consider the MTFs that correspond to diffraction-limited systems with square (width l) and circular (diameter D) exit pupils. When the exit pupil of the system is circular, the MTF is circularly symmetric, with ξ profile:

$$\text{MTF}(\xi) = \begin{cases} \frac{2}{\pi} \left\{ \cos^{-1}(\xi/\xi_{\text{cutoff}}) - \xi/\xi_{\text{cutoff}} [1 - (\xi/\xi_{\text{cutoff}})^2] \right\}^{1/2} & \text{for } \xi \leq \xi_{\text{cutoff}} \\ 0 & \text{otherwise} \end{cases}.$$

Optics MTF: Calculations (cont'd)

The square aperture has a linear MTF along the spatial frequency ξ given by

$$\text{MTF}(\xi, \eta) = \frac{M_{\text{img}}(\xi, \eta)}{M_{\text{obj}}(\xi, \eta)}.$$

The MTF curve for a system with appreciable geometric aberrations is upwardly bounded by the diffraction-limited MTF curve. Aberrations broaden the impulse response $h(x, y)$, resulting in a narrower, lower MTF with a smaller integrated area. The area under the MTF curve relates to the **Strehl-intensity ratio (SR)**, which measures image quality degradation, and is the irradiance at the center of the impulse response, divided by that at the center of a diffraction-limited impulse response. Small aberrations reduce the intensity at the principal maximum of the diffraction pattern, or the diffraction focus, and that of the removed light is distributed to the outer parts of the pattern. Using the **central-ordinate theorem** for the Fourier transforms, SR is written as the ratio of the area under the actual MTF curve to that under the diffraction-limited MTF curve yielding

$$\text{SR} = \frac{\iint \text{MTF}_{\text{actual}}(\xi, \eta) d\xi d\eta}{\iint \text{MTF}_{\text{diff-limited}}(\xi, \eta) d\xi d\eta}.$$

The Strehl ratio falls between 0 and 1, however, its useful range is ~ 0.8 to 1 for highly corrected optical systems. Geometrical-aberration OTF is calculated from ray-trace data by Fourier transforming the spot-density distribution without regard for diffraction effects. The OTF is obtained accurately if the aberration effects dominate the impulse-response size. The OTF of a uniform blur spot is written as

$$\text{OTF}(\xi) = \frac{J_1(\pi\xi d_{\text{blur}})}{\pi\xi d_{\text{blur}}},$$

where $J_1(\cdot)$ is the first-order Bessel function, and d_{blur} is the diameter of the blur spot. The overall optics portion MTF of an infrared system is determined by multiplying the ray-trace data MTF with the diffraction-limited MTF of the proper $F/\#$ and wavelength.

Electronics MTF: Calculations

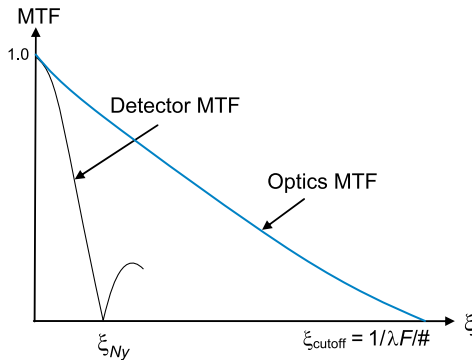
Two integral parts of modern infrared imaging systems are the electronic subsystems, which handles the signal and image processing functions, and the sensor(s) of the imaging system. Characterization of the electronic circuitry and components is well established by the temporal frequency in hertz. In order to cascade the electronic and optical subsystems, the temporal frequencies must be converted to spatial frequencies. This is achieved by dividing the temporal frequencies by the scan velocity of the imaging device. In contrast to the optical transfer function, the electronic MTF is not necessarily maximized at the origin, and can either amplify or attenuate the system MTF curve at certain spatial frequencies.

The detector MTF is expressed as

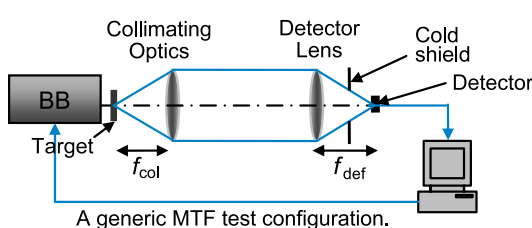
$$\text{MTF}_d(\xi, \eta) = \text{sinc}(d_h \xi) \text{sinc}(d_v \eta),$$

where d_h and d_v are the photosensitive detector sizes in the horizontal and vertical directions, respectively. Although the detector MTF is valid for all spatial frequencies, it is typically plotted up to its cutoff frequencies ($\xi = 1/d_h$ and $\eta = 1/d_v$). The spatial **Nyquist frequency** (ξ_{Ny}) of the detector array must be taken into consideration to prevent aliasing effects.

It is the combination of the optical and electronic responses that produce the overall system MTF, even though the detector MTF usually becomes the limiting factor of the electro-optical system since in general $\xi_{Ny} \ll \xi_{\text{cutoff}}$.



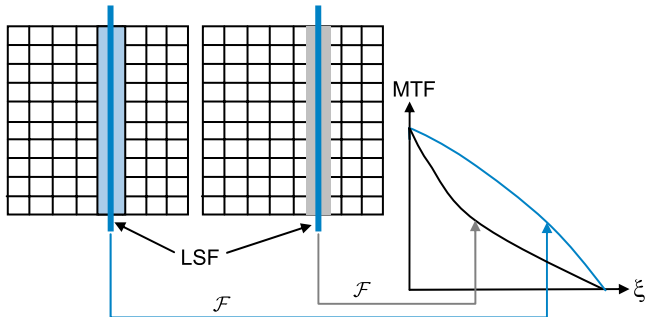
MTF Measurement Setup and Sampling Effects



All optical and electro-optical components comprising the infrared-imaging system should

be placed on a vibration-isolated optical table. The aperture of the collimator should be large enough to overfill the aperture of the system under test. The optical axis of the infrared camera has to be parallel to and centered on the optical axis of the collimator, to insure that its entrance pupil is perpendicular to the collimator optical axis. The display gain and brightness should be optimized prior to the start of the MTF measurements to assure that the display setting is not limiting the performance of the detector array.

Sampling effects alter the MTF and affect the fidelity of the image. The discrete location of the detectors in the staring array creates the sampling lattice. **Phasing effects** between the sampling lattice and the location of the target introduce problems at nearly all spatial frequencies. **Digitalization** alters signal amplitude and distorts the pulse shape. Sampling causes sensor systems like **focal plane arrays (FPAs)** to have a particular kind of shift variance (i.e., spatial phase effects); in which case, they depend on the position of the target relative to the sampling grid to measure the MTF of the system.



MTF Measurement Techniques: PSF and LSF

Different measurement techniques can be used to assess the MTF of an infrared-imaging system. These include the measurement of different types of responses such as point-spread function, line-spread function, edge-spread function, sine-target response, square-target response, and noiselike target response. All targets, except the ones that are random, should be placed in a micro-positioning mount containing three degrees of freedom (x, y, θ) to account for phasing effects.

The imaging of a point source $\delta(x, y)$ of an optical system has an energy distribution called the **point-spread function (PSF)**. The 2D Fourier transform of the PSF yields the complete 2D OTF(ξ, η) of the system in a single measurement. The absolute value of the OTF gives the MTF of the system. The impulse response technique is practically implemented by placing a small pinhole at the focal point of the collimator. If the flux passing through the pinhole produces an SNR that is below a usable value, a slit target can be placed at the focal plane of the collimating optics; the output is called the **line-spread function (LSF)**. The cross-section of the LSF is obtained by integrating the PSF parallel to the direction of the line source, because the line image is simply the summation of an infinite number of points along its length. The LSF only yields information about a single profile of the 2D OTF. Therefore, the absolute value of the Fourier transform of the LSF yields the 1D MTF(ξ, η) of the system.

To obtain other profiles of the MTF, the line target can be reoriented as desired. The slit angular subtense must be smaller than the IFOV with a value of 0.1 IFOV. The phasing effects are tested by scanning the line target relative to the sampling sensor grid until maximum and minimum signals are obtained at the sensor. The measurements are performed and recorded at different target positions, and averaging the output over all locations yields an average MTF. However, this average MTF is measured using a finite-slit aperture, in which case, this undesirable component is removed by dividing out the Fourier transform of the finite slit, yielding a more accurate MTF.

MTF Measurement Techniques: ESF and CTF

The MTF is also obtained from a **knife-edge spread response (ESF)**, the response of the system under test to an illuminated knife-edge target. There are two advantages in using this target over the line-target: it is simpler to build than a narrow slit, and there is no MTF correction. The edge is differentiated to obtain the line-spread function and is then Fourier transformed. However, the derivative operation accentuates the system noise presented in the data, which can corrupt the resulting MTF. The edge must be straight with no raggedness. To increase the SNR for both the line and edge-spread techniques, the 1D Fourier transform is averaged over all the rows of the image. In addition, reducing the system gain reduces noise, and the target signal can be increased if possible.

The MTF is also obtained by measuring the system's response to a series of sine-wave targets, where the image modulation depth is measured as a function of spatial frequency. Sinusoidal targets can be fabricated on photographic films or transparencies for the visible spectrum; however, they are not easy to fabricate for the testing of infrared systems due to materials limitations. A less expensive, more convenient target is the bar target, a pattern of alternate bright and dark bars of equal width. The square-wave response is called **contrast transfer function (CTF)**, and is a function of the **fundamental spatial frequency ξ_f** of the specific bar target under test. The CTF is measured on the peak-to-valley variation of the image irradiance, and is defined as

$$\text{CTF}(\xi_f) = \frac{M_{\text{square-response}}(\xi_f)}{M_{\text{input-square-wave}}(\xi_f)}.$$

The CTF is higher than the MTF at all spatial frequencies because of the contribution of the odd harmonics of the infinite-square wave test pattern to the modulation depth in the image. The CTF is expressed as an infinite series of MTFs. A square wave can be expressed as a Fourier-cosine series. The output amplitude of the square wave at frequency ξ_f is an infinite sum of the input cosine amplitudes modified by the system's MTF:

MTF Measurement Techniques: ESF and CTF (cont'd)

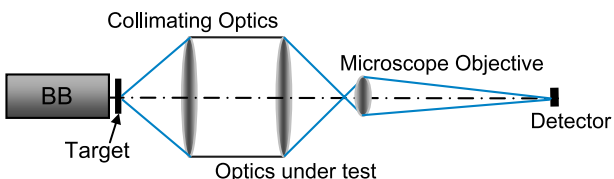
$$\text{CTF}(\xi_f) = \frac{4}{\pi} \left[\text{MTF}(\xi_f) - \frac{1}{3} \text{MTF}(3\xi_f) + \frac{1}{5} \text{MTF}(5\xi_f) - \frac{1}{7} \text{MTF}(7\xi_f) + \dots \right],$$

conversely, the MTF can be expressed as an infinite sum of CTFs as

$$\text{MTF}(\xi_f) = \frac{\pi}{4} \left[\text{CTF}(\xi_f) + \frac{1}{3} \text{CTF}(3\xi_f) - \frac{1}{5} \text{CTF}(5\xi_f) + \frac{1}{7} \text{CTF}(7\xi_f) + \dots \right].$$

Optical systems are characterized with three- and four-bar targets and not by infinite square-wave cycles. Therefore, the CTF might be slightly higher than the CTF curve for an infinite square wave. For bar targets with a spatial frequency above one-third the cutoff frequency, where the MTF approaches zero, the MTF is equal to $\pi/4$ times the measured CTF. Electronic nonlinearity, digitization effects, and sampled-scene phase effects can make these MTF and CTF measurements difficult.

The MTF of optics is measured, without including the detector MTF, by placing a microscope objective in front of the detector FPA. The microscope objective is used as a relay lens to reimaging the system's response formed by the optics under test onto the FPA with the appropriate magnification. Here, the detector is no longer the limiting component of the imaging system, since its MTF response becomes appreciably higher than the optical MTF curve. The microscope objective must be high quality to reduce degradation of the measured response function, and have high enough NA to capture the entire image-forming cone angle.



Imaging systems containing a detector FPA are nonisoplanatic, and their responses depend on the location of the deterministic targets relative to the sampling grid, introducing problems at nearly all spatial frequencies. The use of random-target techniques for measuring the MTF of a digital imaging system tends to average out the phase effects.

MTF Measurement Techniques: Noiselike Targets

Using noiselike test targets of known spatial frequency content allow measurement of shift-invariant MTF because the target information is positioned randomly with respect to the sampling sites of the digital imaging system.

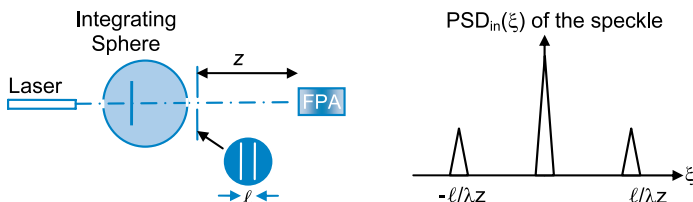
The MTF of the system is calculated because the input power density $\text{PSD}_{\text{input}}(\xi)$ of the input random pattern is known, and an accurate estimate of the output power density $\text{PSD}_{\text{output}}(\xi)$ is made from the FPA response. The MTF is then calculated from the following relationship:

$$\text{MTF}(\xi) = \sqrt{\frac{\text{PSD}_{\text{output}}(\xi)}{\text{PSD}_{\text{input}}(\xi)}}.$$

This approach is commonly used to characterize time domain electrical networks, and its application to the MTF testing of digital imaging systems provides an average of the shift variation, which eases alignment tolerances and facilitates MTF measurements at spatial frequencies beyond Nyquist.

Two different techniques are used for the generation of random targets: laser speckle and transparency-based noise targets. The former is used to characterize the MTF of FPAs alone, while the latter one is used to characterize the MTF of a complete imaging system (i.e., imaging optics together with the FPA).

A laser speckle pattern of known PSD is generated by the illustrated optical train.

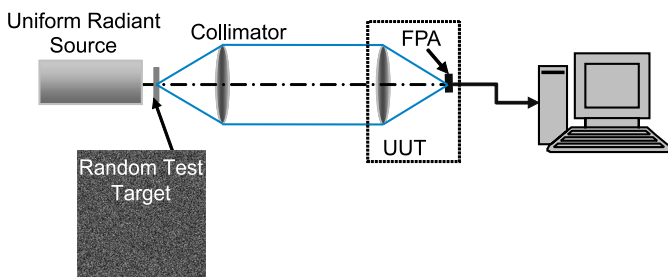


The integrating sphere produces a uniform irradiance with a spatially random phase. The aperture following the integrating sphere (typically a double slit is used), determines the $\text{PSD}_{\text{input}}(\xi)$ of the speckle pattern at the FPA, which is proportional to the aperture transmission function.

MTF Measurement Techniques: Noiselike Targets (cont'd)

The spatial frequency of the resulting narrowband speckle pattern can be tuned by changing the aperture-to-focal-plane distance z . The MTF is calculated from the relative strength of the sideband center of the $\text{PSD}_{\text{output}}(\xi)$.

To characterize a complete imaging system, a 2D uncorrelated random pattern with uniform band-limited white-noise distribution is created using a random generator computer algorithm. This random gray level pattern is printed onto a transparency and placed in front of a uniform radiant extended source, producing a 2D radiance pattern with the desired input power spectrum $\text{PSD}_{\text{input}}$.



The output spectral density is estimated by imaging the target through the optical system onto the FPA. The output data is then captured by a frame grabber and processed to yield the output power spectrum $\text{PSD}_{\text{output}}(\xi)$ as the absolute value squared of the Fourier transform of the output image data. The MTF is then calculated using the equation from the previous page.

In the infrared region, the transparency must be replaced by a random thermoscene made of a chrome deposition on an infrared material substrate. Microlithographic processes enable production of square apertures of various sizes on a 2D matrix to achieve the desirable random pattern. To avoid diffraction-induced nonlinearities of transmittance, the minimum aperture size must be five times the wavelength.

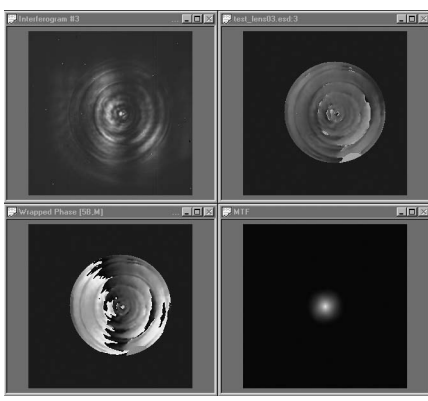
MTF Measurement Techniques: Interferometry

Common path interferometers may be employed for measuring the transfer functions of optical systems. An interferogram of the wavefront exiting the system is reduced to find the phase map. The distribution of amplitude and phase across the exit pupil contains the necessary information for calculating the OTF by pupil autocorrelation.

The performance of a lens at specific conjugates can be measured by placing the optical element in one of the arms of an interferometer. The process begins by computing a single wrapped phase map from the resultant wavefront information or **optical path difference (OPD)** exiting the pupil of the system under test.

The wrapped phase map is represented in multiples of 2π with phase values ranging from $-\pi$ to π . Removal of the 2π modulus is accomplished by using an unwrapping algorithm, thus producing an unwrapped phase map also known as the surface map. The PSF is obtained

by multiplying the conjugate Fourier transform of the surface map data (i.e., element by element multiplication of the amplitude complex function). The inverse Fourier transform of the PSF yields the complex OTF, with the modulus that corresponds to the MTF of the optical system.



In summary, the MTF is a powerful tool used to characterize imaging system's ability to reproduce signals as a function of spatial frequency. It is a fundamental parameter that determines where the limitations of performance in optical and electro-optical systems occur, and which crucial components must be enhanced to yield a better overall image quality. It guides system design, and predicts system performance.

Noise Equivalent Temperature Difference

Noise equivalent temperature difference (NETD) is the target-to-background temperature difference that produces a peak signal-to-rms-noise ratio of unity. Its analytical formula is given by:

$$\text{NETD} = \frac{4}{\pi} \left[\frac{F_{/\#}^2 \sqrt{\Delta f}}{D^* \sqrt{A_d} \partial L / \partial T} \right],$$

where Δf is the electronic bandwidth, D^* and A_{det} are respectively the normalized detectivity and the effective area of the detector, and partial derivative of the radiance with respect to temperature is the exitance contrast. This equation applies strictly to detector-limited situations.

A smaller NETD indicates better thermal sensitivity. For the best NETD, D^* is peaked near the wavelength of maximum exitance contrast of the source. A smaller $F/\#$ collects more flux, yielding a more accurate estimate NETD. A smaller electronic bandwidth yields a larger dwell time, obtaining a smaller noise voltage and lowering the NETD. A larger detector area gives a larger IFOV, collecting more flux and resulting in a better NETD. The drawback of NETD as a system-level performance descriptor is that while the thermal sensitivity improves for larger detectors, the image resolution deteriorates. Thus, while the NETD is a sufficient operational test, it cannot be applied as a designed criterion.

When the system operates under BLIP conditions, the equation for NETD becomes

$$\text{NETD}_{\text{BLIP}} = \frac{2\sqrt{2} hc}{\sqrt{\pi} \lambda} \left[\frac{F_{/\#} \sqrt{\Delta f} \sqrt{L_{\text{bkg}}}}{\sqrt{A_d} \sqrt{\eta} \partial L / \partial T} \right],$$

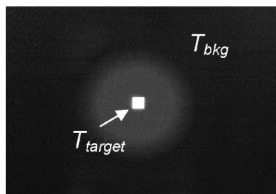
where λ is the wavelength, h is the Planck constant, c is the velocity of light in vacuum, L_{bkg} is the background radiance, and η is the quantum efficiency of the detector. Notice that the NETD is inversely proportional to the square root of the quantum efficiency and proportional to the square root of the in-band background flux. Under BLIP conditions, it has a linear dependence on $F/\#$ rather than a square dependence as in the detector-limited condition case.

NETD Measurement Technique

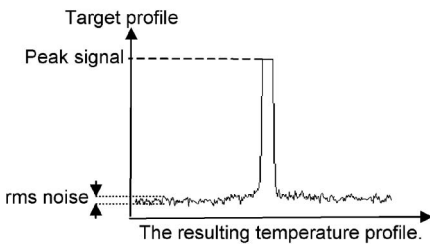
The NETD measurement is usually carried out using a square target. The size of the square must be several times the detector angular substance (i.e., several IFOV's) of the extended source to ensure that the spatial response of the system does not affect the measurement. This target is usually placed in front of an extended area blackbody source, so that the temperature difference between the square target and the background is several times the expected NETD to ensure a response that is clearly above the system noise. The peak signal and rms noise data are obtained by capturing, averaging, and taking the standard deviation of several images. The NETD is then calculated from the experimental data as follows:

$$\text{NETD} = \frac{\Delta T}{\text{SNR}},$$

where $\Delta T = T_{\text{target}} - T_{\text{bkg}}$, and the SNR is the signal-to-noise ratio of the thermal system.



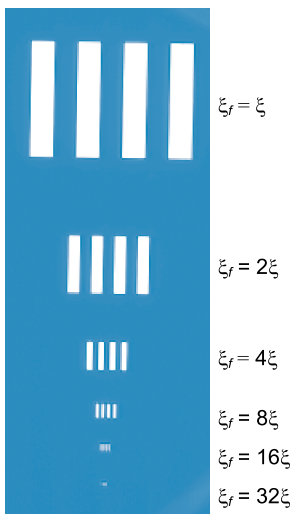
The NETD test imaged pattern



Care must be taken to ensure that the system is operating linearly and that no noise sources are included. Because of the dependence of noise on bandwidth, and to obtain the proper dwell time and bandwidth, the NETD must be measured with the system running at its full operational scan rate.

Minimum Resolvable Temperature Difference

The **minimum resolvable temperature difference (MRTD)** simultaneously characterizes both the spatial resolution and the thermal sensitivity. It is a subjective measurement for which the SNR-limited thermal sensitivity is outlined as a function of spatial frequency.



The bars and spaces of the target are blackbody radiators of different but uniform temperatures, and the bar height is seven times the bar width.

$$\xi_f = \xi$$

$$\xi_f = 2\xi$$

$$\xi_f = 4\xi$$

$$\xi_f = 8\xi$$

$$\xi_f = 16\xi$$

$$\xi_f = 32\xi$$

Conceptually, the MRTD is the image SNR required for an observer to resolve four-bar targets at several **fundamental spatial frequencies** ξ_f , so that the bars are just discernable by a trained observer with unlimited viewing time. The noise-limited rationale is essential in this case, because an infrared imaging system displays its utmost sensitivity when the highest noise is visible to the observer (i.e., gain is increased to compensate for adverse atmospheric and/or scene conditions).

These tests depend on decisions made by the observer. The results vary with training, motivation, and visual capacity, as well as the environmental setting. Because of the considerable inter- and intra-observer variability, several observers are required. The underlying distribution of observer responses must be known, so that the individual responses can be appropriately averaged together.

MRTD is a better system-performance descriptor than the MTF alone because the MTF measures the attenuation in modulation depth, without regard for a noise level. MRTD is also a more complete measurement than the NETD because it accounts for both spatial resolution and noise level. Therefore, the MRTD is a useful overall analytical and design tool that is indicative of system performance.

MRTD: Calculation

MRTD measures the ability to resolve detail imagery, and is directly proportional to the NETD and inversely proportional to the MTF:

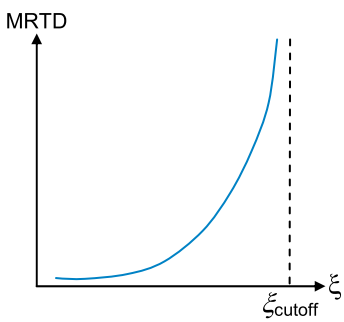
$$\text{MRTD} \propto \frac{\text{NETD} \xi_t \sqrt{\text{HIFOV} \cdot \text{VIFOV}}}{\text{MTF}(\xi_t) \sqrt{\tau_{\text{eye}} \cdot \tau_{\text{frame}}}},$$

where ξ_f is the spatial frequency of the target being observed, τ_{eye} is the integration time of the human eye, τ_{frame} is the frame time, MTF is the transfer function of the system at that particular target frequency, and HIFOV and VIFOV are the horizontal and vertical IFOV's of the system, respectively.

The derivation of an exact analytical expression for MRTD is complex because of the number of variables in the calculation; therefore, computer-aided performance models such as the NVTherm model are used. Substituting the NETD equation into the MRTD equation yields

$$\text{MRTD} \propto \frac{\xi_t \sqrt{\text{HIFOV} \cdot \text{VIFOV}}}{\text{MTF}(\xi_t) \sqrt{\tau_{\text{eye}} \cdot \tau_{\text{frame}}}} \times \frac{F_{/\#}^2 \sqrt{\Delta f}}{D^* \sqrt{A_d} \partial L / \partial T}.$$

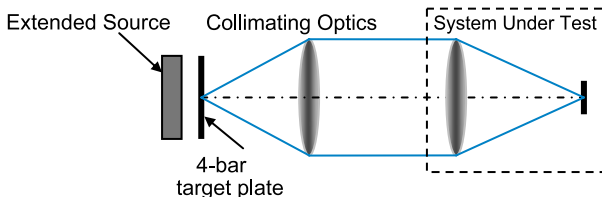
MRTD depends on the same variables as NETD (i.e., $F_{/\#}$, Δf , D^* , and radiance contrast). However, the thermal performance of the system cannot be increased by increasing the area of the detector or IFOV; the MTF decreases at higher frequencies. Therefore, the amount of ΔT required for a 4-bar target to be discernable increases as the size of the bars decrease. The MRTD increases when MTF decreases, but the MRTD increases faster due to the extra



factor ξ_f in the numerator. The effect of the observer is included in the factor $\tau_{\text{eye}} \tau_{\text{frame}}$. Increasing the frame rate gives more observations within the temporal integration time of the human eye, and then the eye-brain system tends to average out some of the noise, leading to a lower MRTD.

MRTD Measurement Technique

A generic MRTD test configuration is shown:



$$\Delta T = T_{\text{BB}} - T_{\text{target plate}}$$

The four-bar target is located in front of the blackbody source at the focal plane of the collimator to collimate the radiation from each point of the surface of the target. To achieve high-spatial frequency, the MRTD setup is mounted on a vibration-isolated optical table. Since the MRTD is a detection criterion for noisy imagery, the gain of the infrared imaging system must be set high enough that the image is noisy. Infrared imaging systems are subject to sampling effects. The MRTD does not have a unique value for each spatial frequency, but has a range of values depending on the location of the target with respect to the detector array. Therefore, the targets must be adjusted to achieve the best visibility. An observer must count the number of bars to ensure that all four are present and discernable. The targets should range from low-spatial frequencies to just past the system cutoff, and span the entire spatial frequency response.

Problems associated with the MRTD measurements include the related distance between the display screen and the observer, background brightness, and strain. The contrast sensitivity increases with background radiance; however, during the MRTD tests, the observer can adjust the system's gain and level, and monitor the brightness and contrast to optimize the image for detection criterion. Inconsistencies between the results obtained by different observers can occur, and over a long period of time, the human eye-brain sensitivity decreases, causing unreliability. The use of the MRTD is also somewhat limited because all the field scenes are spectrally selective (i.e., emissivity is a function of wavelength), while most MRTD tests are performed with extended-area blackbodies.

MRTD Measurement: Automatic Test

It is of practical interest to measure the MRTD without the need of a human observer. Automatic tests or objective tests are desirable because of an insufficient number of trained personnel and because the subjective test is time consuming. The MRTD equation can be written as

$$\text{MRTD} = \mathcal{K}(\xi_f) \frac{\text{NETD}}{\text{MTF}(\xi_f)},$$

where the constant of proportionality and any spatial-frequency-dependent terms, including the effect of the observer, are taken up into the function $\mathcal{K}(\xi_f)$. To characterize the average effects of the observer, for a given display and viewing geometry, an MRTD curve is measured for a representative sample of the system under test. Along with the MRTD data, the NETD and MTF are measured and recorded for the system. From these data, the function $\mathcal{K}(\xi_f)$ can be determined, and subsequent tests of similar systems can be performed without the observer.

A comprehensive automatic laboratory test station, which provides the means to measure the performance of an infrared imaging system, and a field-tester apparatus measuring the FLIR parameters of an Apache helicopter, is shown below.



Pictures courtesy of CI Systems, Inc.

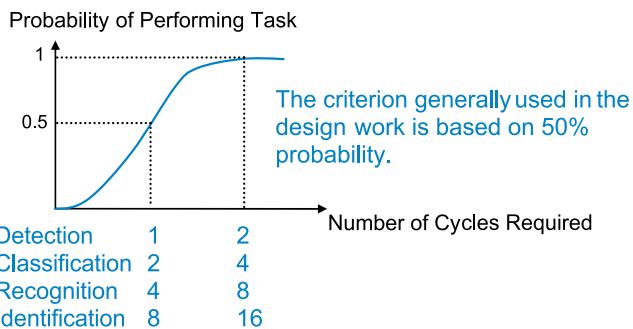
Johnson Criteria

The **Johnson criteria** accounts for both the thermal sensitivity and the spatial resolution of a thermal imaging system. It provides a way of discriminating real targets in terms of equivalent bar chart resolvability patterns.

Eight military targets and a standing man were placed in front of television imagery. Sets of square-wave patterns were placed along these targets. These square arrangements have the same apparent ΔT as the military targets and are viewed under the same conditions. The theory relating equivalent bar target resolvability to target discrimination is that the level of discrimination (i.e., detection, classification, recognition, or identification), can be predicted by determining the number of resolved cycles within the equivalent chart that would fit across the minimum dimension of the target. A more complex decision task requires finer spatial resolution.

The target remains the same in all cases, and it is portrayed as having an average apparent blackbody temperature difference ΔT between the target and the background. The image quality limitations to performance are classified in the table.

Degradation	Performance Limited	Discrimination Level
1	Random noise-limited	Detection
2	Magnification-limited	Classification
3	MTF-limited	Recognition
4	Raster-limited	Identification



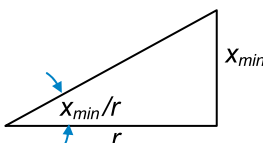
Johnson Criteria (cont'd)

Equivalent bar resolvability pattern for the fundamental degradations



Once the required numbers of cycles for a particular task are determined, the required angular spatial frequency in cycles/rad is calculated by

$$\xi = \frac{n_{\text{cycles}}}{x_{\min}/r}$$



where n_{cycles} is the number of cycles, x_{\min} is the minimum target dimension, r is the range; and therefore, x_{\min}/r is the angular subtense of the target.

To discriminate a target, two IFOVs are required per cycle of the highest spatial frequency (i.e., Nyquist sampling theorem). Therefore, the IFOV can be written in terms of the Johnson parameters as

$$\frac{1}{2 \cdot \text{FOV}} = \frac{f}{2\sqrt{A_d}} = \frac{n_{\text{cycles}}}{x_{\min}/r} \Rightarrow \frac{f}{\sqrt{A_d}} = \frac{2rn_{\text{cycles}}}{x_{\min}},$$

where f is the effective focal length of the optical system and A_d is the area of the detector.

This information allows setting the resolution requirements for the system, including the detector size, focal length of the optical system, the dimensions of the target, and the target distance.

The detection of simple geometrical targets embedded in random noise is a strong function of the SNR when all other image quality parameters are held constant. Classification is important because, for example, if a certain type of vehicle is not supposed to be in a secured area, it is not only necessary to detect the target but to classify it before firing on it. Recognition is enhanced with the area under the MTF curve and identification performance is improved by incrementing the number of lines per scans per target.

Infrared Applications

Applications for thermal sensing and thermal imaging are found in almost every aspect of the military and industrial worlds. Infrared sensing offers high-quality passive and active night vision because it produces imagery in the absence of visible light. It also provides considerable intelligence about the self-state of objects by sensing their self-emissions, indicating both surface and sub-surface conditions.

Infrared military systems enable on-board passive and active defense or offense capabilities for aircraft that could defeat or destroy incoming missiles, and providing effective shield against adversary cruise and ballistic attacks. Other applications include target designation, surveillance, target discrimination, active and passive tracking, battle-space protection, asset protection, defense satellite control, warning devices, etc. Thermal offensive weapons are particularly suited for those missions where precision, adjustability, and minimum collateral damage are required.

Infrared observations in astrophysics are important because its radiation penetrates more easily through the vast stretches of interstellar gas and dust clouds than does the visible and ultraviolet light, thus revealing regions hidden to normal telescopes.

With the development of fast, high-resolution thermal workstations, infrared thermography has become an important practical non-destructive technique for the evaluation, inspection, and quality assurance of industrial materials and structures. A typical approach consists of subjecting the work piece to a surface thermal excitation, and observing perturbations of the heat propagation within the material. This technique is capable of revealing the presence of defects by virtue of temperature distribution profile anomalies. It is attractive technique because it provides non-contact, rapid scanning, and full-inspection coverage in just milliseconds. It can be used either for qualitative or quantitative applications.

Infrared Applications (cont'd)

Some of these applications are as follows: Building diagnostics such as roofing and moisture detection; material evaluation such as hidden corrosion in metals, turbine blades and vanes blockage; plant condition monitoring such as electrical circuits, mechanical friction and insulation, gas leakage, effluent thermal plumes; and aircraft and ship-board surveyors where power generating system failures produce signatures that can be detected with IR devices.

Infrared spectroscopy is the study of the composition of organic compounds. An infrared beam is passed through a sample, and the amount of energy absorbed at each wavelength is recorded. This may be done by scanning through the spectrum with a monochromatic beam, which changes in wavelength over time, or by using a Fourier transform spectrometer to measure all wavelengths at once. For this, a transmittance or absorbance spectrum may be plotted, showing at which wavelengths the sample absorbs the infrared light, and allows an interpretation of what covalent bonds are present. Infrared spectroscopy is widely used in both research and industry as a simple and reliable technique for static and dynamic measurements, as well as quality control.

Equation Summary

Thin lens equations:

$$\frac{1}{f} = \frac{1}{p} + \frac{1}{q} \text{ Gaussian} \quad x_{\text{obj}}x_{\text{img}} = f^2 \text{ Newtonian}$$

Thick lens equation:

$$\frac{1}{f_{\text{eff}}} = (n - 1) \left[\frac{1}{R_1} - \frac{1}{R_2} + \frac{(n - 1)t}{n} \frac{1}{R_1 R_2} \right]$$

Lateral or transverse magnification:

$$M = -\frac{q}{p} = \frac{h_{\text{img}}}{h_{\text{obj}}}$$

Area or longitudinal magnification:

$$M^2 = \frac{A_{\text{img}}}{A_{\text{obj}}} = \left(-\frac{q}{p} \right)^2$$

F-number and numerical aperture:

$$F/\# \equiv \frac{f_{\text{eff}}}{D_{\text{enp}}} \quad \text{NA} \equiv n \sin \alpha$$

$$F/\# = \frac{1}{2 \tan(\sin^{-1} \text{NA})} \quad \text{NA} = \sin \left(\tan^{-1} \frac{1}{2F/\#} \right)$$

$$F/\# \cong \frac{1}{2 \text{NA}} \quad \text{paraxial approximation}$$

Field-of-view:

$$\text{FOV}_{\text{half-angle}} = \theta_{1/2} = \left| \tan^{-1} \frac{h_{\text{obj}}}{p} \right| = \left| \tan^{-1} \frac{h_{\text{img}}}{q} \right|$$

$$\text{FOV}_{\text{full-angle}} = \theta = \frac{d}{f} \quad \text{paraxial approximation}$$

Diffraction-limited expressions:

$$d_{\text{diff}} = 2.44 \lambda F/\# \text{ blur spot} \quad \beta = 2.44 \frac{\lambda}{D} \text{ angular blur}$$

Refractive index:

$$n = \frac{c}{v}$$

Law of Reflection:

$$\theta_i = \theta_r$$

Equation Summary (cont'd)

Snell's law:

$$n_1 \sin \theta_i = n_2 \sin \theta_t$$

Fresnel equation (normal incidence):

$$\rho = \left(\frac{n_2 - n_1}{n_1 + n_2} \right)^2 \quad \tau = \frac{4n_1 n_2}{(n_1 + n_2)^2}$$

Internal transmittance

$$\tau_{\text{int}} = \frac{\phi(z)}{\phi_{\text{inc}}} = e^{-\alpha z}$$

External transmittance:

$$\tau_{\text{ext}} = \tau^2 e^{-\alpha z} = \tau^2 \tau_{\text{internal}}$$

Reciprocal relative dispersion or Abbe number:

$$V = \frac{n_{\text{mean}} - 1}{\Delta n} = \frac{n_{\text{mean}} - 1}{n_{\text{final}} - n_{\text{initial}}}$$

Relative partial dispersion:

$$P = \frac{n_{\text{mean}} - n_{\text{initial}}}{n_{\text{final}} - n_{\text{initial}}}$$

Solid angle equations:

$$\Omega = 4\pi \sin^2 \frac{\theta_{\max}}{2}$$

$$\Omega \cong \frac{a}{r^2} \quad a \ll r^2 \quad \text{paraxial approximation}$$

Fundamental equation of radiation transfer:

$$\partial^2 \phi = L \partial A_s \cos \theta_s \partial \Omega_d$$

$$\phi \cong L A_s \cos \theta_s \Omega_d \quad \text{finite quantities}$$

Intensity:

$$I = \frac{\partial \phi}{\partial \Omega_d} \cong \frac{\phi}{\Omega_d} \quad I = \frac{\partial \phi}{\partial \Omega_d} = L A_s \cos \theta_s$$

Exitance and Radiance:

$$M = \frac{\partial \phi}{\partial A_s} \cong \frac{\phi}{A_s} \quad M = \frac{\partial \phi}{\partial A_s} = \pi L \quad \text{Lambertian radiator}$$

Equation Summary (cont'd)

Irradiance:

$$E_{\text{extended source}} = \frac{\partial \phi}{\partial A_d} = \pi L \sin^2 \theta = \frac{\pi L}{4F_{/\#}^2 + 1}$$

$$E_{\text{point source}} = \frac{\phi}{A_d} \times 0.84 = \frac{0.84I\Omega_{\text{optics}}}{\frac{\pi}{4}d_{\text{diff}}^2} = \frac{0.84I\Omega_{\text{optics}}}{\frac{\pi}{4}[2.44\lambda(F/\#)]^2}$$

$A\Omega$ product or optical invariant:

$$A_s \Omega_d = A_d \Omega_s$$

Planck's radiation law:

$$M_{e,\lambda} = \frac{2\pi hc^2}{\lambda^5} \frac{1}{\exp(hc/\lambda kT) - 1} \quad [\text{Watt/cm}^2 \cdot \mu\text{m}]$$

$$M_{p,\lambda} = \frac{2\pi c}{\lambda^4} \frac{1}{\exp(hc/\lambda kT) - 1} \quad [\text{photon/sec} \cdot \text{cm}^2 \cdot \mu\text{m}]$$

Rayleigh-Jeans radiation law $\frac{hc}{\lambda kT} \ll 1$:

$$M_{e,\lambda} \cong \frac{2\pi ckT}{\lambda^4}$$

$$M_{p,\lambda} \cong \frac{2\pi kT}{\lambda^3 h}$$

Wien's radiation law $\frac{hc}{\lambda kT} \gg 1$:

$$M_{e,\lambda} \cong \frac{2\pi hc^2}{\lambda^5} \exp\left(-\frac{hc}{\lambda kT}\right) \quad M_{p,\lambda} \cong \frac{2\pi c}{\lambda^4} \exp\left(-\frac{hc}{\lambda kT}\right)$$

Stefan-Boltzmann law:

$$M_e(T) = \sigma_e T^4 \quad \sigma_e = 5.7 \times 10^{-12} \text{ W/cm}^2 \text{K}^4$$

$$M_p(T) = \sigma_p T^3 \quad \sigma_p = 1.52 \times 10^{-11} \text{ photons/sec} \cdot \text{cm}^2 \cdot \text{K}^3$$

Wien's displacement law:

$$\lambda_{\max,e} T = 2898 \text{ } [\mu\text{m} \cdot \text{K}] \quad \lambda_{\max,p} T = 3662 \text{ } [\mu\text{m} \cdot \text{K}]$$

Peak exitance contrast:

$$\lambda_{\text{peak-contrast},e} T = 2410 \text{ } [\mu\text{m} \cdot \text{K}]$$

Emissivity:

$$\varepsilon(\lambda, T) = \frac{M_{\lambda,\text{source}}(\lambda, T)}{M_{\lambda,BB}(\lambda, T)}$$

Equation Summary (cont'd)

Kirchhoff's law:

$$\begin{aligned}\text{Integrated absorptance} &= \alpha(\lambda, T) \equiv \varepsilon(\lambda, T) \\ &= \text{integrated emittance}\end{aligned}$$

Power Spectral Density:

$$\text{PSD} = N(f) = \mathcal{F}\{c_n(\tau)\} = \int_{-\infty}^{\infty} c_n(\tau) e^{-j2\pi f \tau} d\tau$$

Noise-equivalent bandwidth:

$$\text{NE}\Delta f \equiv \frac{1}{G^2(f_0)} \int_{-\infty}^{\infty} |G(f)|^2 df \quad \text{NE}\Delta f = \frac{1}{2\tau} \quad \text{square function}$$

$$\text{NE}\Delta f = \frac{1}{4\tau} \quad \text{exponential function}$$

Shot noise:

$$i_{n,\text{shot}} = \sqrt{2q\bar{i}\Delta f}$$

Johnson noise:

$$v_{n,j} = \sqrt{4kT R \Delta f} \quad i_{n,j} = \sqrt{\frac{4kT \Delta f}{R}}$$

$$i_{n,j} = \sqrt{i_d^2 + i_L^2} = \sqrt{4k\Delta f \left[\frac{T_d}{R_d} + \frac{T_L}{R_L} \right]} \quad \text{for cryogenic detector conditions}$$

1/f noise:

$$i_{n,f} = \sqrt{\mathcal{K} \frac{\bar{i}^\alpha \Delta f}{f^\beta}}$$

Temperature Noise:

$$\overline{\Delta T^2} = \frac{4kKT^2}{K^2 + (2\pi f)^2 C^2}$$

Responsivity (frequency, spectral, blackbody, and \mathcal{W} -factor (see page 56)):

$$|\mathcal{R}_v(f)| = \frac{v_0 \tau}{\sqrt{1 + (2\pi f \tau)^2}}$$

$$\mathcal{R}_v(\lambda) = \frac{v_{\text{sig}}}{\phi_{\text{sig}}(\lambda)} \quad \mathcal{R}_i(\lambda) = \frac{i_{\text{sig}}}{\phi_{\text{sig}}(\lambda)}$$

Equation Summary (cont'd)

$$\begin{aligned}\mathcal{R}_{v,e}(\lambda) &= \mathcal{R}_{v,e}(\lambda_{\text{cutoff}}) \frac{\lambda}{\lambda_{\text{cutoff}}} \\ \mathcal{R}(T) &= \frac{\mathcal{R}_v(\lambda_{\text{cutoff}})}{\lambda_{\text{cutoff}}} \int_0^{\lambda_{\text{cutoff}}} M_{e,\lambda}(\lambda) \lambda d\lambda \\ \mathcal{W}(\lambda_{\text{cutoff}}, T) &= \frac{\mathcal{R}_v(\lambda_{\text{cutoff}})}{\mathcal{R}(T)} = \frac{\sigma T^4}{\frac{1}{\lambda_{\text{cutoff}}} \int_0^{\lambda_{\text{cutoff}}} M_{e,\lambda}(\lambda) \lambda d\lambda} \\ &= \frac{\sigma T^4}{\frac{hc}{\lambda_{\text{cutoff}}} \int_0^{\lambda_{\text{cutoff}}} M_{p,\lambda}(\lambda) d\lambda}\end{aligned}$$

Noise Equivalent Power (NEP):

$$\text{NEP} = \frac{v_n}{\mathcal{R}_v} = \frac{v_n}{v_{\text{sig}}/\phi_{\text{sig}}} = \frac{\phi_{\text{sig}}}{\text{SNR}} \quad [\text{watt}]$$

Specific or normalized detectivity (D^*):

$$D^* = \frac{\sqrt{A_d \Delta f}}{\text{NEP}} = \frac{\sqrt{A_d \Delta f}}{\phi_d} \text{SNR} = \frac{\sqrt{A_d \Delta f}}{v_n} \mathcal{R}_v \quad [\text{cm} \sqrt{\text{Hz}}/\text{watt}]$$

D^{} :**

$$D^{**} = \sin \theta D^*$$

Photovoltaic detectors under BLIP conditions:

$$\text{SNR}_{\text{PV}} = \frac{\phi_{e,\text{sig}} \eta q \frac{\lambda}{hc}}{\sqrt{2q^2 \phi_{e,\text{bkg}} \eta \frac{\lambda}{hc} \Delta f}}$$

$$\text{NEP}_{\text{PV,BLIP}}(\lambda) = \sqrt{\frac{hc}{\lambda} \frac{2\phi_{e,\text{bkg}} \Delta f}{\eta}}$$

$$\begin{aligned}D_{\text{PV,BLIP}}^*(\lambda) &= \frac{\lambda_{\text{cutoff}}}{hc} \sqrt{\frac{\eta}{2 \int_0^{\lambda_{\text{cutoff}}} E_{\text{bkg}}(\lambda) d\lambda}} \\ &= F_{/\#} \frac{\lambda_{\text{cutoff}}}{hc} \sqrt{\frac{2\eta}{\pi \int_0^{\lambda_{\text{cutoff}}} L_{\text{bkg}}(\lambda) d\lambda}}\end{aligned}$$

Equation Summary (cont'd)

Photovoltaic detectors under JOLI conditions:

$$\text{SNR}_{\text{PV,JOLI}} = \frac{q\eta\phi_{e,\text{sig}}\frac{\lambda}{hc}}{4k\Delta f\left(\frac{T_d}{R_d} + \frac{T_f}{R_f}\right)} \cong \frac{q\eta\phi_{e,\text{sig}}\frac{\lambda}{hc}}{4k\Delta f\frac{T_d}{R_d}} \quad R_f \gg R_d$$

$$D_{\text{PV,JOLI}}^* = \frac{\lambda q\eta}{2hc} \sqrt{\frac{R_d A_d}{kT_d}}$$

Generation recombination noise:

$$i_{n,G/R} = 2qG\sqrt{\eta E_p A_d \Delta f + g_{th} \Delta f} \cong 2qG\sqrt{\eta E_p A_d \Delta f}$$

$$i_{n,G/R} = \sqrt{2}i_{n,\text{shot}}G$$

Photoconductive detectors under BLIP conditions:

$$\text{NEP}_{\text{PC,BLIP}} = \frac{2hc}{\lambda G} \sqrt{\frac{E_{\text{bkg}} A_d \Delta f}{\eta}}$$

$$D_{\text{PC,BLIP}}^* = \frac{\lambda}{2hc} G \sqrt{\frac{\eta}{E_{\text{bkg}}}}$$

Photoconductive detectors under JOLI conditions:

$$\text{NEP}_{\text{PC,JOLI}} \equiv \frac{i_j}{\mathcal{R}_{i,\text{PC}}} = \frac{\sqrt{4k\Delta f T / R_{\text{eq}}}}{\frac{\lambda q\eta}{hc} G}$$

$$D_{\text{PC,JOLI}}^* = \frac{\lambda q\eta}{2hc} G \sqrt{\frac{R_{\text{eq}} A_d}{kT}}$$

Pyroelectric detectors:

$$\mathcal{R}_i = \frac{A_d R_{th} \mathbf{p} \varepsilon \omega}{\sqrt{1 + \omega^2 \tau_{th}^2}} \quad \mathcal{R}_v = \frac{A_d R_d R_{th} \mathbf{p} \varepsilon \omega}{\sqrt{1 + \omega^2 \tau_{th}^2} \sqrt{1 + \omega^2 (R_d C_d)^2}}$$

$$\text{NEP} = \frac{v_{\text{johson}}}{\mathcal{R}_v} = \frac{\sqrt{4kT \Delta f} \sqrt{1 + \omega^2 \tau_{th}^2} \sqrt{1 + \omega^2 (R_d C_d)^2}}{A_d \sqrt{R_d} R_{th} \mathbf{p} \varepsilon \omega}$$

$$D^* = \frac{\sqrt{A_d^3 R_d} R_{th} \mathbf{p} \varepsilon \omega}{\sqrt{4kT} \sqrt{1 + \omega^2 \tau_{th}^2} \sqrt{1 + \omega^2 (R_d C_d)^2}}$$

Equation Summary (cont'd)

Bolometer detectors:

$$\mathcal{R}_v = \frac{\alpha \varepsilon v_{\text{bias}}}{2K \sqrt{1 + \omega^2 \tau_{th}^2}}$$

$$\text{NEP} = \frac{4K \sqrt{1 + \omega^2 \tau_{th}^2} \sqrt{kTR_d \Delta f}}{\alpha \varepsilon v_{\text{bias}}}$$

$$D^* = \frac{\alpha \varepsilon v_{\text{bias}} \sqrt{A_d}}{4K \sqrt{1 + \omega^2 \tau_{th}^2} \sqrt{kTR_d}}$$

Thermoelectric detectors:

$$\mathcal{R}_v = \frac{\varepsilon \Theta N}{K \sqrt{1 + \omega^2 \tau_{th}^2}}$$

Scanning and Staring Systems:

$$\text{SNR} \propto \sqrt{\text{number of sensor elements}} = \sqrt{n_d}$$

Range equation:

$$r = \sqrt{\frac{\pi D_{\text{opt}} \tau_{\text{opt}}}{4F/\#}} \sqrt{I \tau_{\text{atm}}} \sqrt{D^*} \sqrt{\frac{1}{\text{SNR} \sqrt{\Omega_d \Delta f}}}$$

$$r_{\text{BLIP}} = \sqrt{\frac{\pi D_{\text{opt}} \tau_{\text{opt}}}{4}} \sqrt{I \tau_{\text{atm}}} \frac{\lambda}{hc} \sqrt{\frac{2\eta}{\pi L_{\text{bkg}}}} \sqrt{\frac{1}{\text{SNR} \sqrt{\Omega_d \Delta f}}}$$

Noise equivalent irradiance (NEI)

$$\text{NEI} = \frac{4F/\# \sqrt{\Omega_d \Delta f}}{\pi D_{\text{opt}} D^* \tau_{\text{opt}} \tau_{\text{atm}}}$$

$$\text{NEI}_{\text{BLIP}} = \frac{4hc}{\lambda A_{\text{opt}} \tau_{\text{opt}} \tau_{\text{atm}}} \sqrt[4]{\frac{L_{\text{bkg}} \Omega_d \Delta f}{2\pi\eta}}$$

Modulation depth or contrast:

$$M = \frac{A_{\max} - A_{\min}}{A_{\max} + A_{\min}}$$

Equation Summary (cont'd)

Optics MTF—calculations (square & circular exit pupils):

$$\text{MTF}(\xi, \eta) = \frac{M_{\text{img}}(\xi, \eta)}{M_{\text{obj}}(\xi, \eta)}$$

$$\text{MTF}(\xi) = \begin{cases} \frac{2}{\pi} \left\{ \cos^{-1}(\xi/\xi_{\text{cutoff}}) - \xi/\xi_{\text{cutoff}} [1 - (\xi/\xi_{\text{cutoff}})^2] \right\}^{1/2} \\ \quad \text{for } \xi \leq \xi_{\text{cutoff}} \\ 0 \quad \text{otherwise} \end{cases}$$

Detector MTF—calculation:

$$\text{MTF}_d(\xi, \eta) = \text{sinc}(d_h \xi) \text{sinc}(d_v \eta)$$

MTF Measurement techniques:

Point spread function response:

$$\text{MTF}(\xi, \eta) = |\mathcal{F}\{\text{PSF}\}|$$

Line spread function response:

$$\text{MTF}(\xi) = |\mathcal{F}\{\text{LSF}\}|$$

Edge spread function response:

$$\frac{d(\text{ESF})}{dx} = \text{LSF}$$

Bar target response:

$$\text{CTF}(\xi_f) = \frac{M_{\text{square-response}}(\xi_f)}{M_{\text{input-square-wave}}(\xi_f)}$$

$$\text{CTF}(\xi_f) = \frac{4}{\pi} \left[\text{MTF}(\xi_f) - \frac{1}{3} \text{MTF}(3\xi_f) + \frac{1}{5} \text{MTF}(5\xi_f) - \frac{1}{7} \text{MTF}(7\xi_f) + \dots \right]$$

$$\text{MTF}(\xi_f) = \frac{\pi}{4} \left[\text{CTF}(\xi_f) + \frac{1}{3} \text{CTF}(3\xi_f) - \frac{1}{5} \text{CTF}(5\xi_f) + \frac{1}{7} \text{CTF}(7\xi_f) + \dots \right]$$

Random noise target response:

$$\text{MTF}(\xi) = \sqrt{\frac{\text{PSD}_{\text{output}}(\xi)}{\text{PSD}_{\text{input}}(\xi)}}$$

Equation Summary (cont'd)

Strehl intensity ratio (SR):

$$\text{SR} = \frac{\iint \text{MTF}_{\text{actual}}(\xi, \eta) d\xi d\eta}{\iint \text{MTF}_{\text{diff-limited}}(\xi, \eta) d\xi d\eta}$$

Noise Equivalent Temperature Difference (NETD):

$$\text{NETD} = \frac{4}{\pi} \left[\frac{F_{/\#}^2 \sqrt{\Delta f}}{D^* \sqrt{A_d} \partial L / \partial T} \right]$$

$$\text{NETD}_{\text{BLIP}} = \frac{2\sqrt{2} hc}{\sqrt{\pi}} \frac{\lambda}{\lambda} \left[\frac{F_{/\#} \sqrt{\Delta f} \sqrt{L_{\text{bkg}}}}{\sqrt{A_d} \sqrt{\eta} \partial L / \partial T} \right]$$

$$\text{NETD} = \frac{\Delta T}{\text{SNR}}$$

Minimum Resolvable Temperature Difference (MRTD):

$$\begin{aligned} \text{MRTD} &\propto \frac{\xi_t \sqrt{\text{HIFOV} \cdot \text{VIFOV}}}{\text{MTF}(\xi_t) \sqrt{\tau_{\text{eye}} \cdot \tau_{\text{frame}}}} \times \frac{F_{/\#}^2 \sqrt{\Delta f}}{D^* \sqrt{A_d} \partial L / \partial T} \\ &= \mathcal{K}(\xi_f) \frac{\text{NETD}}{\text{MTF}(\xi_f)} \end{aligned}$$

Johnson criteria:

$$\frac{f}{\sqrt{A_d}} = \frac{2rn_{\text{cycles}}}{x_{\min}}$$

Bibliography

- J. E. Greivenkamp, *Field Guide to Geometrical Optics*, SPIE Press, 2004.
- M. Bass, *Handbook of Optics*, Vol. I & II, McGraw-Hill, New York, 1995.
- E. Hecht and A. Zajac, *Optics*, Addison-Wesley, Massachusetts, 1974.
- F. A. Jenkins and H. E. White, *Fundamentals of Optics*, McGraw-Hill, New York, 1981.
- M. Born and E. Wolf, *Principles of Optics*, Pergamon Press, New York, 1986.
- W. J. Smith, *Modern Optical Engineering*, McGraw-Hill, New York, 2000.
- J. M. Lloyd, *Thermal Imaging Systems*, Plenum, New York, 1975.
- R. D. Hudson, *Infrared System Engineering*, Wiley, New York, 1969.
- E. L. Dereniak and G. D. Boreman, *Infrared Detectors and Systems*, John Wiley & Sons, New York, 1996.
- W. L. Wolfe and G. J. Zissis, *The Infrared Handbook*, Infrared Information Analysis (IRIA) Center, 1989.
- G. D. Boreman, *Fundamentals of Electro-Optics for Electrical Engineers*, SPIE Press, 1998.
- G. D. Boreman, *Modulation Transfer Function in Optical and Electro-Optical Systems*, SPIE Press, 2001.
- R. W. Boyd, *Radiometry and the Detection of Optical Radiation*, Wiley, New York, 1983.
- R. H. Kingston, *Detection of Optical and Infrared Radiation*, Springer-Verlag, New York, 1979.

Bibliography

- R. J. Keyes, "Optical and infrared detectors," *Topics in Applied Physics*, Vol. 19, Springer-Verlag, New York, 1980.
- W. L. Wolfe, *Introduction to Infrared Systems Design*, SPIE Press, 1996.
- G. C. Holst, *Testing and Evaluation of Infrared Imaging Systems*, JCD Publishing, 1993.
- G. C. Holst, *Common Sense Approach to Thermal Imaging Systems*, SPIE Press, 2000.
- J. D. Gaskill, *Linear Systems, Fourier Transforms, and Optics*, Wiley, New York, 1978.
- J. W. Goodman, *Introduction to Fourier Optics*, McGraw Hill, New York, 1968.
- W. Wittenstain, J. C. Fontanella, A. R. Newbery, and J. Baars, "The definition of OTF and the measurement of aliasing for sampled imaging systems," *Optica Acta*, Vol. **29**, pp. 41–50 (1982).
- S. K. Park, R. Schwengerdt, and M. Kaczynski, "MTF for sampled imaging systems," *Applied Optics*, Vol. **23**, pp. 2572–2582 (1984).
- S. E. Reinchenbach, S. K. Park, and R. Narayanswamy, "Characterizing digital image acquisition devices," *Opt. Eng.*, Vol. **30**(2), pp. 170–177 (1991).
- A. Daniels, G. D. Boreman, A. D. Ducharme, and E. Sapir, "Random transparency targets for MTF measurement in the visible and infrared," *Opt. Eng.*, Vol. **34**(3), pp. 860–868, March 1995.
- G. D. Boreman and A. Daniels, "Use of spatial noise targets in image quality assessment," (invited), *Proceedings of International Congress of Photographic Science*, pp. 448–451, 1994.

Bibliography

- A. Daniels and G. D. Boreman, "Diffraction Effects of infrared halftone transparencies," *Infrared Phys. Technol.*, Vol. **36**(2), pp. 623–637, July 1995.
- A. D. Ducharme and G. D. Boreman, "Holographic elements for modulation transfer function testing of detector arrays, *Opt. Eng.*, Vol. **34**(8), pp. 2455–2458, August 1995.
- M. Sensiper, G. D. Boreman, and A. D. Ducharme, "MTF testing of detector arrays using narrow-band laser speckle," *Opt. Eng.*, Vol. **32**(2), pp. 395–400 (1993).
- G. D. Boreman, Y. Sun, and A. B. James, "Generation of random speckle with an integrating sphere," *Opt. Eng.*, Vol. **29**(4), pp. 339–342 (1993).

Index

- 1/f noise, 52, 106
 Δf , 46
 Abbe number, 19
 absorption, 15, 21
 absorption coefficient, 15
 advantage, 72
 afocal systems, 10
 aluminum, 38
 angular magnification, 10
 $A\Omega$ product or optical invariant, 26, 105
 aperture stop (AS), 6
 area or longitudinal magnification, 4, 103
 assumption, 72
 astronomical telescope, 10
 autocorrelation, 44
 axial ray, 6
 back focal length (*b.fl.*), 5
 background-limited infrared photodetector (BLIP), 49, 63
 blackbody (BB), 30
 blackbody responsivity $\mathcal{R}(T, f)$, 56
 blur spots, 12
 bolometer, 42, 66
 bolometer detectors, 109
 brass, 38
 brick, 38
 brightness temperature (T_b), 39
 carbon, 38
 cardinal points, 5
 cavity radiation, 30
 central-ordinate theorem, 84
 chief ray, 6
 cold shield, 11
 cold stop, 11
 cold-stop efficiency, 11
 color temperature (T_c), 40
 common path interferometers, 92
 concrete, 38
 contrast, 2
 contrast transfer function (CTF), 88
 converging beam scanner, 70
 copper, 38
 cryogenic temperatures, 11
 current responsivity, 53
 D^{**} , 61, 107
 $D_{PV, BLIP}^*$, 61
 detection, warning, or go-no-go systems, 75
 detectivity, 42
 detector MTF—calculation, 110
 detector output voltage, 56
 Dewar, 11
 diameter, 7
 diffraction, 12
 diffraction limited, 12, 83
 diffraction-limited expressions, 103
 digitization, 86
 dispersion, 19
 durable, protected, or hard coated, 17
 dwell time (τ_{dwell}), 70
 effective focal lengths, 5
 electromagnetic radiation, 1
 electromagnetic spectrum, 1
 emission, 21
 emissivity, 36, 38, 105
 enhanced, 17
 enlarging lenses, 9
 entrance pupil (D_{enp}), 6
 erecting telescope, 10
 exit pupil (D_{exp}), 6
 exitance and radiance, 24, 104
 extended-area source, 28
 external transmittance, 16, 104

Index (cont'd)

- F-number and numerical aperture, 103
F-number ($F/\#$), 7
 F_F and F_B , front and back focal points, 5
 field lens, 11
 field stop, 8
 field-of-view (FOV), 2, 8, 103
 first and second principal points P_o and P_i , 5
 flux, 24
 flux collection efficiency, 2
 flux transfer, 8
 focal plane arrays (FPAs), 86
 footprint, 8
 frequency range, 1
 Fresnel equation (normal incidence), 15, 104
 front focal length ($f.f.l$), 5
 fundamental equation of radiation transfer, 104
 fundamental spatial frequency ξ_f , 88, 95
 Galilean telescope, 10
 Gaussian lens equation, 3
 generation-recombination (G/R) noise, 50, 108
 glass, 38
 Golay cells, 42
 gold, 38
 good absorbers are good emitters, 37
 hard coated, 17
 human skin, 38
 image irradiance, 28
 image quality, 2, 8, 80
 immersion lens, 11
 impulse response, 80
 index of refraction, 11
 infrared-imaging systems, 2
 instantaneous field-of-view (IFOV), 70
 intensity, 24, 28, 104
 internal transmittance, 16, 104
 iron, 38
 irradiance, 24, 105
 isoplanatism, 81
 Johnson criteria, 79, 99, 111
 Johnson noise, 51, 106
 Johnson-limited noise performance (JOLI), 61, 63
 Keplerian telescope, 10
 Kirchhoff's law, 37, 106
 knife-edge spread response (ESF), 88
 lacquer, 38
 Lambertian disc, 28
 Lambertian radiator, 25
 lateral or transverse magnification, 4, 103
 law of reflection, 15, 103
 line-spread function (LSF), 87
 linearity, 81
 longitudinal magnification, 4
 lubricant, 38
 magnification, 8
 marginal ray, 6
 material dispersion, 15
 mean, 43
 metals and other oxides, 38
 minimum resolvable temperature difference (MRTD), 79, 95, 111
 mirrors, 16
 modulation depth or contrast, 109

Index (cont'd)

- modulation transfer function (MTF), 79
 MTF measurement techniques, 110
- narcissus effect, 14
 $\text{NE}\Delta f$, 46
 Newtonian lens equation, 3
 nickel, 38
 nodal points N_o and N_i , 5
 noise equivalent irradiance (NEI), 78, 109
 noise equivalent power (NEP), 57, 107
 noise equivalent temperature difference (NETD), 79, 93, 111
 noise-equivalent bandwidth, 46, 106
 noise-equivalent power, 42
 nonmetallic materials, 38
 numerical aperture (NA), 7
 Nyquist frequency, 85
- objective lens, 9
 oil, 38
 open circuit, 59
 optical aberrations, 8, 12
 optical axis, 3
 optical invariant, 26
 optical path difference (OPD), 92
 optical transfer function (OTF), 81
 optics MTF—calculations (square & circular exit pupils), 110
- paint, 38
 paper, 38
 parallel beam scanner, 70
 parallel scanning, 73
 paraxial approximation, 3
 peak exitance contrast, 105
- phase transfer function (PTF), 81
 phasing effects, 86
 photoconductive (PC) detector, 62
 photoconductive detector under BLIP conditions, 108
 photoconductive detector under JOLI conditions, 108
 photoconductor, 62, 63
 photodiode, 59
 photon detector, 42
 photons, 1
 photovoltaic detectors under BLIP conditions, 107
 photovoltaic detectors under JOLI conditions, 108
 photovoltaic (PV) detectors, 59
 Planck's equation, 2
 Planck's radiation equation, 34
 Planck's radiation law, 105
 plaster, 38
 point source, 24, 28
 point-spread function (PSF), 87
 power spectral density, 106
 power spectral density (PSD), 44, 106
 primary and secondary principal planes, 5
 protected, 17
 pyroelectric, 42
 pyroelectric detector, 64, 108
- \mathcal{R}_i , 53
 \mathcal{R}_v , 53
 radiance, 25, 28
 radiation temperature (T_{rad}), 39

Index (cont'd)

- radiation transfer, 25
 radiometry, 23
 range equation, 75, 109
 Rayleigh-Jeans radiation law, 34, 105
 reciprocal relative dispersion or Abbe number, 19, 104
 reflection loss, 15
 refractive index n , 15, 103
 relative partial dispersion, 19, 104
 resolution, 2
 responsive time constant, 54
 responsivity (frequency, spectral, blackbody, and K -factor), 42, 53, 106
 reverse bias, 59
 rupture modulus, 15
 sampling effects, 86
 sand, 38
 scan noise, 14
 scanning and staring systems, 74, 109
 scattered flux density, 21
 search systems, 75
 Seebeck coefficient Θ , 69
 self-radiation, 2
 shading, 14
 shift invariance, 81
 short circuit, 59
 shot noise, 48, 106
 signal-to-noise ratio (SNR), 23, 49
 silver, 38
 Snell's law, 3, 15, 104
 soil, 38
 solid angle equations, 104
 solid angle " Ω ", 22
 spatial frequency, 80
 spatial resolution, 79
 specific or normalized detectivity (D^*), 58, 107
 spectral radiometric quantities, 30
 spectral responsivity $\mathcal{R}(\lambda, f)$, 55
 stainless steel, 38
 standard deviation, 43
 staring systems, 74
 steel, 38
 Stefan-Boltzmann constant, 33
 Stefan-Boltzmann law, 33, 34, 105
 steradians [ster], 22
 stray radiation, 11
 Strehl intensity ratio (SR), 84, 111
 superconductors, 42
 telecentric stop, 6
 telecentric system, 6
 temperature, 2
 temperature noise, 52, 106
 terrestrial telescope, 10
 thermal detector, 42
 thermal conductivity, 15
 thermal equations in photon-derived units, 34
 thermal expansion, 15
 thermal imaging system (TIS), 79
 thermal noise, 11
 thermal sensitivity, 79
 thermistors, 66
 thermocouple, 69
 thermoelectric detector, 69, 109
 thermopile, 42, 69
 thick lens equation, 103
 thin lens, 3
 thin lens equation, 103
 through-put, 26
 time delay and integration (TDI), 72
 tin, 38
 transfer function, 80
 transmission range, 15
 type of radiation, 1

Index (cont'd)

- variance or mean-square, 43
voltage responsivity, 53
water, 38
water-erosion resistance, 15
wavelength range, 1
- white noise, 45
Wien's displacement law, 33, 34, 105
Wien's radiation law, 34, 105
wood, 38



Arnold Daniels is a senior engineer with extensive experience in the development of advanced optical and electro-optical systems. His areas of expertise include applications for infrared search and imaging systems, infrared radiometry testing and measurements, thermographic nondestructive testing, Fourier analysis, image processing, data acquisition systems, precision optical alignment, and adaptive optics. He received a B.S. in Electro-Mechanical engineering from the University Autonomous of Mexico and a B.S. in Electrical engineering from the Israel Institute of Technology (Technion). He earned an M.S. in Electrical engineering from the University of Tel-Aviv and received a doctoral degree in Electro-Optics from the school of Optics (CREOL) at the University of Central Florida. In 1995 he received the Rudolf Kingslake medal and prize, which is awarded in recognition of the most noteworthy original paper to appear in SPIE's journal Optical Engineering. He is presently developing aerospace systems for network centric operations and defense applications at Boeing-SVS.